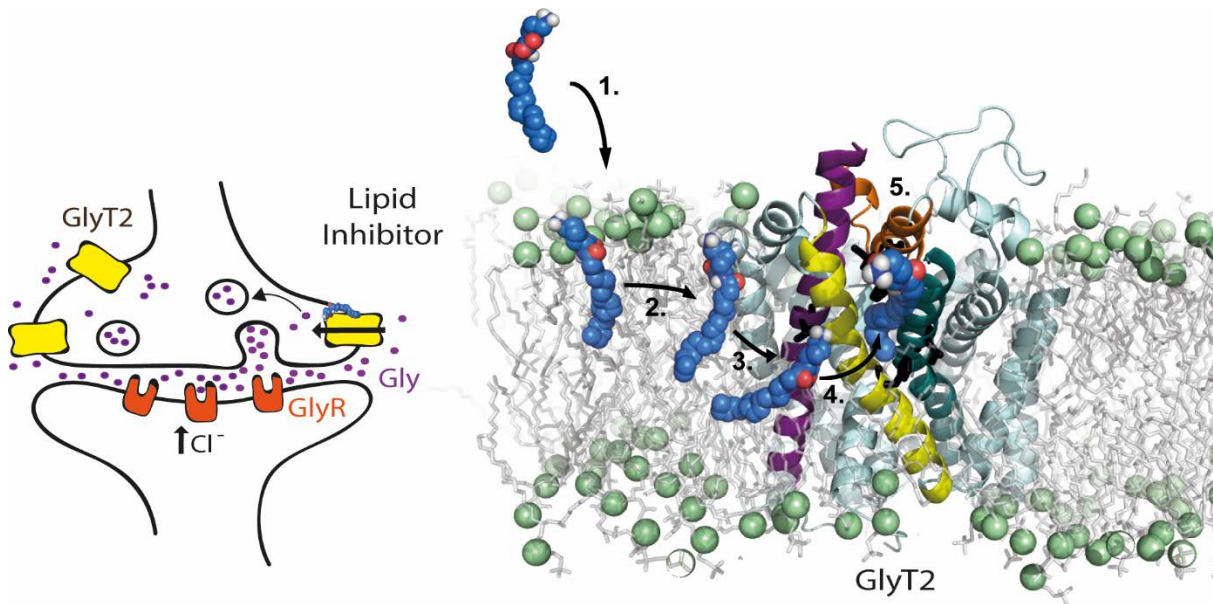


HEADS OR TAILS: LIPID INHIBITORS OF THE GLYCINE TRANSPORTER, GLYT2



Shannon Narelle Mostyn

Supervised by:

Professor Robert Vandenberg
Professor Renae Ryan
Dr Jane Carland

The Discipline of Pharmacology, School of Medical Sciences

The University of Sydney

This thesis is submitted in fulfilment of the requirements for the degree
of Doctor of Philosophy (Medicine)

April 2018

Abstract

Membrane proteins are influenced by the dynamic lipid membrane environment, which can impart stability, mediate protein interactions, and provide highly selective contacts essential for function. Membrane proteins can also bind endogenous lipid ligands or are able to be allosterically modulated by lipids, many of which are thought to access their specific binding sites via the cell membrane.

N-arachidonyl glycine (NAGly) is a bioactive lipid that is found in its highest concentrations within the spinal cord and may play an important role in endogenous regulation of glycinergic neurotransmission and pain perception through inhibition of the glycine transporter, GlyT2. In addition to NAGly, a number of lipid inhibitors of GlyT2 have been identified. These compounds are comprised of a long flexible unsaturated acyl tail conjugated to an amino acid or amino acid derivative head group. The aims of my study were two-fold; first to identify new, more potent, lipid inhibitors and develop a structure activity relationship for these compounds; and second, to elucidate the molecular mechanisms of inhibition. Wild type and mutant GlyT2 transporters were expressed in *Xenopus laevis* oocytes with glycine transport and the subsequent inhibition of transport measured using two-electrode voltage clamp electrophysiology, and radiolabelled uptake of glycine.

A library of 55 N-acyl amino acids with varying head and tail groups were synthesised and tested at both GlyT2 and the closely related glycine transporter, GlyT1. Two distinct groups of compounds were tested: the first group maintaining a glycine head group and altering the lipid tail; and the second conjugating the [C18 ω9] oleoyl tail to amino acids with varying properties. I found the lipid constituent of the acyl-glycine analogues is essential for specific interactions and the mechanism of inhibition and is not merely a non-selective, sticky adjunct. There was an ideal chain length, with an order of potency C18 > C16 > C14, and stringently defined double bond conformation and position. Conservative differences between compounds are sufficient to impart or remove inhibitory activity which validates highly specific binding to a

subtype specific, allosteric pocket. While changing the tail did not greatly alter potency, analogues where the head group was altered significantly influenced apparent affinity. Acyl amino acids containing an aromatic or positively charged side chain conferred the highest apparent affinity, with C16 ω 3 L-Lys possessing the highest potency (10.7 nM). 12 compounds inhibited GlyT2 < 100nM, and one of these inhibitors, oleoyl D-Lys, is also metabolically stable and produces analgesia in a rat model of neuropathic pain.

Mutagenesis of extracellular loop 4 (EL4), and transmembrane helices TM5 and TM8 suggest that the allosteric binding site is comprised of a cluster of aromatic residues which may strongly coordinate aromatic or positively charged head groups of the most potent analogues. Additionally, changing the properties of a membrane facing residue alters the otherwise slow washout of lipids. From these results, in addition to dynamic docking studies, it is proposed that acyl amino acids may first diffuse into the lipid bilayer and interact with regions of GlyT2 at the protein-membrane interface. Acyl amino acids then access their final binding site formed by aliphatic and aromatic residues from TM5, TM8, and EL4. It has previously been shown that EL4 undergoes important conformational changes in this family of transporters, where EL4 shifts into the outward facing vestibule to occlude the extracellular side and continue the transport cycle. Acyl amino acids may therefore inhibit GlyT2 by stabilising EL4 in a conformation that does not favour transport. The combination of structure-activity studies with molecular insights provides key information on the mechanism of inhibition which will drive further generation of GlyT2 inhibitors for the treatment of neuropathic pain.

Statement of contribution

I hereby declare that this submission is my own work and that, to the best of my knowledge and belief, it contains no material previously published or written by another person nor material which to a substantial extent has been accepted for the award of any other degree or diploma of a university of higher learning, except where due acknowledgement is made in this text.

Chapter 3 is published as “Synthesis and characterisation of novel acyl-glycine inhibitors of GlyT2” (2017) ACS Chemical Neuroscience, 8, 1949-1959. I co-designed the study with Dr Jane Carland, Dr Tristan Rawling, Prof Renae Ryan, and Prof Robert Vandenberg. Susan Shimmon performed the chemical synthesis and analysis. I conducted the electrophysiology and uptake experiments, analysed data, and prepared the manuscript with feedback from co-authors, Dr Tristan Rawling, Prof Renae Ryan, and Prof Robert Vandenberg.

Chapter 4 is currently being prepared for publication. I co-designed the study with Dr Tristan Rawling, Dr Sarasa Mohammadi, Prof Renae Ryan, Prof Macdonald Christie, and Prof Robert Vandenberg. Susan Shimmon performed the chemical synthesis and analysis. I conducted the electrophysiology and uptake experiments and analysed data with help from Zachary Frangos. Stability and blood brain barrier permeability assays were a service provided by the Centre for Drug Candidate Optimisation (CDCO), Monash University. Dr Sarasa Mohammadi performed the analgesia experiments and analysed data. I prepared the manuscript with Dr Tristan Rawling, with contributions from co-authors Dr Sarasa Mohammadi, Prof Renae Ryan, Prof Macdonald Christie, and Prof Robert Vandenberg.

Chapter 5 is currently being prepared for publication. I co-designed the study with Dr Megan O'Mara, Prof Renae Ryan, and Prof Robert Vandenberg. Mitchell Blyth performed dynamic docking experiments and analysed data. I conducted molecular biology and electrophysiology experiments, analysed data, and am currently preparing the manuscript with help from co-authors.

In all chapters where experiments were performed by collaborators their contributions are highlighted. Where data was provided to me, I created figures, described results, and drew conclusions for inclusion in my thesis.

Code of ethics

All experiments were performed in accordance with the “Australian code of practice for the care and use of animals for scientific purpose” Australian Government Publishing Service, Canberra, 1990.

Acknowledgements

First and foremost, I would like to thank my supervisor Professor Robert Vandenberg. You are a truly caring and concerned mentor and always made yourself available to provide guidance. You are a logical and well-reasoned researcher and yet still get excited at small victories when I run down the hall to your office with the latest from the lab. You are a strong advocate for all your students and I greatly value your advice for my future career in science.

To Professor Renae Ryan, thank you for being such a supportive supervisor. You have counselled me through multiple ups and downs, and helped me to push through and see the bigger picture. I admire how you fight to give opportunities to others and are always looking out for the wellbeing of your students.

Thank you to Dr Jane Carland for teaching me two-electrode voltage clamp electrophysiology and for introducing me to the wonderful world of glycine transporters. To Cheryl Handford, you are an absolute star! You are so kind and generous and always have time to teach students or lend a helping hand.

I would also like to thank everyone involved in the glycine grant for their contributions and for propelling my project forward with their own hard work. In particular, thank you Dr Tristan Rawling and Susan Shimmon for the unbelievably timely synthesis of compounds; thank you Dr Megan O'Mara, Dr Nandhitha Subramanian, Dr Michael Thomas, and Mitchell Blyth for your work in helping me understand how our slippery lipids work; thank you Professor Macdonald Christie, Professor Michael Murray, and Dr Sarasa Mohammadi for helping me see the future of our inhibitors.

To all past and present members of the Transporter Biology Group, I have spent more time with you over these past few years than anyone, and you have made the lab a second home (with a bed under my desk to match). Thank you Dr Ben McIlwain, Dr Rosie Cater, and Dr Amanda Scopelliti for being so welcoming; seeing all of the fabulous things you have gone on

to do gives me hope for my own future. To Dr Pep Font, I look forward to being bac-to-bac with you.

To Keith and Silvana, thank you! You have saved me more times than I can count!

Thank you to all of my Pharmacology pals who make work fun. Ben Harris you are a fabulous desk buddy. Gabi “DJ” Gregoriou you are a pool shark. I have so many great memories of the fun times in Newtown and umbrella wine time we shared.

To my friends and housemates who have given me sanity, and to Jess and Nelly (who have done the opposite) – a huge thank you for being around for the times when things weren't going so smoothly.

Finally, I would like to give a special thanks to my family. To my brother, Mick, you have made my PhD so much more rewarding. I have loved having you with me every step of the way. To my father and grandparents, Simon, Janice, and Lachie, thank you for giving me a place to get away for some much needed relaxation and refuelling. And to my beautiful mother, Bernadette, you have made us both strong women. You inspire me to keep going.

Patent

Vandenberg R, Ryan R, Rawling T, Imlach W, Christie M, Carland J and Mostyn S Novel glycine transport inhibitors for the treatment of pain. PCT/AU2018/050035

Publications

Carland JE, Thomas M, Mostyn SN, Subramanian N, O'Mara ML, Ryan RM, Vandenberg RJ (2018) Molecular determinant for substrate interactions with the glycine transporter, GlyT2 , ACS Chemical Neuroscience, 9 (3), 603-614

Mostyn SN, Carland JE, Shimmon S, Ryan R, Rawling T, Vandenberg RJ (2017) Synthesis and characterisation of novel acyl-glycine inhibitors of GlyT2, ACS Chemical Neuroscience, 8, 1949-1959

Vandenberg RJ, Mostyn SN, Carland JE, Ryan RM (2016), Glycine transporter 2 inhibitors: Getting the balance right, Neurochemistry International 98: p89-93

Table of contents

List of figures and tables	1
Abbreviations	5
Chapter 1: Literature review	7
1.1 Chronic pain	7
1.1.1 Neuropathic pain	8
1.1.2 Nociception	8
1.1.3 The role of glycine in neuropathic pain	9
1.2 Glycinergic neurotransmission	11
1.3 Glycine transporters	12
1.4 Glycine transport inhibitors	14
1.5 Lipids as glycine transport inhibitors	17
1.6 Molecular basis for lipid inhibition of GlyT2	20
1.6.1 Structures of the bacterial homologue LeuT	20
1.6.2 Structures of the dopamine and serotonin transporters	22
1.6.3 GlyT2 homology model	24
1.7 Lipid interactions with membrane proteins	25
1.7.1 Living in the membrane environment	25
1.7.2 Lipid ligands of membrane proteins	29
1.8 Development of lipids as drugs	33
Thesis objectives	36
Chapter 2: Methods	38
2.1 Materials	38
2.2 Creation of wild type (WT) or mutant mRNA encoding glycine transporters	38
2.3 Harvesting and preparing oocytes	39
2.4 Two electrode voltage clamp electrophysiology	39
2.4.1 Glycine concentration responses	41
2.4.2 Critical micelle concentrations of acyl amino acids	41
2.4.3 Acyl inhibitor concentration responses	42
2.4.4 Acyl inhibitor washout time course	43
2.4.5 Oleoyl L-Lys competition assay	43
2.5 Radiolabelled uptake	43
2.5.1 [³ H]-glycine uptake time course	43

2.5.1 [3H]-glycine uptake on oocytes expressing GlyT1 and GlyT2	44
2.6 Pharmacokinetics of oleoyl L-Lys and oleoyl D-Lys	44
2.6.1 Stability in plasma and liver microsomes	44
2.6.2 Blood brain barrier permeability	44
2.7 Analgesia testing in a partial nerve ligation model of pain	45
2.8 GlyT2 homology model and docking of lipid inhibitors	45
Chapter 3: Characterisation of novel acyl-glycine inhibitors of GlyT2	47
3.1 Introduction	47
3.2 Results and discussion	49
3.2.1 Inhibitory activity of acyl-glycine analogues at GlyT2 and GlyT1	50
3.2.2 Activity of C18 acyl-glycine analogues	52
3.2.3 Activity of C16 and C14 acyl-glycine analogues	54
3.2.4 C18 ω8 gly and C16 ω6 gly inhibit [3H]-glycine uptake by oocytes expressing GlyT2	57
3.2.5 There is a preferred double bond position and chain length for conferring affinity and extent of inhibition	58
3.2.6 Reversibility of acyl-glycine inhibitors	61
3.3 Conclusions	62
Chapter 4: N-acyl amino acid inhibitors of GlyT2 for the treatment of neuropathic pain	63
4.1 Introduction	63
4.2 Results and discussion	65
4.2.1 Activity of N-acyl amino acid analogues on GlyT2 and GlyT1	65
4.2.2 Activity of N-acyl L-amino acids	67
4.2.3 Activity of N-acyl D-amino acids	72
4.2.4 Structure activity of acyl inhibitors on GlyT2	72
4.2.5 Maximal level of inhibition	73
4.2.6 Oleoyl L-Lys reduces radiolabelled uptake of GlyT2 expressing oocytes in a dose dependent manner	78
4.2.7 Reversibility of N-acyl amino acid inhibitors	79
4.2.8 Metabolism of oleoyl L-Lys and oleoyl D-Lys	82
4.2.9 Blood brain barrier permeability of oleoyl D-Lys	83
4.2.10 Analgesic activity of oleoyl D-Lys on a partial nerve ligation rat model of neuropathic pain	84
4.3 Conclusions	86

Chapter 5: Molecular determinants for acyl amino acid inhibition of GlyT2	87
5.1 Introduction	87
5.2 Results and discussion	90
5.2.1 Oleoyl L-Lys is not a competitive inhibitor of GlyT2	90
5.2.2 Screening of residues which may be involved in the mechanism of inhibition by lipid inhibitors	93
5.2.3 Glycine affinity of mutant transporters	96
5.2.4 Differential selectivity of GlyT1 and GlyT2	98
5.2.5 Y550 is important in the mechanism of inhibition by lipid GlyT2 inhibitors	100
5.2.6 Mutations to the top of TM8 disrupt lipid head group interactions	102
5.2.7 Mutations of membrane exposed medial TM5 and TM8 residues disrupt lipid tail group interactions	105
5.2.8 Docking of C18 ω 9 D-Lys suggests a lipid binding cavity comprised of residues from EL4, TM5, and TM8	108
5.2.9 Comparison with lipid binding membrane proteins	110
5.2.10 F515W in TM7 increases efficacy and the reversibility of OLCarn	113
5.3 Conclusions	119
Chapter 6: Final discussion and future directions	121
6.1 Summary of key findings	121
6.2 Future directions: Resolving protein-lipid interactions	124
6.2.1 Measuring lipid binding to membrane proteins	124
6.2.2 Advances in structural biology to study membrane proteins in a more native environment	127
6.3 Monitoring conformational dynamics of transport and inhibition	130
6.4 Functional implications of glycine transport inhibitors	133
6.5 Conclusion	135
References	136

List of figures and tables

Figure 1.1. Nociceptive and non-noxious pathways in the dorsal horn of the spinal cord	9
Figure 1.2. Glycinergic neurotransmission is reduced in radial neurons of superficial dorsal horn after partial nerve ligation	10
Figure 1.3. The cycle of glycine action at inhibitory and excitatory synapses	12
Figure 1.4. Glycine receptor mediated post synaptic currents	14
Figure 1.5. Structures of GlyT2 inhibitors	15
Figure 1.6. Structures of known glycine conjugated and carnitine conjugated GlyT2 lipid inhibitors	19
Figure 1.7. Schematic of transport in LeuT	22
Figure 1.8. Alignment of SERT versus dDAT	23
Figure 1.9. Homology model of GlyT2 shown in plane of the membrane	24
Figure 1.10. Cholesterol binding site of the dopamine transporter dDAT	28
Figure 1.11. Surface rendering of the sphingosine-1-phosphate crystal structure	31
Figure 2.1. Setup of two-electrode voltage clamp electrophysiology	40
Figure 3.1. Structures of NAGly and NOGly	49
Figure 3.2. Example glycine induced transport current traces from oocytes expressing GlyT2 and clamped at -60 mV	51
Figure 3.3. Monounsaturated C18 acyl-glycines inhibit glycine transport currents of GlyT2 and GlyT1 transporters expressed in <i>Xenopus laevis</i> oocytes	53
Figure 3.4. Monounsaturated C16 and C14 acyl-glycines inhibit glycine transport currents of GlyT2 and GlyT1 transporters expressed in <i>Xenopus laevis</i> oocytes	55
Figure 3.5. Rates of [³ H]-glycine uptake in the presence and absence of acyl-glycine inhibitors	57
Figure 3.6. Possible conformations of acyl tails	60
Figure 4.1. Representative current traces from oocytes expressing glycine transporters, clamped at -60 mV	66

Figure 4.2. Aliphatic acyl amino acids inhibit glycine transport currents of GlyT2 transporters expressed in <i>Xenopus laevis</i> oocytes	68
Figure 4.3. Polar and negatively charged acyl amino acids inhibit glycine transport currents of GlyT2 transporters expressed in <i>Xenopus laevis</i> oocytes	69
Figure 4.4. Aromatic acyl amino acids inhibit glycine transport currents of GlyT2 transporters expressed in <i>Xenopus laevis</i> oocytes	70
Figure 4.5. Positively charged acyl amino acids inhibit glycine transport currents of GlyT2 transporters expressed in <i>Xenopus laevis</i> oocytes	71
Figure 4.6. Radiolabelled uptake of [³ H]-glycine by GlyT2 but not GlyT1 is inhibited by oleoyl L-Lys	79
Figure 4.7. Reversibility time course for N-acyl amino acids	80
Figure 4.8. Representative traces for reversibility of select N-acyl amino acids	81
Figure 4.9. Von Frey threshold for partial nerve ligation injured rats following injection of oleoyl D-Lys	85
Figure 5.1. Homology model of GlyT2 shown in plane of the membrane	90
Figure 5.2. Oleoyl L-Lys reduces concentration-dependent glycine currents	92
Figure 5.3. Sequence alignment of GlyT2, GlyT1, DAT, and LeuT	94
Figure 5.4. Location of mutated residues on GlyT2	95
Figure 5.5. Inhibition of WT and mutant GlyT2 transporters by 1 μM OLCarn	96
Figure 5.6. Glycine dependent transport currents for WT and mutant transporters	97
Figure 5.7. Acyl amino acids inhibit glycine transport currents of I545L mutant GlyT2 transporters expressed in <i>Xenopus laevis</i> oocytes	98
Figure 5.8. Acyl amino acids inhibit glycine transport currents of L425I mutant GlyT1 transporters expressed in <i>Xenopus laevis</i> oocytes	99
Figure 5.9. Location of mutations in EL4	100
Figure 5.10. Acyl amino acids inhibit glycine transport currents of Y550L mutant GlyT2 transporters expressed in <i>Xenopus laevis</i> oocytes	101
Figure 5.11. Location of mutations at the top of TM8	102

Figure 5.12. Acyl amino acids inhibit glycine transport currents of P561S mutant GlyT2 transporters expressed in <i>Xenopus laevis</i> oocytes	103
Figure 5.13. Acyl amino acids inhibit glycine transport currents of W563L mutant GlyT2 transporters expressed in <i>Xenopus laevis</i> oocytes	104
Figure 5.14. Location of membrane exposed mutants in TM5 and TM8	105
Figure 5.15. Acyl amino acids inhibit glycine transport currents of L569F mutant GlyT2 transporters expressed in <i>Xenopus laevis</i> oocytes	106
Figure 5.16. Acyl amino acids inhibit glycine transport currents of F428A mutant GlyT2 transporters expressed in <i>Xenopus laevis</i> oocytes	107
Figure 5.17. Structures of select acyl-glycine analogues	108
Figure 5.18. GlyT2 model with oleoyl D-Lys docked in site A and site B	109
Figure 5.19. Sphingosine-1-phosphate receptor bound to antagonist ML056	111
Figure 5.20. Potential LPA binding obtained from docking simulations from top down and in plane of the membrane	112
Figure 5.21. Location of F515 on GlyT2 in plane of the membrane	113
Figure 5.22. Acyl amino acids inhibit glycine transport currents of F515W mutant GlyT2 transporters expressed in <i>Xenopus laevis</i> oocytes	114
Figure 5.23. Washout of 1 μ M OLCarn on WT GlyT2 and TM7 F515W mutant GlyT2 transporters	115
Figure 5.24. Molecular dynamics simulation of acyl inhibitors in a POPC/cholesterol membrane	116
Figure 5.25. Proposed mechanism of inhibition by acyl inhibitors of GlyT2	119
Figure 6.1. Residues lining (within 3 Å) the oleoyl D-Lys site A and site B	123

Table 3.1. Structure-activity relationships of C14, C16, and C18 glycine compounds at GlyT2 and GlyT1	56
Table 4.1. Structure-activity relationships of amino acid conjugated lipid compounds at GlyT2 and GlyT1	75
Table 4.2. Degradation half-lives of N-acyl amino acids in rat plasma and liver microsomes	83
Table 4.3. Pharmacokinetic parameters of 28 after intraperitoneal administration of a single 27.5 mg/kg dose in Sprague Dawley rats	84
Table 5.1. EC ₅₀ values for glycine transport of WT and mutant GlyT2 and GlyT1 transporters	97
Table 5.2. IC ₅₀ values and % max. inhibition for mutant GlyT2 transporters	117

Abbreviations

2-AG	2-arachidonoyl glycerol
95% CI	95% confidence interval
AmtB	ammonia channel
ANOVA	analysis of variance
BBB	blood brain barrier
CB ₁ and CB ₂	cannabinoid receptors
CMC	critical micelle concentration
CNS	central nervous system
COX	cyclooxygenase
cryo-EM	cryo-electron microscopy
dDAT	<i>Drosophila melanogaster</i> dopamine transporter
DEER	double electron-electron resonance
EL	extracellular loop
EPSCs	excitatory post synaptic currents
FAAH	fatty acid amide hydrolase
GABA	gamma-aminobutyric acid
GlyR	glycine receptor
GlyT1	glycine transporter 1
GlyT2	glycine transporter 2
hSERT	human serotonin transporter
IPSC	inhibitory post-synaptic currents
ITC	isothermal titration calorimetry
Kir	inwardly rectifying K ⁺ channel
LCP	lipidic cubic phase
LeuT	bacterial leucine transporter from <i>Aquifex aeolicus</i>
LPA	lysophosphatidic acid receptor
MD	molecular dynamics
MSP	membrane scaffold protein
MUFA	monounsaturated fatty acid
NAGly	N-arachidonoyl glycine
native-MS	mass spectrometry of intact membrane proteins
NMDAR	N-methyl D-aspartate receptors
NOGly	N-oleoyl glycine

NSS	neurotransmitter sodium symporters
OLCarn	oleoyl L-carnitine
PNL	partial nerve ligation
PO	1-palmitoyl-2-oleoyl
POPC	1-palmitoyl-2-oleoyl- <i>sn</i> -glycero-3-phosphocholine
POPG	1-palmitoyl-2-oleoyl- <i>sn</i> -glycero-3-phosphoglycerol
RMSD	root mean square deviation
S1P ₁	sphingosine-1-phosphate receptor
SEM	standard error of the mean
siRNA	small interfering RNA
SMALP	styrene maleic acid lipo-particles
smFRET	Single molecule [Förster] fluorescence resonance energy transfer
TM	transmembrane
VIAAT	vesicular inhibitory amino acid transporter
WT	wild type

Chapter 1: Literature review

1.1 Chronic pain

Approximately 29% of the Australian population are suffering from chronic pain conditions (Stollznow Research, 2010), with a high proportion of those affected being of working age, causing a deficit of \$34 billion annually to the Australian economy through health care costs and loss of productivity (most recent figures by Access Economics, 2007). Chronic pain cases make up the majority of visits to general practitioners and are additionally associated with a number of psychiatric comorbidities (Gatchel *et al.*, 2007). In a study of 1,595 chronic pain patients, 64% also suffered from a psychiatric condition compared with 15% in the general population (Dersh *et al.*, 2002). These concomitant conditions are often a greater predictor of disability than the severity of chronic pain (Ormel *et al.*, 1994), and are likely a direct consequence of the debilitating nature of the disease, as only 16% of patients are satisfied with their pain management (Stollznow Research, 2010)

There is a great need to develop new drugs to treat chronic pain as current analgesics are ineffective, or have an unacceptable side effect profile and potential for abuse. For example, opioids have traditionally been used for the treatment of chronic pain due to their analgesic effects via action on mu (μ) opioid receptors. However, concerns about long-term safety and efficacy have limited their use (Rosenblum *et al.*, 2008). Other therapeutics indicated for treatment of other diseases, such as tricyclic antidepressants and anticonvulsants, are often prescribed to treat chronic pain (Fornasari, 2017), but majority of cases are refractory to these conventional drugs. It is clear that current treatments are ineffective at treating the complex spectrum of symptoms that underlies neuropathic pain, and new targets which are involved in the formation and progression of the disease must be explored.

1.1.1 Neuropathic pain

Neuropathic pain is a prevalent form of chronic pain, characterised by associated hyperalgesia and allodynia, which produce distinctive symptoms of numbness, burning, shooting, and electric-like pain in sufferers (Costigan *et al.*, 2009). Hyperalgesia is defined as a lowered reduction in the pain threshold, which amplifies pain sensation, and often occurs alongside allodynia, an inappropriate pain response to innocuous stimuli (Scholz & Woolf, 2002).

Disease or injury to peripheral nerves can cause long-term neuropathic pain which persists well after the site of injury has healed. Damage and inflammation at the peripheral site alone, however, cannot explain the ongoing symptoms. Changes within the central nervous system produce disordered synaptic pathways and central sensitisation, which contribute to the pathology of neuropathic pain (Latremliere & Woolf, 2009).

1.1.2 Nociception

In normal nociception, sensory receptors have a typical threshold of activation. Certain stimuli such as intense heat and pressure, but not light touch and low temperature, will stimulate nociceptors (Julius & Basbaum, 2001). Following activation, primary sensory neurons innervate the spinal cord dorsal horn as the first point of dispatch before transmission to the brain for cognitive processing (Todd, 2010).

Primary afferent neurons terminate in distinctive locations within the spinal cord, with nociceptive fine myelinated A δ -, and unmyelinated C-fibers innervating the superficial region (laminae I-II), and lower- threshold, non-noxious mechanoreceptive A β -fibers terminating in deeper laminae II_i-VI (Todd, 2010) (Figure 1.1, Vandenberg *et al.*, 2014). Nociceptive projection neurons in lamina I express neurokinin 1 receptors (NK1) which are activated following direct stimulation by C-fibres, or by excitatory interneurons in lamina II (Takazawa & MacDermott, 2010). Inhibitory glycinergic interneurons in lamina III synapse onto excitatory

neurons, including protein kinase C γ (PKC γ) positive neurons, where they inhibit low-threshold, non-noxious information from entering the pain pathway.

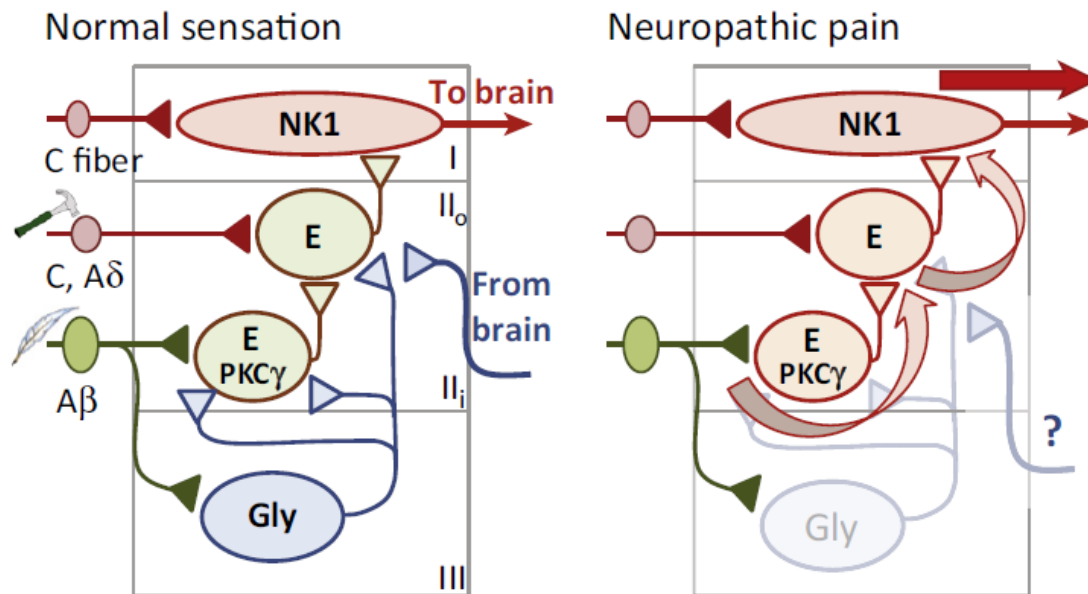


Figure 1.1. Nociceptive and non-noxious pathways in the dorsal horn of the spinal cord.

Left panel: in normal physiological states, excitatory A β (light touch) sensory inputs converge onto excitatory interneurons [green cells; E, some of which are protein kinase C γ (PKC γ)-positive] in lamina II of the superficial dorsal horn, as well as glycinergic neurons in lamina III [blue cells; Gly]. Concurrent activation of these glycinergic interneurons produces strong feed-forward inhibition of lamina II excitatory interneurons (green; E) that prevents non-noxious sensory information from invading pain transmission neurons in lamina I [red cell; neurokinin 1 (nk1) receptor positive] (Vandenberg *et al.*, 2014). Right panel: a loss of glycinergic inputs allow for innocuous stimuli to enter the pain pathway and increase transmission to the brain.

1.1.3 The role of glycine in neuropathic pain

A dysfunction of synaptic transmission can give rise to neuropathic pain, whereby a dominance of excitatory tone in the superficial neurons of the dorsal horn causes an excess of nerve firing in the ascending pain pathway (Latreoliere & Woolf, 2009; Takazawa & MacDermott, 2010). Nerve injury can, among other mechanisms, reduce the control

maintained by inhibitory neurons and allow for disinhibition of pain signalling to occur. Loss of inhibition can be due to a reduced synthesis and release of neurotransmitters or, more significantly, a loss of inhibitory neurons through N-methyl D-aspartate receptors (NMDAR) induced toxicity and apoptosis (Scholz *et al.*, 2005).

A recent study has shown that in a partial nerve ligation rat model of neuropathic pain, there is a reduction in electrically evoked glycinergic inhibitory post-synaptic currents (eIPSCs) of radial interneurons in the spinal cord (Figure 1.2, Imlach *et al.*, 2016). These excitatory radial neurons in the spinal cord received reduced glycinergic inhibitory inputs. This may generate hyperexcitability and disinhibition of pain signalling. Disinhibition has been shown to increase the low-threshold activation of lamina II neurons, and the subsequent increase in excitatory post synaptic currents (EPSCs) activated by A β and A δ fibres, which would allow for mechanical allodynia (Takazawa & MacDermott, 2010).

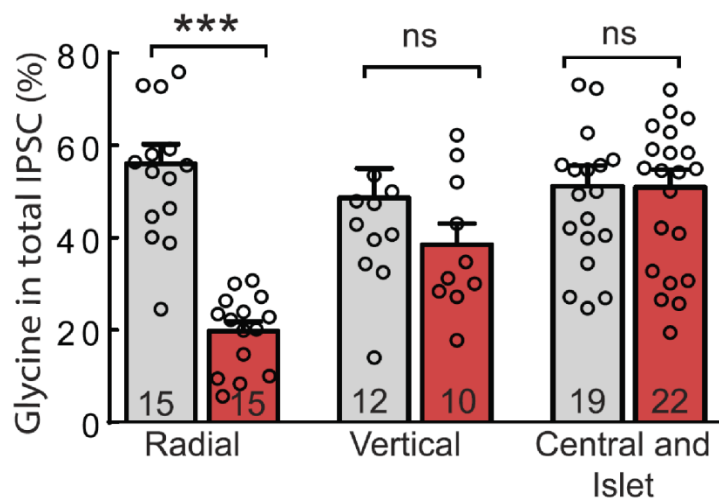


Figure 1.2. Glycinergic neurotransmission is reduced in radial neurons of superficial dorsal horn after partial nerve ligation. Normalised glycinergic eIPSC values as a percentage of the total eIPSC for the neuron types following partial nerve ligation (red) and sham (grey) surgeries (***) $p < 0.001$, two way ANOVA, Sidak post-hoc multiple comparisons test) (adapted from Imlach *et al.*, 2016).

Peripheral nerve injury can also lead to degeneration of peripheral C-fiber terminals and subsequent sprouting of A β fibers into higher regions of the spinal cord (laminae I-II), where they innervate nociceptive neurons (Scholz & Woolf, 2002). This muddling of sensory pathways can lead to stimulation of nociceptive transmission by innocuous stimuli.

The network of altered synaptic transmission in the dorsal horn allows for excessive nerve firing in the ascending pain pathway. Glycine is the predominant inhibitory neurotransmitter in the spinal cord responsible for suppressing excitatory tone, and so it follows that a novel therapy involved in increasing glycine at inhibitory synapses may dampen spontaneous nerve activity and result in a reduction of associated pain symptoms.

1.2 Glycinergic neurotransmission

Inhibitory glycine receptors (GlyR) are pentameric ligand gated ion channels composed of subunits (α 1- α 4, β) which direct their differential expression and defines the physiological role of the receptor (Lynch, 2004; Malosio *et al.*, 1991). When expressed postsynaptically in the brain stem and spinal cord, GlyRs are activated by glycine to generate hyperpolarisation to reduce neuronal firing and have been implicated in pain processing (Ahmadi *et al.*, 2001). Presynaptic homomeric α 3 glycine receptors have also been proposed to have a role in pain pathways, where activation of these receptors prompts presynaptic glycine release (Jeong *et al.*, 2003). In addition to its actions at inhibitory synapses, glycine can diffuse to excitatory synapses where it can act as a co-agonist with glutamate at NMDARs (Supplisson & Bergman, 1997).

Following glycine release into inhibitory synapses, glycine levels increase from a resting concentration of 0.1-0.2 μ M to millimolar concentrations (Eulenburg *et al.*, 2005). Rapid removal of glycine is then required to terminate transmission and reduce diffusion to adjacent synapses. In order to sustain this tightly regulated concentration requirement, Na⁺/Cl⁻ coupled transporters are employed to actively remove glycine from the synapse, resulting in a subsequent restoration of resting glycine levels (Zafra *et al.*, 1995).

1.3 Glycine transporters

There are two subtypes of glycine transporters which have been identified within the mammalian central nervous system, glycine transporter 1 (GlyT1) and glycine transporter 2 (GlyT2) which share 48% amino acid sequence identity (Morrow *et al.*, 1998). GlyT1 is preferentially expressed on astrocytes adjacent to both excitatory and inhibitory neurons allowing for regulation of glycine concentrations at both glutamatergic and glycinergic synapses. GlyT2 is almost exclusively expressed on presynaptic inhibitory glycinergic neurons (Zafra *et al.*, 1995) (Figure 1.3, Vandenberg *et al.*, 2014).

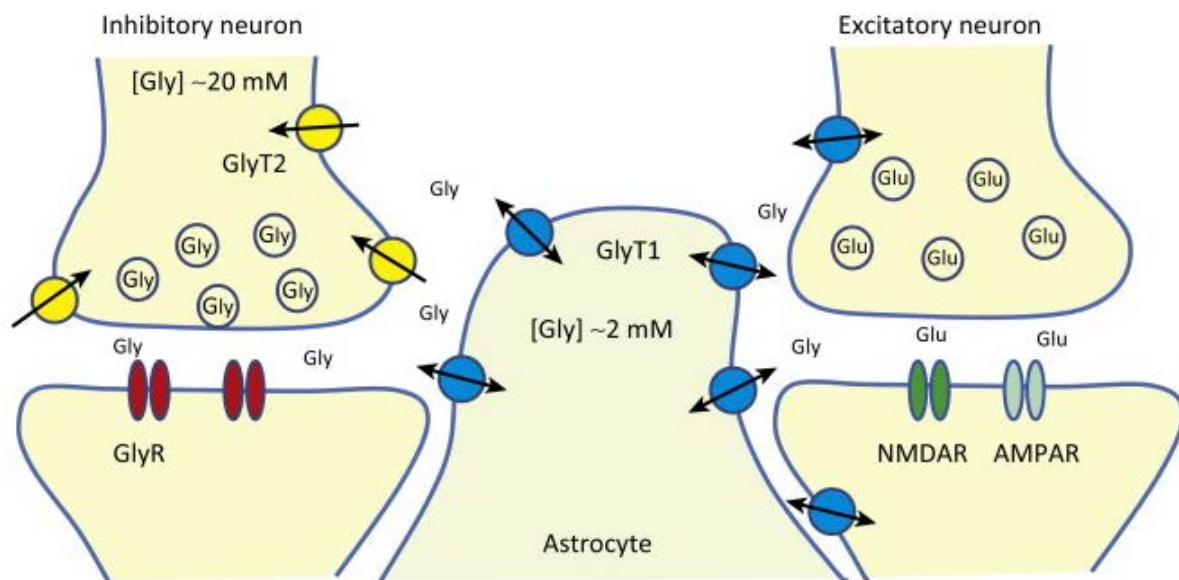


Figure 1.3. The cycle of glycine action at inhibitory and excitatory synapses. Glycine is released into inhibitory synapses where it activates postsynaptic GlyRs (red). Glycine is cleared from the inhibitory synapse via GlyT2 (yellow) transporters on the presynaptic neuron and via GlyT1 (blue) transporters on adjacent astrocytes. At excitatory synapses glycine acts as a co-agonist with glutamate on NMDARs (green). The glycine is then cleared by GlyT1 on astrocytes and glutamatergic neurons (Vandenberg *et al.*, 2014).

The transport of glycine is thermodynamically unfavourable. To account for this GlyT1 and GlyT2 couple substrate transport to one Cl⁻ ion and two Na⁺ ions or three Na⁺ ions respectively,

exploiting the ion gradients generated by Na⁺/K⁺-ATPase (Roux & Supplisson, 2000). As a result of the additional Na⁺ ion carried by GlyT2, the concentrating capacity for the transport of glycine by this subtype is greater. This facilitates the rapid reuptake of glycine into presynaptic terminals where the low affinity vesicular inhibitory amino acid transporter (VIAAT) can load glycine into vesicles to be recycled for further release (Roux & Supplisson, 2000).

The substrate binding site of GlyT1 is somewhat larger than GlyT2 and is able to accommodate sarcosine, an *N*-methyl derivative of glycine, as well as the transport of glycine itself (Vandenberg *et al.*, 2007). Conversely, there are no known substrates other than glycine for GlyT2 (Carland *et al.*, 2018).

The importance of GlyT1 and GlyT2 is demonstrated through knockout, or small interfering RNA (siRNA) knockdown of protein expression. Homozygous (GlyT1^{-/-}) knockout mice experience severe motorsensory and respiratory deficits, which are fatal 6-14 hours following birth (Gomez *et al.*, 2003a). These mice also exhibit constant activation of glycine receptors, which suggests that in the absence of GlyT1, glycine is unable to be sufficiently cleared from the synapse. Conversely, electrophysiological recordings from GlyT2^{-/-} mice show a reduction in postsynaptic glycinergic currents (Figure 1.4, Gomez *et al.*, 2003b), supporting the crucial role of GlyT2 in the recycling and release of glycine. The GlyT2 knockout phenotype is fatal 2 weeks postnatal, where mice develop severe neuromotor disease, with symptoms reflective of hyperekplexia; strong tremor could be easily induced through touch, and mice experienced extreme muscle rigidity and were unable to right themselves (Gomez *et al.*, 2003b). Mutation of the human GlyT2 gene (SLC6A5) is the most common cause of presynaptic hyperekplexia, where mutations have been shown to affect GlyT2 localisation and expression, and/or a reduction in glycine reuptake through disruption of the glycine and ion binding sites (Carta *et al.*, 2012; Eulenburg *et al.*, 2006; Rees *et al.*, 2006).

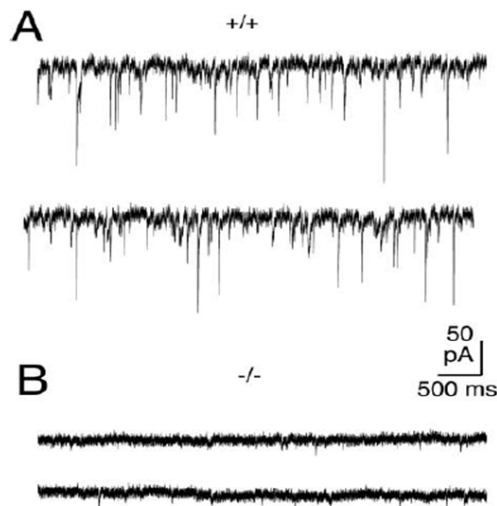


Figure 1.4. Glycine receptor mediated post synaptic currents in **A.** wild type GlyT2 (+/+) and **B.** knockout GlyT2 (-/-) mice (Gomez *et al.*, 2003b)

Partial knockdown of glycine transporters using targeted siRNA reduces protein expression to ~30% 3 days after injection (Morita *et al.*, 2008). No apparent behavioural symptoms were observed. Furthermore, siRNA has an antiallodynic effect in rat models of neuropathic pain (Morita *et al.*, 2008), further validating an analgesic role for glycine. While total removal of GlyT2 eliminates this route of glycine recycling, partial knockdown instead slows clearance from the synapse while still preserving glycine reuptake for vesicular refilling and further release.

1.4 Glycine transport inhibitors

Intrathecal injection of glycine reduces spontaneous nociception and neuronal dystrophy in rats (W. Huang & Simpson, 2000). Conversely, hyperalgesia and allodynia can be induced using the glycine receptor antagonist, strychnine (Yaksh, 1989). The role of glycine in the development of pain and its utility in producing analgesia has driven the development of a number of glycine transport inhibitors (Figure 1.5) for the treatment of neuropathic pain.

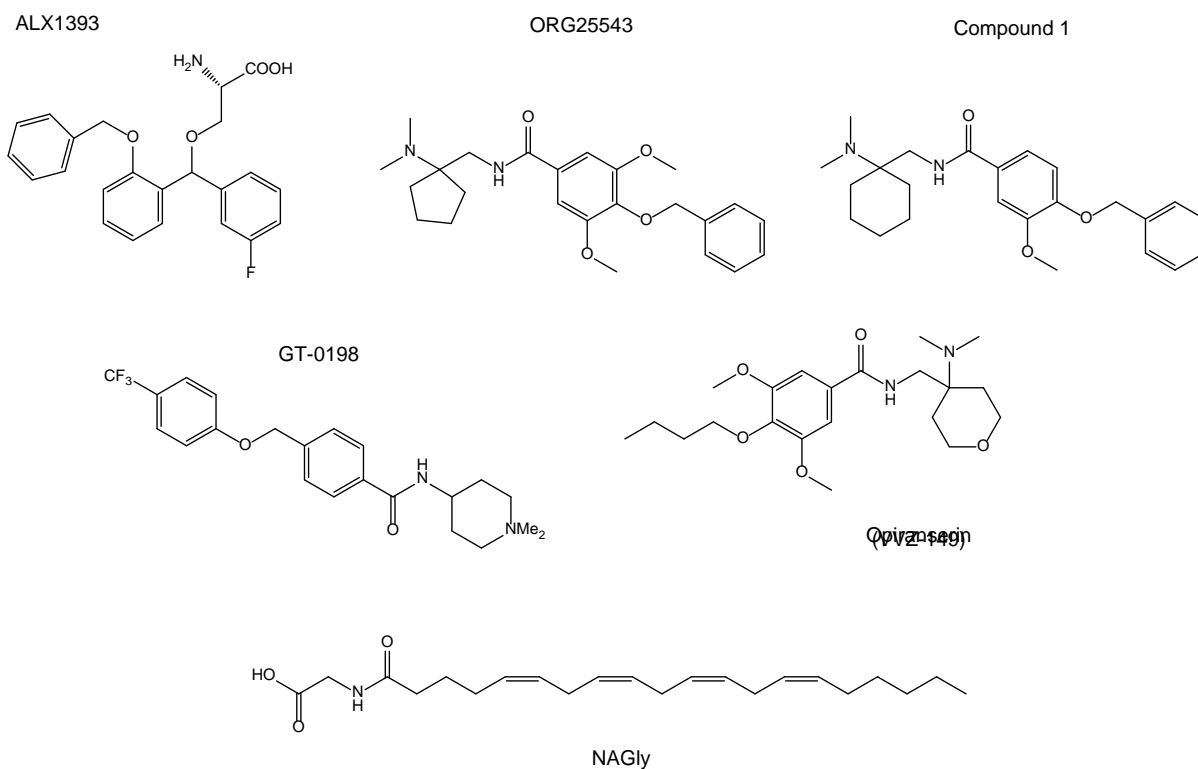


Figure 1.5. Structures of GlyT2 inhibitors.

ALX1393 (Xu *et al.*, 2005) and ORG25543 (Caulfield *et al.*, 2001) were among the first potent inhibitors of GlyT2 to be developed. ALX1393 inhibits GlyT2 with an IC_{50} of 100 nM (Mingorance-Le Meur *et al.*, 2013) and has been shown to be anti-allodynic when intrathecally or intravenously injected into rodents suffering from neuropathic pain (Haranishi *et al.*, 2010; Morita *et al.*, 2008; Xu *et al.*, 2005). These anti-allodynic effects could be reversed using strychnine (Haranishi *et al.*, 2010), confirming a glycinergic mechanism of analgesia where inhibition of GlyT2 by ALX1393 results in an increase of GlyR activation, probably through transient increases in the concentration of glycine within the synapse.

Chronic application of ALX1393 does not affect the frequency of glycinergic miniature inhibitory postsynaptic currents (mIPSCs), but rather alters the ratio of gamma-aminobutyric acid (GABA) and glycine signalling (Xu *et al.*, 2005). This is likely through the inhibition of glycine recycling by GlyT2 which would influence the VIAAT mediated loading of presynaptic vesicles and ultimately favour the release of GABA. This potential to alter the balance of

inhibitory neurotransmission may limit the use of ALX1393. Application of ALX-1393 has since been implicated in producing significant adverse symptoms, including paresis or plegia, and severe respiratory depression (Hermanns *et al.*, 2008), with similar respiratory effects, such as irregular respiratory rhythm, observed in mice deficient in presynaptic $\alpha 3$ receptors (Manzke *et al.*, 2010), which suggests the symptoms occur through obstruction of presynaptic recycling mechanisms. Additionally, in a study measuring the *in vivo* target exposure of ALX1393 following intravenous injection (Mingorance-Le Meur *et al.*, 2013), the free brain/plasma ratio was >0.05 , 60 minutes post administration. At the maximal dose, the free concentration was 3-fold below the IC_{50} which suggests that ALX1393 may be unable to cross the blood brain barrier (BBB) in sufficient quantities to bind to the glycine transporter. ALX1393 has also been shown to inhibit glycine uptake of GlyT1 expressing cells (IC_{50} 4 μM) (Mingorance-Le Meur *et al.*, 2013). Despite ALX1393's analgesic properties, adverse side effects, poor BBB permeability, and non-selectivity may limit its therapeutic use.

ORG25543 is a potent inhibitor of GlyT2 (IC_{50} 16 nM, Caulfield *et al.*, 2001), and unlike ALX1393, has no appreciable activity at GlyT1. ORG25543 ameliorates hyperalgesia and allodynia in a number of pain models (Morita *et al.*, 2008; Mingorance-Le Meur *et al.*, 2013). Application of ORG25543 to mouse spinal cord slices shows changes in glycinergic neurotransmission and a decrease in the decay constant of mIPSCs (Bradaia *et al.*, 2004), however exposure >10 minutes resulted in a long term reduction in IPSCs, likely through decreased glycine release into the synapse. Furthermore, glycinergic currents are not able to be restored following a washout period after ceasing ORG25543 application (Mingorance-Le Meur *et al.*, 2013). This sustained, complete block of GlyT2 may prevent the recycling of glycine and lead to toxicity, mimicking the symptoms of a GlyT2 knockout phenotype. Acute dosing of ORG25543 produces excitotoxicity, hyperekplexia like symptoms such as tremor, and in severe cases death, as a result of its irreversibility (Mingorance-Le Meur *et al.*, 2013). To prevent this, a series of analogues based on the structure of ORG25543 were synthesised and tested for their BBB permeability and toxicity profiles (Mingorance-Le Meur *et al.*, 2013).

Compound 1 is one such compound with an IC₅₀ of 100 nM, high BBB permeability, and reversibility and restoration of glycine currents following inhibition. Application of Compound 1 to mice displayed no adverse side effects and so it is predicted that a GlyT2 inhibitor should be reversible to improve its therapeutic potential.

More recently, Takahashi *et al.*, (2014) synthesised a series of phenoxyethylbenzamides which are potent inhibitors of GlyT2. One analogue, GT-0198, displayed high selectivity at GlyT2 (IC₅₀ 105 nM) and a high brain/plasma ratio of 0.167 1 hr following oral administration (Takahashi *et al.*, 2014). Intravenous, oral or intrathecal administration of GT-0198 has also been shown to be analgesic in a partial nerve ligation model of pain (Omori *et al.*, 2015).

Opiranserin (previously VVZ-149) is a drug under development by Vivozon indicated for post-operative pain relief, and is currently in phase II clinical trials. Unlike classical GlyT2 inhibitors, opiranserin was developed with the aim of binding to multiple targets with similar affinity that may generate synergistic effects (Nedeljkovic *et al.*, 2017; Pang *et al.*, 2012). Opiranserin inhibits GlyT2 (IC₅₀ 860 nM), and is an antagonist at purine P2X₃ receptors (IC₅₀ 870 nM) and serotonin 5-HT_{2A} receptors (IC₅₀ 1.3 µM). This multi-target approach may help to identify more efficacious analgesics for the treatment of neuropathic pain.

1.5 Lipids as glycine transport inhibitors

Another compound with multiple antinociceptive targets is N-arachidonyl glycine or NAGly (Figure 1.5, 1.6A), which in addition to inhibiting GlyT2 (Wiles *et al.*, 2006), also targets T-type Ca²⁺ channels (Ross *et al.*, 2009), COX-2 (Prusakiewicz *et al.*, 2002), inhibitory glycine receptors (Yang *et al.*, 2008), and may also activate orphan receptors including GPR55 (Console-Bram *et al.*, 2017) and GPR18 (Kohno *et al.*, 2006). NAGly is a carboxylic acid derivative of anandamide and is endogenously produced through two distinct enzymatic pathways in the central nervous system (Bradshaw *et al.*, 2009). NAGly is found in highest concentrations within the spinal cord and may play an important role in modulating pain (Huang *et al.*, 2001). NAGly reduces mechanical allodynia and thermal hyperalgesia, which

are characteristic of chronic pain in both neuropathic and inflammatory rat models of pain, and does not generate any overt side effects (Succar *et al.*, 2007; Vuong *et al.*, 2008). Additionally, NAGly prolongs the time course of glycine at glycinergic synapses in lamina II of the superficial dorsal horn, an area responsible for integrating ascending pain information, and also prolongs the decay phase of evoked inhibitory postsynaptic currents, which suggests that NAGly may exert analgesia by increasing inhibitory tone at glycinergic neurons (Jeong *et al.*, 2010).

NAGly is a reversible, non-competitive inhibitor of GlyT2 (IC₅₀ 9 μM) and has no appreciable activity at GlyT1 (Wiles *et al.*, 2006), or at the CB₁ or CB₂ cannabinoid receptors (Sheskin *et al.*, 1997). Other N-arachidonyl amino acid conjugates (Figure 1.6A) also inhibit the GlyT2 transporter, with an order of potency of NAGly > N-arachidonyl alanine > N-arachidonyl GABA (Wiles *et al.*, 2006). These inhibitors are amphipathic and have the propensity to spontaneously form micelles at a characteristic critical micelle concentration (CMC). The CMC for NAGly is >30 μM which would limit the free diffusion and binding to GlyT2 above this concentration. For NAGly, the solubility of the compound is likely to limit the maximal level of inhibition and produce partial inhibition in *in vivo* and *in vitro* assays. N-oleoyl glycine (NOGly) similarly contains a glycine head group and has instead an ω9 monounsaturated 18-carbon tail. NOGly inhibits GlyT2 (Carland *et al.*, 2013) with a lower level of maximal inhibition than NAGly, which plateaus at concentrations below its CMC, suggesting that the partial inhibition is a reflection of how the lipid binds to the transporter.

Similarly, an endogenous acylcarnitine, oleoyl L-carnitine (OLCarn) inhibits GlyT2 (IC₅₀ 340 nM, Carland *et al.*, 2013). Two additional compounds containing the L-carnitine head group with tails of differing length and degree of saturation (Figure 1.6B), palmitoyl-L-carnitine and lauroyl-L-carnitine inhibit GlyT2 with IC₅₀ values of 600 nM and > 10 μM respectively (Carland *et al.*, 2013). Unlike the glycine conjugated inhibitors which were fully reversible 5 minutes after inhibition, OLCarn is very slowly reversible, with glycine currents not restored in the time frame of the assay (Carland *et al.*, 2013). The reversibility of OLCarn can be accelerated by

adding bovine serum albumin or the lipid extruding compound β -cyclodextrin, which suggests that OLCarn may inhibit GlyT2 by binding within a membrane exposed site.

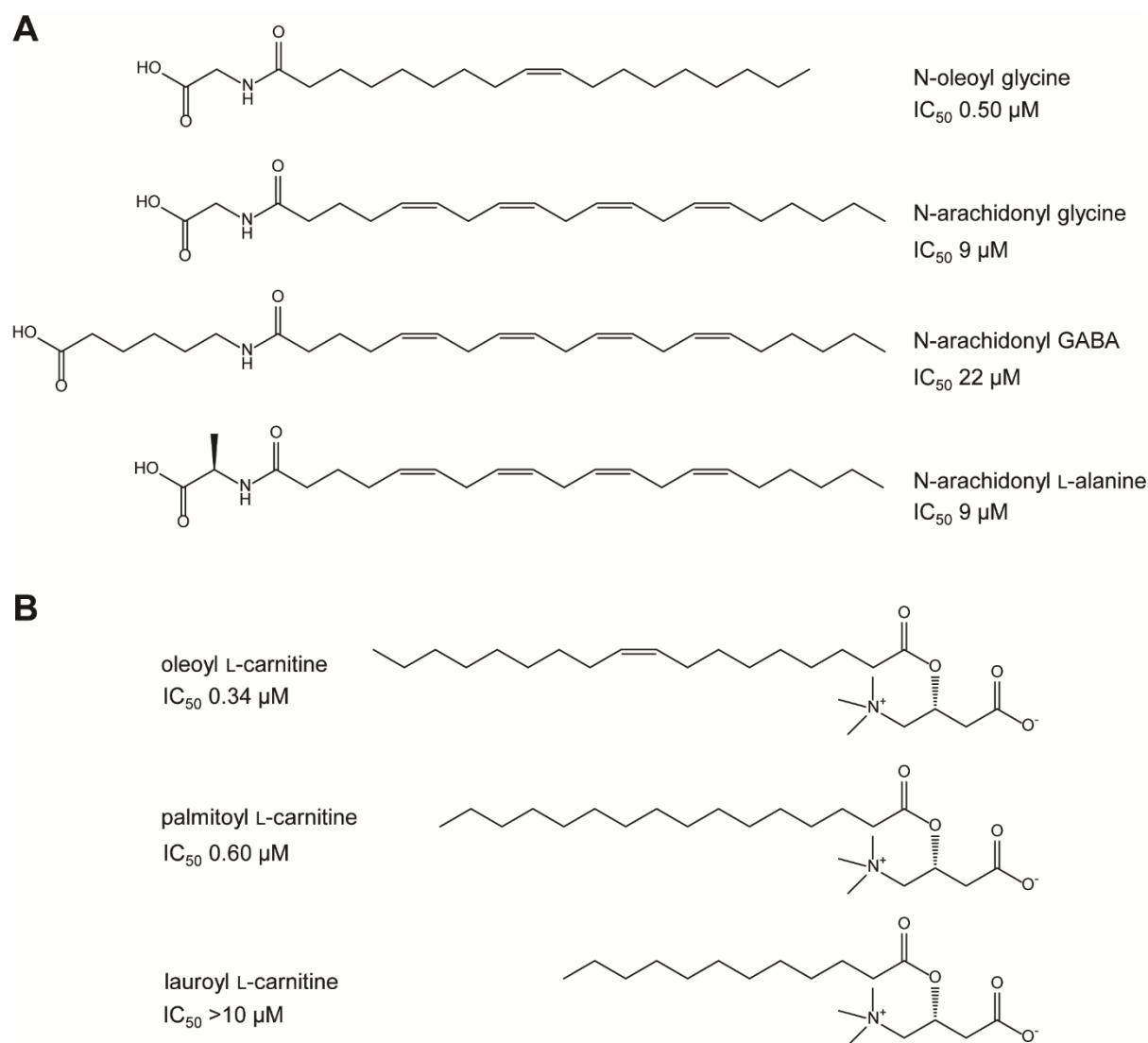


Figure 1.6. Structures of known A. glycine conjugated and B. carnitine conjugated GlyT2 lipid inhibitors.

Bioactive lipid inhibitors of GlyT2 are amphiphilic; comprised of a long flexible lipid tail and a polar head group. It has been demonstrated that both the head and tail group are important in conferring activity of these compounds (Carland *et al.*, 2013, Wiles *et al.*, 2006), though little is known about the molecular interactions with their target. A comprehensive structure activity relationship of these compounds is also yet to be understood.

1.6 Molecular basis for lipid inhibition of GlyT2

Unlike other known inhibitors of GlyT2, which likely bind their bulky aromatic groups within the central cavity of GlyT2, lipid inhibitors are non-competitive (Wiles *et al.*, 2006) and thought to act at an allosteric site. Previous studies using site-directed mutagenesis and chimeric GlyT1/GlyT2 transporters have revealed that extracellular loop 4 (EL4) plays an important role in the mechanism of inhibition by both glycine- and carnitine- conjugated lipid inhibitors (Edington *et al.*, 2009; Carland *et al.*, 2013), though the binding site has not been elucidated. No structures of the glycine transporter are available, and so crystal structures of homologues are utilised to understand the important conformational changes required for transport of glycine by GlyT2.

GlyT2 belongs to the neurotransmitter sodium symporters (NSS) or SLC6 family of transporters, which are secondary active transporters that exploit the Na⁺ gradient to drive transport of amino acid and amino acid derivatives across cell membranes (Kristensen *et al.*, 2011). In addition to glycine transporters, members of this family include transporters for serotonin, dopamine, noradrenalin, and GABA. To date, crystal structures of the bacterial leucine transporter, LeuT_{Aa} (Krishnamurthy & Gouaux, 2012; Yamashita *et al.*, 2005); the *Drosophila melanogaster* dopamine transporter, dDAT (Penmatsa *et al.*, 2013, 2015; Wang *et al.*, 2015); and the human serotonin transporter, hSERT (Coleman *et al.*, 2016), have been resolved in a number of conformations and either, apo, substrate or inhibitor bound.

1.6.1 Structures of the bacterial homologue LeuT

LeuT_{Aa} (herein referred to as LeuT) is a bacterial leucine transporter from *Aquifex aeolicus* with homology to the NSS transporter family and shares ~20% amino acid identity with the glycine transporters. LeuT is well characterised and has been crystallised in a number of conformations; outward-facing, outward-facing with substrate bound (Yamashita *et al.*, 2005), and inward-facing (Krishnamurthy & Gouaux, 2012) conformations which have been used to model the movement of LeuT through different stages of the transport cycle (Figure 1.7,

Krishnamurthy & Gouaux, 2012) (Chen & Chung, 2015; Forrest *et al.*, 2008; Kazmier *et al.*, 2014; Penmatsa & Gouaux, 2014).

LeuT contains twelve α -helical transmembrane (TM) domains oriented by a pseudosymmetrical axis whereby the first five transmembrane helices (TM1-5) mirror the second five helices (TM6-10) (Forrest *et al.*, 2008). Two pairs of helices, TM1 and 6, and TM3 and 8, form the core of the transporter and hold the leucine binding site and coordinate two Na^+ ions for co-transport (Krishnamurthy *et al.*, 2009). These sites are conserved in GlyT1 and GlyT2 (Vandenberg *et al.*, 2007), with GlyT2 containing a third Na^+ binding site located on the intracellular half of the transporter (Subramanian *et al.*, 2016).

The leucine binding site is dehydrated during transport, employing a conserved salt bridge between R30 (TM1) and D404 (TM10) (Figure 1.7) to reinforce the extracellular hydrophobic vestibule, and a thick intracellular gate comprising a complex hydrogen bond network and salt bridge to occlude water (Yamashita *et al.*, 2005). The disruption and creation of these bonds generates significant structural changes which enable LeuT to oscillate between the outward facing and inward facing conformations (Forrest *et al.*, 2008; Tavoulari *et al.*, 2016), consistent with the alternating access mechanism of transport.

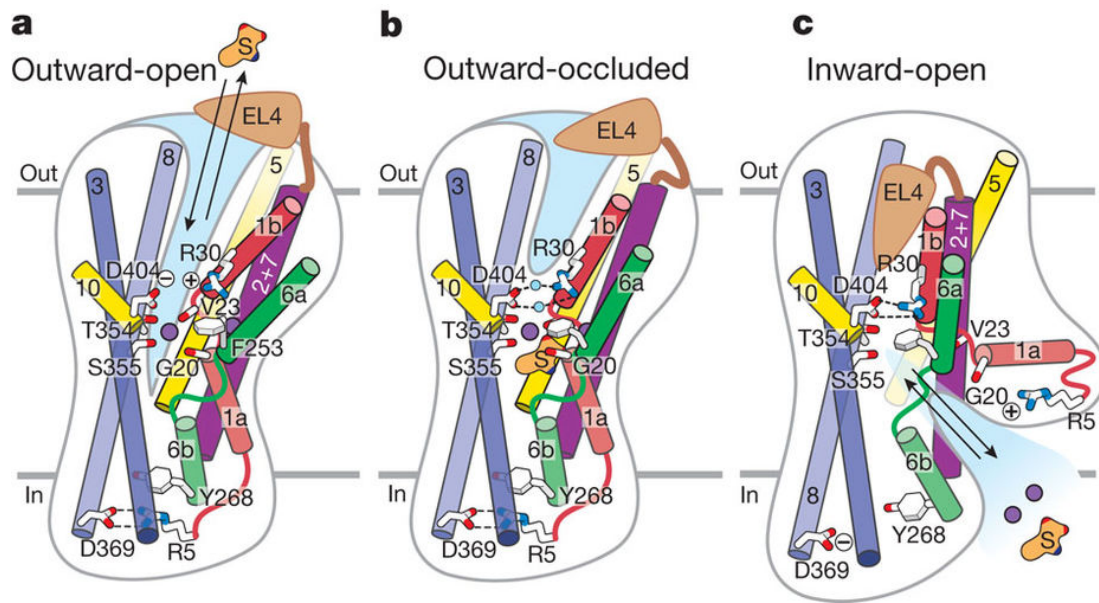


Figure 1.7. Schematic of transport in LeuT. Shown are structural elements and gating residues instrumental to conformational changes associated with the transition from the outward-open (a) to the outward-occluded state (b), and the inward-open state (c) (Krishnamurthy & Gouaux, 2012).

In the outward-facing conformation, LeuT allows leucine and two Na⁺ ions to bind resulting in the movement of the extracellular loop EL4 into the extracellular facing hydrophobic vestibule (Figure 1.7a). EL4 packs adjacent to TM1b, TM3, TM7 and TM8, closing the extracellular gate and preventing release of the substrate into the extracellular space (Figure 7b). Unwound regions of TM1 and TM6 form hinge domains, permitting their intracellular halves to swing outward and expel leucine into the cytoplasm (Figure 7c, Krishnamurthy & Gouaux, 2012).

1.6.2 Structures of the dopamine and serotonin transporters

More recently, outward-open crystal structures of the related dDAT (Penmatsa *et al.*, 2013, 2015; Wang *et al.*, 2015) and hSERT (Coleman *et al.*, 2016) have been determined from *Drosophila melanogaster* and humans respectively. dDAT and hSERT are comprised of twelve TM helices which are pseudosymmetrically oriented, resembling the structure of LeuT. Substrates or inhibitors were observed bound in the primary substrate-binding cavity, with two

Na⁺ ions resolved in the same Na1 and Na2 sites as LeuT, and the co-transported Cl⁻ ion coordinated by residues in TM2, TM6, and TM7 of dDAT (Penmatsa *et al.*, 2013).

Superimposition of dDAT and hSERT show a low (0.5 Å) root mean square deviation (RMSD) between core helices which coordinate substrate and ions; and conformational variation between TMs 9-12 as well as the flexible termini and extracellular loops EL2 and EL4 (Figure 1.8, Coleman *et al.*, 2016). The binding of substrates and inhibitors at dDAT and hSERT closely resemble that of LeuT, which suggests a common mechanism of transport for transporters with a LeuT-like fold.

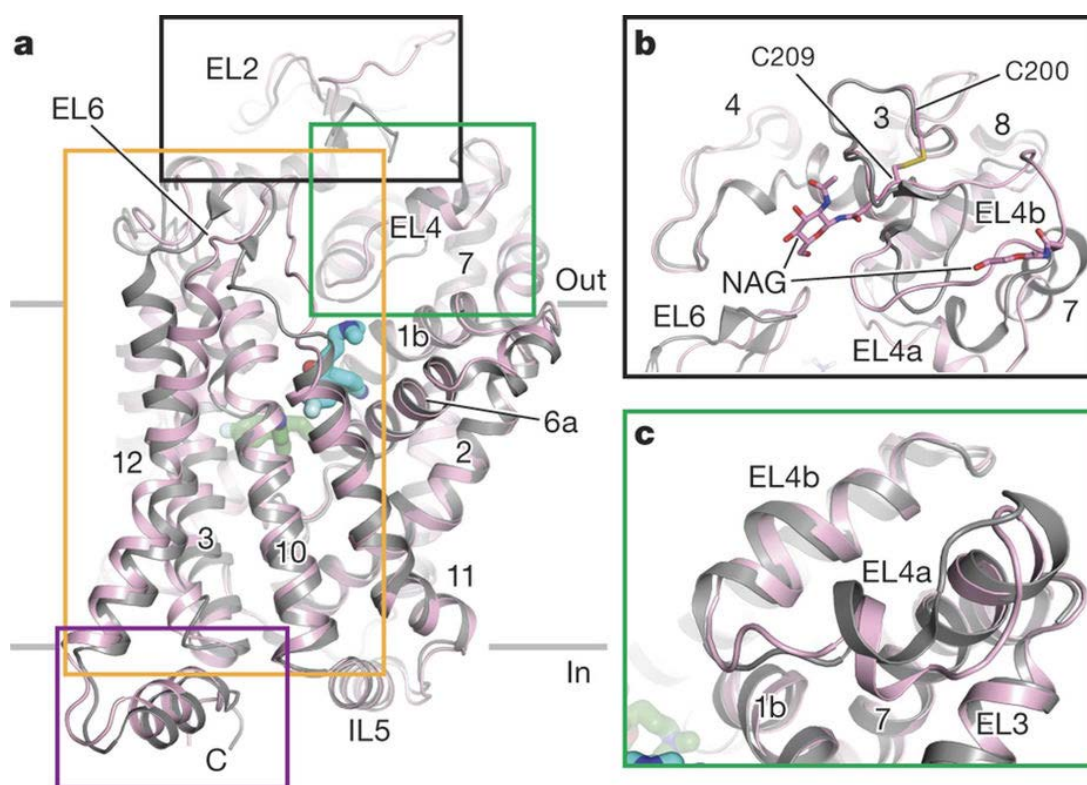


Figure 1.8. Alignment of SERT (pink) versus dDAT (grey) **a**, Overall alignment with TM1-TM12; regions in SERT with structural differences are boxed. (S)-citalopram bound to the central (green) and allosteric (cyan) sites shown as sticks. **b**, Close up view of EL2, N-acetylglucosamine (NAG; SERT) and the disulfide bridge between Cys200 and Cys209 are shown as sticks. **c**, View of EL4 (adapted from Coleman *et al.*, 2016).

1.6.3 GlyT2 homology model

GlyT2 is also predicted to possess the LeuT-like fold common among NSS transporters, and shares 50% sequence identity with dDAT. A homology model of GlyT2 was produced (Figure 1.9, Subramanian *et al.*, 2016) using protein fold recognition, where the amino acid sequence of GlyT2 was threaded onto the outward-occluded dDAT structure (4M48; Penmatsa *et al.*, 2013). Secondary structure predictions were used to increase accuracy of the sequence alignment, with a large unstructured region of EL2 (residues W315-Q362), N-terminus and C-terminus removed from the model. Unrestrained molecular dynamic (MD) simulations were run for 50 ns (Subramanian *et al.*, 2016) and the resulting RMSD was within expected thermal fluctuations (backbone RMSD 1.37 Å). Furthermore, the glycine substrate and Na⁺ ions remain coordinated by residues throughout simulations, suggesting the GlyT2 model is stable.

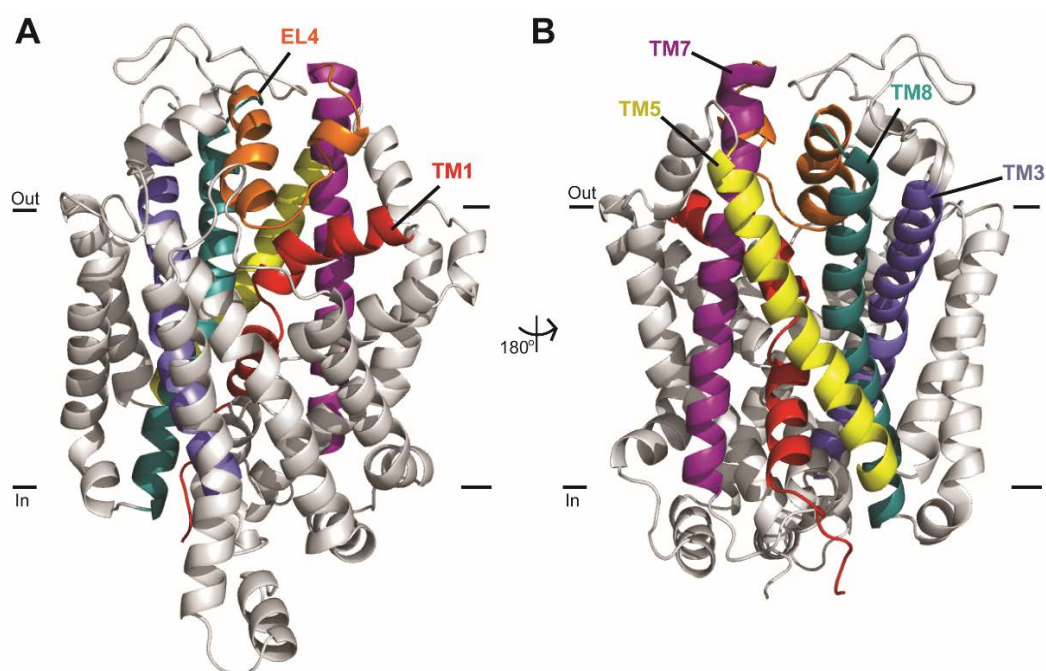


Figure 1.9. Homology model of GlyT2 shown in plane of the membrane **A.** front face and **B.** reverse face. Important helices and loops are coloured, EL4 (orange), TM1 (red), TM3 (blue), TM5 (yellow), TM7 (purple), and TM8 (teal). Model is based on outward-occluded dDAT (PDB: 4M48) using a protein fold recognition (or threading) approach. Model created by Nandhitha Subramanian.

This model has been used to identify a novel third Na⁺ binding site (Na₃) in GlyT2 which is coordinated by residues in TM3 (W263, M276), TM6 (A481), and TM10 (E648) (Subramanian *et al.*, 2016). Additionally, the specificity of the GlyT2 substrate binding site has been explored using functional data and MD using this model, which shows the primary binding site of GlyT2 is unable to accommodate any other amino acids but the smallest amino acid, glycine (Carland *et al.*, 2018). Simulations of GlyT2 are conducted in a typical 1-palmitoyl-2-oleoyl-*sn*-glycero-3-phosphocholine (POPC) bilayer with 20% cholesterol to mimic the mammalian neuronal cell membrane.

1.7 Lipid interactions with membrane proteins

1.7.1 Living in the membrane environment

The mammalian cell is compartmentalised by a lipid bilayer which acts to separate the chemistry of each cell from the external environment. Glycerophospholipids comprise majority of the mammalian cell membrane with the most abundant lipid, phosphatidylcholine, composing ~50%, and the remainder contributed by other phospholipids, sphingolipids, and accessory lipids such as cholesterol and cardiolipin (van Meer *et al.*, 2008). Phospholipids are amphipathic molecules which self-assemble into a bilayer with their fatty acyl chains extending towards each other and their polar head groups facing the aqueous space. The final composition of the membrane can influence membrane curvature, liquid:gel phases, and can accommodate membrane proteins and modulate their activity.

Interactions between proteins and lipid membranes range from non-selective annular lipid contacts which encircle a membrane protein, to highly selective lipid binding essential for function (Landreh *et al.*, 2016). However, there are challenges in observing proteins in a more native, membrane-dissolved state, which has limited our understanding. The bacterial aquaporin has been crystallised at 1.9 Å with a full band of annular membrane lipids surrounding the protein (Gonen *et al.*, 2005). Flexible acyl tails were observed to contour around the gaps and grooves of the protein structure, but did not occupy any tight lipid binding

sites, which suggests that this structure is a typical representation of how membrane lipids may interact with their protein residents. Furthermore, MD studies of this protein structure in a dimyristoyl-phosphocholine bilayer, shows constant exchange of membrane lipids for these protein grooves, and that the acyl tails governed the positioning of lipids around the channel, but that aquaporin did not possess any specific phospholipid binding sites (Aponte-Santamaria *et al.*, 2012). Despite this, protein mobility greatly influenced the localisation of lipids around aquaporin which suggests that even non-selective lipid interactions may be significant for functioning of membrane proteins.

Both proteins and lipids undergo structural changes with respect to each other which can affect their organisation within membranes. In particular, hydrophobic matching to minimise hydrophobic areas of a protein exposed to the aqueous environment is a strong driver of lipid-protein dynamics (Harroun *et al.*, 1999a, 1999b). Often hydrophobic portions of transmembrane helices do not match up with typical membrane thickness (30 Å, van Meer, 2008). This hydrophobic mismatch can change between different protein conformations, and therefore a membrane must be dynamic when accommodating a flexible protein, as in the case of a transporter moving through the different conformations of a transport cycle. LeuT has been crystallised in a number of conformations which represent movements from an outward-open to an inward-open state (Yamashita *et al.*, 2005; Krishnamurthy & Gouaux 2012). Continuum MD allows the energetics of hydrophobic mismatch to be quantified in an elastic membrane, and has been used to monitor LeuT in a phospholipid membrane (Mondal *et al.*, 2013). Differences in hydrophobic mismatch for different conformations of LeuT were observed, in addition to significant membrane thinning and water penetration near a membrane exposed, positively charged residue, K288 (Mondal *et al.*, 2013). Neutralisation of this residue (K288A) yields a faster transporter, likely as a direct consequence of removing unfavourable interactions between K288 and the membrane. Exposure to the lipid environment can either be favourable or unfavourable, and is clearly functionally relevant for the conformational changes required for membrane proteins.

One way to increase membrane protein stability is to form oligomeric interactions with other transmembrane subunits; the majority of membrane proteins are organised into higher order oligomers within the membrane environment. The role membrane lipids may have in stabilising oligomers has also been investigated using mass spectrometry to observe membrane proteins with a predicted weak oligomerisation interface (Gupta *et al.*, 2017). LeuT for example, contains no salt bridges and little buried surface to drive oligomerisation, yet the mass spectrum of LeuT liberated from octylglucoside micelles shows a peak which corresponds to dimer formation (Gupta *et al.*, 2017). In the absence of cardiolipin, however, LeuT forms a delipidated monomer, which suggests that dimerization between LeuT monomers is facilitated by cardiolipin “glue”, which can be knocked out using mutagenesis of the proposed interface.

BetP is a trimeric betaine transporter from *Corynebacterium glutamicum*, with the same structural fold as LeuT (Koshy *et al.*, 2013). The crystal structure of BetP at 2.7 Å revealed 8 1-palmitoyl-2-oleoyl-*sn*-glycero-3-phosphoglycerol (POPG) lipids, 5 of which were non-annular, resolved with the transporter. Many of these lipids were observed in the centre of the trimer and are thought to mediate oligomeric interactions. Additionally, the areas of the transporter in close contact with the lipids are areas of BetP which undergo considerable conformational changes for transport. The negatively charged head groups of POPG are closely interacting with loops important for gating (Koshy *et al.*, 2013), and it is proposed that POPG may be a regulatory mechanism to control gating. This has since been supported through infrared spectroscopy of BetP reconstituted in two-dimensional crystals of negatively charged lipids (Güler *et al.*, 2016).

Other lipid molecules have also been proposed to modulate proteins via distinct interactions. The first crystal structure of the dopamine transporter, dDAT, revealed a cholesterol molecule coordinated in a membrane exposed cleft between TM1a, TM5, and TM7 (Figure 1.10, Penmatsa *et al.*, 2013). The binding site of this cholesterol is comprised of largely branched aliphatic residues, which are conserved among many NSS transporters. Superimposition of the dDAT structure with the inward-open structure of LeuT reveals a potential regulatory

mechanism for cholesterol. For LeuT to enter the inward-open conformation and for substrate to be released, TM1a must shift into the membrane in the space occupied by cholesterol in the dDAT structure. Cholesterol may thus be an endogenous modulator of the dopamine transporter, favouring the outward-open conformation and preventing substrate release into the intracellular space. Increasing cholesterol content in membranes increases binding of cocaine analogues, which enter the central binding cavity in the outward-facing conformation (Hong & Amara, 2010). It has also recently been shown that cholesterol binding to the site identified in the dDAT structure inhibits the transition to an inward-facing conformation, for hDAT, hSERT, and the human noradrenalin transporter (Zeppelin *et al.*, 2018). This specific cholesterol binding site may therefore be functionally relevant and conserved among the family.

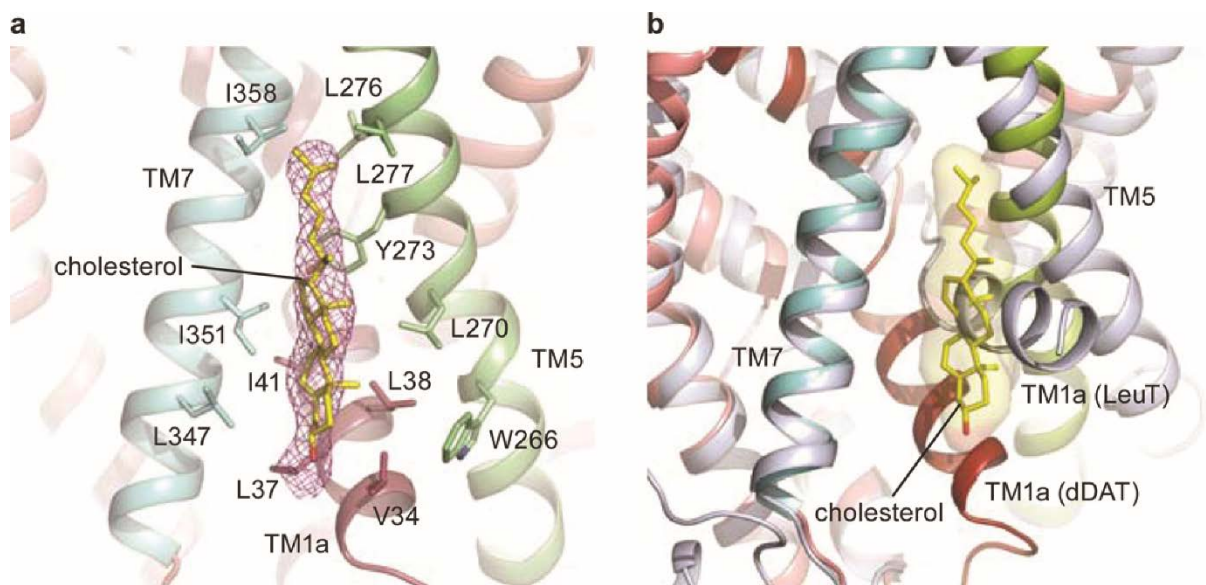


Figure 1.10. Cholesterol binding site of the dopamine transporter dDAT. Cholesterol (yellow sticks) is bound in a cleft between TM1a, TM5, and TM7. **a.** Binding site; residues that coordinate cholesterol are labelled and shown as sticks **b.** dDAT (coloured cartoon) superimposed with LeuT (grey cartoon) showing the relative movements of TM1a (Penmatsa *et al.*, 2013).

While structural visualisation of membrane proteins in their native state remains challenging, it is clear that the membrane environment influences function, and is not merely a solvent for hydrophobic proteins. Emerging techniques such as cryo-electron microscopy (cryo-EM) of membrane proteins in nanodiscs (Efremov *et al.*, 2017), detergent-free protein purification using styrene maleic acid polymers (Scheidelaar *et al.*, 2015), and mass spectroscopy of membrane proteins liberated directly from lipid environments (Laganowsky *et al.*, 2013), may provide more detailed and accurate information on membrane proteins and lipid interactions.

1.7.2 Lipid ligands of membrane proteins

In addition to protein interactions with the membrane environment, lipids have also been demonstrated to be endogenous ligands of a number of membrane proteins. Cannabinoid receptors (CB₁ and CB₂), the lysophosphatidic acid receptor (LPA), and the sphingosine-1-phosphate receptor (S1P₁) are members of the G protein-coupled receptor superfamily, which contain seven TM domains (Chrencik *et al.*, 2015; Hanson *et al.*, 2012; Hua *et al.*, 2016; Taniguchi *et al.*, 2017) and share moderate sequence identity, particularly around the membrane exposed TM helices. Each of these receptors are activated by lipid molecules with either a negatively charged, or neutral, head group conjugated to a long flexible acyl tail (Shimizu, 2009). These agonists contain similar features to the lipid inhibitors of GlyT₂, with endogenous cannabinoids containing a polyunsaturated C₂₀ tail similar to NAGly, and lysophosphatidic acid containing a monounsaturated C₁₈ tail similar to NOGly. Crystal structures of G-protein coupled receptors, with molecular dynamics and modelling of endogenous substrates, can help to infer the mechanism of their lipid ligands and provide insight into lipid-protein binding.

Arachidonylethanolamide (anandamide) and 2-arachidonoyl glycerol (2-AG) are the endogenous agonists of the cannabinoid receptors (Luchicchi & Pistis, 2012). They are highly lipophilic and therefore likely to exist within the membrane, where it has been hypothesised that they may access the binding site of CB receptors (Pei *et al.*, 2008). Nuclear magnetic

resonance (NMR) spectroscopy of anandamide in a dipalmitoylphosphatidylcholine membrane reveals that although it could exist in a number of conformations, anandamide prefers to adopt an extended conformation within the membrane, with its head group next to neighbouring dipalmitoylphosphatidylcholine head groups and the terminal methyl adjacent to the terminal methyl of the phospholipid acyl chain (Tian *et al.*, 2005). Molecular dynamics of 2-AG binding to CB₂ in a POPC bilayer observe the 2-AG lipid first associating with the membrane phospholipids, followed by migration of 2-AG to interact with the CB₂ receptor (Hurst *et al.*, 2010). 2-AG then enters the ligand binding site by moving through an opening between membrane exposed helices TM6 and TM7. Furthermore, the recent crystal structure of the inactive human CB₁ receptor shows the synthetic antagonist, AM6538, bound in a membrane exposed pocket with its aliphatic chain substituted phenyl ring extending into a long hydrophobic channel of the receptor (Hua *et al.*, 2016). Subsequent molecular docking of anandamide and 2-AG also show hydrophobic residues in TM2, TM3, TM6, and TM7 interacting with the hydrophobic acyl tails in the predicted final binding site of these endogenous lipids.

Similarly, the S1P₁ structure bound to the sphingolipid mimic antagonist, ML056, reveals a highly amphipathic binding pocket which can accommodate the zwitterionic head group, and long acyl chain of spingosine-1-phosphate (Hanson *et al.*, 2012). This binding site is occluded by an extracellular helical cap (Figure 1.11; Hanson *et al.*, 2012) which suggests this site is not aqueously accessible. Instead, it is proposed that ligands enter laterally through a membrane exposed opening between helices TM1 and TM7.

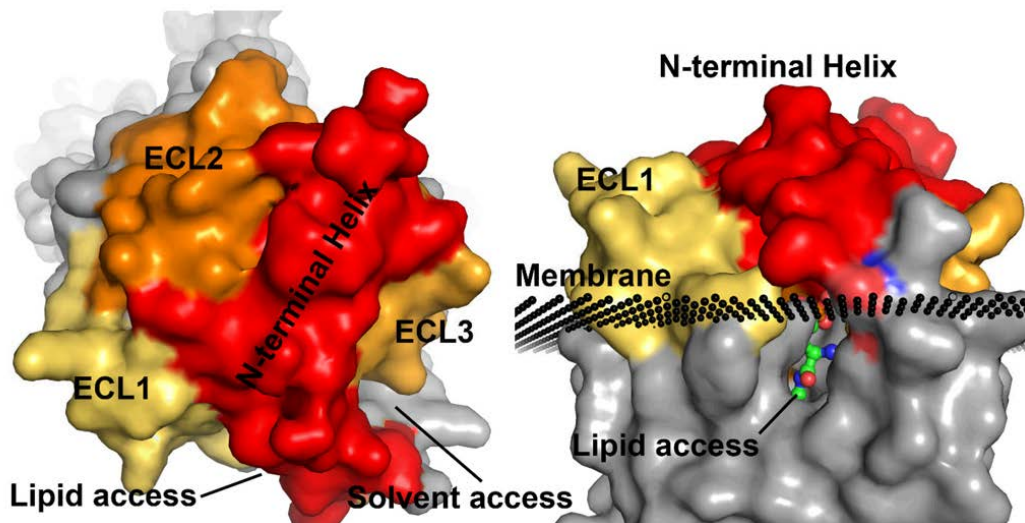


Figure 1.11. Surface rendering of the sphingosine-1-phosphate crystal structure. Top-down view showing the binding pocket occluded by the helical cap formed by extracellular loops ECL1, ECL2, ECL3 and the N-terminal helix. Side view showing the opening between membrane helices I and VII which may provide an access point through the lipid membrane (adapted from Hanson *et al.*, 2012).

Endogenous substrates of the free fatty acid receptor are saturated C12-C16 or unsaturated C18-C20 fatty acids, which act as full agonists (Kotarsky *et al.*, 2003). In a crystal structure of the free fatty acid receptor, the partial agonist, TAK-875, is shown bound between helices 3 and 4 whilst the substituted benzyl ring protrudes into the membrane (Srivastava *et al.*, 2014). TAK-875 additionally possesses a ~ 380 -fold preference for the lipophilic phase over the aqueous phase which suggests that it partitions into the lipid bilayer before interacting with free fatty acid receptor. It is notable that this site differs from the pocket observed for other GPCRs, and that access through helices via the membrane may be a ubiquitous pathway for lipid ligands.

Transporters have also been identified to bind and transport lipids. The diversity of inner and outer membrane leaflets is maintained with unidirectional flippases, bidirectional scramblases, or phospholipid transporters (Montigny *et al.*, 2016). Similarly, some bacteria utilise flippases

to transport bulky lipid molecules from their inner membrane, to the outer leaflet of the outer membrane (Mi *et al.*, 2017). Translocation of lipids is often against a steep gradient and requires energetic coupling to either ATP hydrolysis or the transport of ions (Montigny *et al.*, 2016). Flippases and scramblases have very large phospholipid or lipopolysaccharide substrates which must be accommodated by large, flexible binding pockets and may provide insight into dynamic interactions of lipids with membrane proteins.

For the bacterial lipopolysaccharide transporter, MsbA, a potential mechanism of flipping was postulated using cryo-EM structures bound to lipopolysaccharide and lipid A (Mi *et al.*, 2017). In this model, the lipid is trapped in the inner core with the acyl chains accommodated by a large hydrophobic pocket before being flipped to the outer membrane. Conversely, for the scramblase-Ca²⁺ activated Cl⁻ channel TMEM16, a different flipping mechanism was proposed where the head group traverses the membrane through a membrane exposed protein cavity while the acyl tails make contact with the bilayer (Brunner *et al.*, 2014). In both cases, however, the lipids make contact with the membrane at some point during the transport cycle.

In addition to endogenous substrates, lipids can also allosterically bind to specific sites on membrane proteins. Arachidonic acid has been observed to have a wide range of effects on ion channels, for example stimulating the inwardly rectifying K⁺ channel, Kir1.3 (Liu *et al.*, 2001), but inhibiting the voltage gated K⁺ channel, Kv1.5 (Bai *et al.*, 2015). Arachidonic acid is also selective for Kir2.3 but has no activity on Kir2.1, Kir2.2, or Kir2.4; chimeras between subtypes show it directly interacts with transmembrane domains and is not simply disrupting the membrane to produce non-specific effects (Liu *et al.*, 2001). The binding site of arachidonic acid on Kv1.5 has been mapped using site-directed mutagenesis and docking and reveals a site comprised of charged or polar residues interacting with the head, and a large number of branched aliphatic residues forming the tail binding site (Bai *et al.*, 2015).

It appears that for most lipid ligands of membrane proteins they must interact with both protein and lipid membrane, either navigating the bilayer to access their binding site, or binding at a

position that is comprised of both membrane and protein. Between receptors, transporters, and channels there are conserved features of lipid binding sites; where the acyl tails fit in a large hydrophobic cavity comprised of branched aliphatic residues; and charged or polar amino acids forming the head group binding site. Despite the flexibility and large range of substrates, there are commonalities between known membrane-protein interactions which may provide insight into the mechanisms of lipid inhibition of glycine transporters.

1.8 Development of lipids as drugs

Drug discovery and development are often seen as being incompatible with lipids as they do not fit the guidelines for drug-likeness as defined by Lipinski's rules, where permeability and absorption are optimal (for example; $\log P < 5$; no more than 5 hydrogen bond donors; and a preference for small molecules with a molecular weight < 500) (Lipinski *et al.*, 1997). Additionally, lipids are abundantly present in cell membranes and possess roles as non-specific signalling molecules, which often cause them to be overlooked for development as targeted therapies.

Fingolimod is an orally available, first-in-class therapy to treat multiple sclerosis, which when phosphorylated *in vivo*, resembles sphingosine-1-phosphate and modulates four of the S1P receptors (Brinkmann *et al.*, 2010). Fingolimod is able to traverse the BBB to accumulate in the CNS (Hunter *et al.*, 2016). While fingolimod must then be phosphorylated to become active on central receptors, it is clear that the development of orally-available, lipid-based drugs is not unfeasible.

CNS drugs must negotiate the BBB, either via passive diffusion (such as fingolimod) or through carrier mediated transport. For charged compounds, passage across the BBB occurs via active transport. ABC transporters, such as p-glycoprotein, and the breast cancer resistance protein can regulate the transport of a wide range of large, diverse species across the BBB (Uchida *et al.*, 2011) and are known to participate in the flux of a number of CNS drugs. Organic cation and organic anion transporters are expressed in high amounts in the

human BBB (Uchida *et al.*, 2011). Organic cation transporter 1 transports cationic compounds such as tetraethylammonium, and verapamil, while the high affinity Organic cation transporter 2 transports zwitterionic carnitine (Yabuuchi *et al.*, 1999) and has been shown to be important for acetyl-L-carnitine transport across the BBB (Inano *et al.*, 2003).

Anandamide is normally synthesised in the brain but has been shown to cross the BBB via a saturable uptake system (Maccarrone *et al.*, 2005). Uptake is proposed to be via an endocannabinoid membrane transporter, which may provide a pathway for lipid ligands to rapidly accumulate. This transport system has not been identified and there remains some controversy as to its existence (Fowler, 2013); passive diffusion of uncharged anandamide is likely to contribute to BBB accumulation to some degree.

Fatty acid transport into the brain is necessary to supply components for cell membranes and lipid precursors for fatty acids that cannot be synthesised in the brain. Fatty acid transport proteins, fatty acid binding proteins, and fatty acid translocase have been shown to be essential in the transport of long chain fatty acids across the BBB (Mitchell *et al.*, 2011). There are many routes of passage for lipids into the CNS which may facilitate the movement of lipid-based drugs.

In addition to acyl-carnitines, acyl-glycines, endocannabinoids, and other lipid signalling molecules, there are believed to be a number of other bioactive lipids whose roles have not yet been elucidated. In 2010, a group began to identify the large number of endogenous lipids using nano-high performance liquid chromatography-tandem mass spectrometry, to identify and quantify acyl amino acids in the rat brain and bovine spinal cord (Tan *et al.*, 2010). Tan and colleagues, identified 50 novel acyl amino acids with glutamic acid, serine, and palmitoyl conjugated compounds being most abundant. It was suggested the isolated species may reflect the populations of amino acids or precursor lipids available for synthesis in the brain.

Lipids in the brain are also metabolised and recycled by a number of enzymes, including fatty acid amide hydrolase (FAAH) and cyclooxygenase (COX). FAAH inactivates fatty acid amide

compounds through hydrolysis of the L- amide bond and has been shown to have activity at anandamide and oleamide, converting each to arachidonic acid and oleic acid respectively (Cravatt *et al.*, 1996). While FAAH is able to inactive head groups, tails can be metabolised through β -oxidation of the double bond, or cyclisation of the tail, for example COX-2 inactivation of anandamide and NAGly (Prusakiewicz *et al.*, 2002; Yu *et al.*, 1997). Lipid compounds containing natural amino acids and unsaturated acyl tails have multiple routes of degradation which will need to be considered when designing lipid-based therapeutics.

Thesis objectives

It is becoming increasingly apparent that lipids interact with membrane proteins through both non selective annular contacts and through specific binding sites, where they are able to greatly influence protein structure and function. While much is known about lipid ligand binding to G-protein coupled receptors, for transporters with the LeuT-like fold the extent that lipid interactions may impact function has only recently begun to be understood in depth. These interactions involve lipids within the natural membrane environment, whereas it is also known that the endogenous signalling lipid, NAGly, is able to bind to and inhibit the glycine transporter, GlyT2. The aims of this thesis were thus to elucidate important interactions that a group of synthesised acyl amino acid analogues have with GlyT2, and to describe the characteristics of these compounds for their use as specific, potent drugs in the treatment of chronic neuropathic pain.

Targeting GlyT2 has proven difficult as it possesses an essential role in the repackaging and recycling of glycine. Many GlyT2 inhibitors which have been developed, block this recycling by acting as full and/or irreversible inhibitors and produce severe side effects which mimic GlyT2 knockout and hyperekplexic phenotypes. The first aim of this thesis was to develop a library of lipid compounds with different head and tail groups that possess different inhibitory characteristics, as well as improving upon the potency of NAGly (IC_{50} 9 μ M). Using two-electrode voltage clamp electrophysiology and radiolabelled [3 H]-glycine uptake I sought to determine the relative affinities (IC_{50} values), maximal levels of inhibition, and reversibility of a number of lipid compounds which were synthesised for this study. The pharmacokinetic and *in vivo* characteristics for select compounds are also described.

A number of crystal structures of the bacterial homologue, LeuT, in different states have provided detail about different conformational transitions, which have since been described using biophysical techniques. EL4 is thought to undergo large conformational changes from the outward-open to the inward facing states and has also been shown to be important in the

mechanism of GlyT2 inhibition by NAGly. To further resolve the mechanism of inhibition, I created a number of GlyT2 mutations in regions that were either close to EL4 or also important in the mechanism of transport and may influence the way EL4 moves. Using site-directed mutagenesis and electrophysiology, I aimed to unearth molecular determinants for the binding of acyl amino acids and to further develop understanding of how these compounds can stall transport.

Chapter 2: Methods

2.1 Materials

N-arachidonyl glycine and N-oleoyl glycine were obtained from Sapphire Biosciences (NSW, Australia); and oleoyl L-carnitine was obtained from Larodan Fine Chemicals (Malmo, Sweden). All other N-acyl amino acids presented in this thesis were synthesised by Dr Tristan Rawling and Susan Shimmon at the University of Technology (Sydney, Australia). For compounds with typical acyl tails the fatty acid was obtained as a starting material, for example, oleic acid. To create compounds with non-commercially available monounsaturated fatty acids, the Wittig reaction was used to synthesise tails with different carbon lengths and double bonds, as previously described in Mostyn *et al.*, 2017. Amide bonds between the amino acid head group and fatty acid tail were formed using a peptide coupling reagent. All other chemicals were obtained from Sigma Aldrich (Sydney, Australia), unless otherwise stated.

2.2 Creation of wild type (WT) or mutant mRNA encoding glycine transporters

Human GlyT1b or GlyT2a (herein referred to as GlyT1 and GlyT2) cDNA were sub-cloned into the plasmid oocyte transcription vector (pOTV). Site directed mutagenesis was performed using the Q5 site-directed mutagenesis kit (New England Biolabs (Genesearch), Arundel, Australia) using oligonucleotide primers synthesised by Sigma Aldrich (Sydney, Australia). PCR products were then transformed into *E. coli* cells and pure plasmid DNA extracted using the Purelink Quick Plasmid Miniprep Kit (Invitrogen by Life Technologies, Löhne, Germany). Sequences were confirmed by the Australian Genome Research Facility (Sydney, Australia). WT and mutant plasmid DNA were linearised with *SpeI* (New England Biolabs (Genesearch) Arundel, Australia) and RNA transcribed by T7 RNA polymerase using the mMessageMachine kit (Ambion, TX, USA).

2.3 Harvesting and preparing oocytes

An all-female *Xenopus laevis* colony were housed in shared tanks of no more than 3 tank-mates, and kept at constant, comfortable conditions to maintain a healthy colony for year-round production of oocytes, and to maintain a high quality of life in accordance with the *Australian Code of Practice for the Care and Use of Animals for Scientific Purposes*. The colony was kept on a 12 hour light/12 hour dark light cycle, in tanks of filtered 18 °C de-chlorinated water, with water pH, hardness, nitrate levels, salinity, and O₂/CO₂ levels constantly monitored for water quality.

Oocytes were extracted from female *Xenopus laevis* frogs anaesthetised with 0.17% 3-aminobenzoic acid ethyl ester (tricaine). A small incision was made in the abdomen to extract a lobe of oocytes. Oocytes were detached from follicle cell containing lobes by digestion with 2 mg/mL collagenase A (Boehringer, Mannheim, Germany) at room temperature for 60-90 minutes.

Defolliculated stage V-VI oocytes were injected with 4.6 ng of cRNA encoding WT or mutant transporter (Drummond Nanoinject, Drummond Scientific Co., Broomall, PA, USA). The oocytes were stored at 16-18 °C for 2-5 days in ND96 solution (96 mM NaCl, 2 mM KCL, 1 mM MgCl₂, 1.8 mM CaCl₂, 5 mM HEPES, pH 7.55), supplemented with 2.5 mM sodium pyruvate, 0.5 mM theophylline, 50 µg/mL gentamicin and 100 µM/mL tetracycline until transporter expression levels were sufficient to measure transporter function.

2.4 Two electrode voltage clamp electrophysiology

Glycine transport by GlyT2 is coupled to 3 Na⁺ ions and 1 Cl⁻, which creates an electrogenic process that allows two electrode voltage clamp electrophysiology to be used to measure glycine transport (Figure 2.1). 2-5 days following injection, glycine transport currents were measured at -60 mV using Geneclamp 500 amplifier (Axon Instruments, Foster City, CA, USA) with a Powerlab 2/20 chart recorder (ADInstruments, Sydney, Australia) and chart software

(ADInstruments). All data was subsequently analysed using GraphPad Prism 7.02 (GraphPad Software, San Diego, CA).

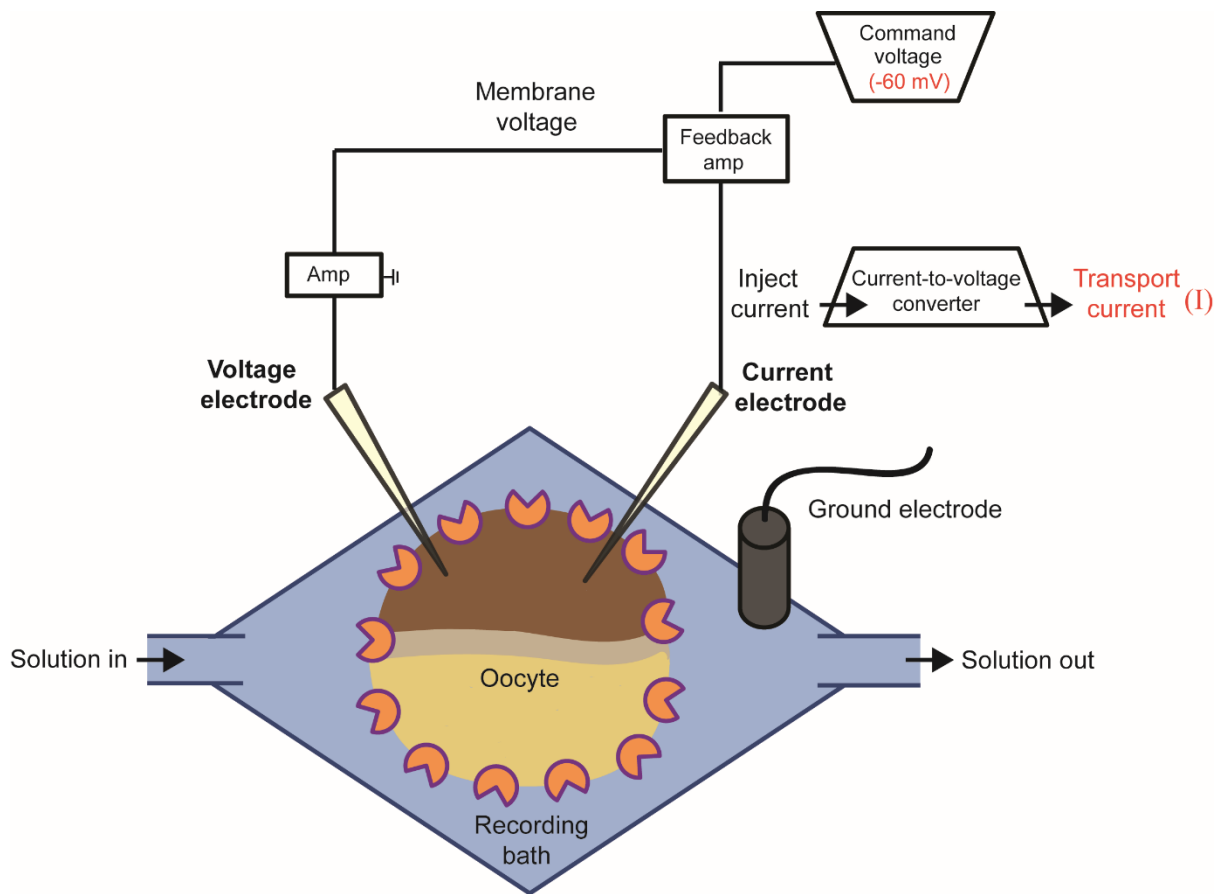


Figure 2.1. Setup of two-electrode voltage clamp electrophysiology. *Xenopus laevis* oocytes expressing GlyT2 (orange sectors) sit in a recording bath with ND96 (reference recording solution) penetrated by two Ag/AgCl₂ microelectrodes; the voltage electrode and the current electrode. The Ag/AgCl₂ ground electrode is placed in the recording bath and voltage and current electrodes referenced to the recording solution prior to setup. The voltage electrode measures membrane potential, and the amplifier “Amp” is compared to the set command voltage (-60 mV for GlyT2). Any differences are corrected by the “Feedback amp” and current is injected into the oocyte via the current electrode to adjust the membrane potential. Currents across the cell membrane are monitored using a current-to-voltage converter providing an amplified output of membrane current (I), indicative of glycine transport.

2.4.1 Glycine concentration responses

Initially, the function of each mutant transporter was tested by measuring glycine concentration dependent transport currents in ND96 (96 mM Na⁺) to drive transport. EC₅₀ values were determined using the modified Michaelis-Menten equation:

$$I = ([\text{Gly}] \cdot I_{\text{max}}) / (EC_{50} + [\text{Gly}]) \quad [\text{Equation 1}]$$

where I is current (nA), [Gly] is the concentration of glycine, I_{max} is the current generated by a maximal concentration of glycine (300 μM) and EC₅₀ is the concentration of glycine that generates a half maximal current. Values are presented as mean ± SEM obtained from n ≥ 3 cells from at least two batches of oocytes. To determine if mutations affected glycine transport, one way ANOVA tests were employed, with a Dunnett's post-hoc test used for comparison with WT GlyT2. For comparison with WT GlyT1 a two-tailed t-test was used. Statistical significance were represented as p < 0.05 *, p < 0.01 **, p < 0.001 *** etc. in the following figures.

2.4.2 Critical micelle concentrations of acyl amino acids

The synthesised lipids are amphipathic with a hydrophobic tail and a polar head group and have the propensity to spontaneously form micelles in solution at a characteristic critical micelle concentration (CMC). Thus, concentrations of lipids higher than the CMC may not freely diffuse to interact with proteins and thereby limit their biological activity. The CMC for OLCarn is approximately 7 μM (Carland *et al.*, 2013) and for NAGly is 100 μM (Wiles *et al.*, 2006). It's also similarly been shown that larger oleic based surfactants with an imidazole ring have a CMC of >10 μM (Bhadani *et al.*, 2017). For acyl-glycine compounds the maximum concentration used was limited to 30 μM. It should be noted that for NAGly, a true plateau of inhibition was not reached for concentrations below its CMC. Curve fitting of this partial concentration response predicts full inhibition at higher concentrations. In the case of NAGly, the solubility of the compound could be limiting the level of inhibition reached in both *in vitro*

and *in vivo* assays. For N-acyl amino acids with larger head groups, the maximum concentration used was limited to 3 μM for positively charged head groups or 10 μM for others.

2.4.3 Acyl inhibitor concentration responses

The majority of N-acyl amino acids are not immediately reversible, and thus inhibitor concentration responses were performed using cumulative application. The EC_{50} concentration of glycine was applied until a stable level of transport was reached. Increasing concentrations of N-acyl amino acid were then co-applied with glycine, with each concentration producing a distinct plateau in response. Currents at each of these plateaus were measured and compared to glycine currents in the absence of any inhibitor.

Inhibitor concentration responses were then fit by the method of least squares using:

$$Y = \text{Bottom} + (\text{Top} - \text{Bottom}) / (1 + 10^{(X - \text{LogIC}_{50})}) \quad [\text{Equation 2}]$$

where X is $\log[\text{acyl amino acid}]$ (μM), Y is current normalised to glycine in the absence of inhibitor and Top and Bottom are the maximal and minimal plateau responses respectively. This equation was constrained to have the bottom value > 0 , but not $= 0$, as to capture partial levels of inhibition, and the standard hill slope -1.0 . Concentration response curves were thus able to generate IC_{50} values as well as % maximum (max.) inhibition values.

IC_{50} values are presented as mean and 95% confidence intervals, and % max inhibition are presented as mean \pm SEM. Data are from $n \geq 3$ cells from at least two batches of oocytes. Where significant inhibition was not reached, the IC_{50} value is recorded as greater than the highest concentration of N-acyl amino acid used. For mutant inhibitor concentration responses, one way ANOVA tests with Dunnett's post-hoc tests for comparison with WT GlyT2 were performed, for both IC_{50} and % max. inhibition values, and presented as $p < 0.05$ *, $p < 0.01$ **, $p < 0.001$ *** etc. in Table 5.2.

2.4.4 Acyl inhibitor washout time course

In addition to apparent affinity and % max. inhibition, acyl inhibitors also possess a characteristic reversibility. Reversibility was determined by a washout time course using the IC_{50} concentration of each compound. Glycine (EC_{50}) was applied, followed by co-application of glycine and inhibitor until stable inhibition was reached. Application of inhibitor was ceased (time 0) and ND96 buffer was then perfused into the recording bath to wash the oocyte. At 5 minute intervals the EC_{50} concentration of glycine was reapplied to measure transport recovery. Recovery was expressed as I/I_{max} , where I_{max} is the current produced by glycine in the absence of inhibitor.

2.4.5 Oleoyl L-Lys competition assay

Glycine concentration responses were performed on oocytes expressing GlyT2 first in the absence of inhibitor, and then in the presence of 10 nM, 30 nM, or 1 μ M oleoyl L-Lys. Oleoyl L-Lys is not immediately reversible so glycine concentration responses were generated by first applying ND96 with oleoyl L-Lys for 2 minutes and then adding increasing concentrations of glycine and measuring the plateau response for each value. Currents were normalised to the I_{max} at the maximal glycine concentration (300 μ M) in the absence of inhibitor for each individual cell. EC_{50} values were determined using Equation 1. Data was then transformed using an Eadie-Hofstee plot. One way ANOVA analysis with Dunnett's post-hoc tests were performed for both EC_{50} and I_{max} values, and presented as $p < 0.05$ *, $p < 0.01$ **, $p < 0.001$ *** etc.

2.5 Radiolabelled uptake

2.5.1 [3 H]-Glycine uptake time course

Oocytes expressing GlyT2 as well as uninjected controls were pre-incubated with 3 μ M acyl-glycine lipids for 2 minutes, incubated with 10 μ M [3 H]-glycine for 0.5, 1, 2, 5, and 10 minutes, and then washed 3 times in ice cold ND96. Oocytes were then placed in 0.1 M NaOH for 30

minutes to lyse the oocytes. Scintillant was added, and the [³H] counted in a Trilux beta counter. The rate of uptake was estimated by fitting the linear portion of the time course to a straight line.

2.5.1 [³H]-Glycine uptake on oocytes expressing GlyT1 and GlyT2

Oocytes expressing GlyT2 or GlyT1 and uninjected controls were pre-incubated with 100 nM or 1 μM oleoyl L-Lys for 2 minutes at room temperature and then incubated with 10 μM [³H]-glycine for a further 2 minutes. Oocytes were then washed 3 times in ice cold ND96 and lysed with 0.1 M NaOH for 30 minutes. Scintillant was added to vials and the [³H] counted using a Trilux beta counter. Background [³H]-glycine uptake by uninjected controls was subtracted, and total counts were normalised to the uptake of [³H]-glycine by GlyT2 or GlyT1 in the absence of inhibitor.

2.6 Pharmacokinetics of oleoyl L-Lys and oleoyl D-Lys

The following experiments were conducted by the Centre for Drug Candidate Optimisation (CDCO) at Monash University (Victoria, Australia).

2.6.1 Stability in plasma and liver microsomes

Rat plasma or liver microsomes from male Sprague Dawley rats were spiked with solutions of either oleoyl L-Lys or oleoyl D-Lys. At various time points over the 240 minutes (plasma) or 60 minutes (liver microsome) incubation period, samples were taken and analysed using liquid chromatography mass spectrometry (LC/MS).

2.6.2 Blood brain barrier permeability

27.5 mg/kg oleoyl D-Lys was administered to male Sprague Dawley rats as a bolus injection into the peritoneal cavity at 5 mL/kg suspended in 10% (v/v) DMSO in 1% Solutol in 50 mM PBS 7.4. Plasma was collected before administration and then 1, 2, 4, 6, and 24 hr following administration. Standard calculations for each pharmacokinetic parameter are listed below.

$$t_{1/2} = \ln(2) / \lambda_z$$

Where $t = t_{1/2}$ is the elimination half-life and λ_z is the terminal elimination rate constant after intraperitoneal administration. AUC is the area under the plasma concentration versus time profile after IP administration, C_{max} is the maximum plasma concentration observed after IP administration, and T_{max} is the time to achieve C_{max} .

2.7 Analgesia testing in a partial nerve ligation model of pain

Male Sprague Dawley rats were anaesthetised, an incision was made at the approximate level of the sciatic nerve, and the nerve was exposed by blunt dissection. The sciatic nerve was isolated from the surrounding fascia, and approximately 1/3-1/2 of the dorsal nerve was ligated with a suture. The wound was closed and sensory signs of allodynia and hyperalgesia developed over 7-14 days. The Von Frey assay was used to measure nociception prior to surgery, after surgery, and at various time points following intraperitoneal injection of either 3 mg/kg (low dose) or 30 mg/kg (high dose) oleoyl D-Lys. Nylon filaments of varying diameters were applied to the rat's hindpaw, and paw withdrawal was observed at each condition. Analgesia experiments were carried out by Dr Sarasa Mohammadi (University of Sydney, Australia).

2.8 GlyT2 homology model and docking of lipid inhibitors

The GlyT2 homology model was created using the outward-occluded dopamine transporter structure from *Drosophila melanogaster* (dDAT) (PDB: 4M48) as a template using a threading approach implemented in the Phyre2 webserver. A sequence alignment of NSS transporters was performed, with GlyT2 sharing 50% identity with dDAT. The model was further refined using secondary structure prediction and alteration of protonation states of ionisable side chains. GlyT2 was then solvated and equilibrated in a POPC bilayer. After 41 nanoseconds of simulation, the representative structure of GlyT2 was obtained (methods described in further

detail in Subramanian *et al.*, 2016). The GlyT2 homology model was created by Dr Nandhitha Subramanian (Australian National University).

Docking of oleoyl D-Lys onto GlyT2 was performed using AutoDock Vina, a program that obtains energetically favourable binding conformations of a ligand by scoring binding conformations (scoring function and methods described in more detail in Trott & Olson, 2010). Majority of protein was static, while Ile545, Tyr550, Trp563, Pro561, Phe428, Leu569, and Phe515 residues were allowed to freely rotate about flexible bonds. Oleoyl D-Lys was also permitted to freely rotate. Docking simulations were performed by Mitchell Blyth (Australian National University).

Chapter 3: Characterisation of novel acyl-glycine inhibitors of GlyT2

The work presented in this chapter has been published in ACS Chemical Neuroscience. Mostyn SN, Carland JE, Shimmon S, Ryan R, Rawling T, Vandenberg RJ (2017) Synthesis and characterisation of novel acyl-glycine inhibitors of GlyT2, ACS Chemical Neuroscience, 8, 1949-1959

3.1 Introduction

N-arachidonyl glycine (NAGly) is an endogenous amino acid-conjugated lipid, derived from the well characterised bioactive lipid, anandamide. It is produced in its greatest quantities in the spinal cord, an important area for the dispatch of sensory signalling, and may have a role in the regulation of pain signalling. Intrathecal injection of NAGly has been shown to reduce mechanical allodynia and thermal hyperalgesia in rat models of both neuropathic and inflammatory chronic pain (Succar *et al.*, 2007; Vuong *et al.*, 2008). Furthermore, co-application of NAGly with CB₁ or CB₂ receptor antagonists does not disrupt the analgesic effects of NAGly which is consistent with early binding studies of anandamide derivatives that show NAGly has negligible activity at cannabinoid receptors (Sheskin *et al.*, 1997), which raises the question as to how NAGly mediates its analgesic activity. One possible mechanism of action is modulation of glycinergic neurotransmission. NAGly prolongs the time course of glycine in glycinergic synapses of lamina II of the superficial dorsal horn (Jeong *et al.*, 2010), an area responsible for integrating ascending pain information. It has been shown that NAGly inhibits the glycine transporter GlyT2, but has no effect on the closely related glycine transporter GlyT1 (Wiles *et al.*, 2006), which suggests that NAGly may exert analgesia by increasing inhibitory tone at glycinergic synapses.

GlyT2 is an essential protein; knock out of the GlyT2 gene in mice produces severe neuromotor symptoms and is lethal 2 weeks postnatal (Gomez *et al.*, 2003b). The consequences of this deletion are presynaptic in origin, which suggests GlyT2 plays a crucial role in maintaining the pool of glycine to be loaded into vesicles for exocytotic release.

ORG-25543 is a full and irreversible GlyT2 inhibitor which also exhibits an excitotoxic phenotype that may mimic GlyT2 knock out effects, and is likely a result of disrupted vesicle filling and therefore a decrease in glycine in the synapse in the long term (Mingorance-Le Meur *et al.*, 2013; Vandenberg *et al.*, 2016). Conversely, partial reduction in GlyT2 expression using siRNA does not produce the hyperekplexia like symptoms generated by GlyT2 knock outs or full inhibitors. Additionally, targeted partial knock down of GlyT2 has been shown to be analgesic in neuropathic pain models in mice (Morita *et al.*, 2008), validating the value of partial inhibitors of GlyT2. Partial, non-competitive glycine transport inhibitors are likely to slow the clearance rate of glycine from the synapse, but not block it completely, and thereby still allow accumulation of presynaptic glycine that is sufficient for recycling. NAGly is also a partial, non-competitive inhibitor of GlyT2 and does not generate any overt motor side effects (Succar *et al.*, 2007; Vuong *et al.*, 2008), suggesting that compounds like NAGly have potential for the treatment of pain with minimal side effects.

Although exogenous NAGly has been shown to be efficacious for the treatment of pain, its utility is limited by its rapid metabolism (Prusakiewicz *et al.*, 2002), low potency at GlyT2 (IC₅₀ 9 µM, Wiles *et al.*, 2006), and role as a nonspecific signalling molecule (Huang *et al.*, 2001; Prusakiewicz *et al.*, 2002). COX-2 is present in high concentrations in tissues rich in NAGly and inactivates the molecule through a cyclization reaction at its ω6 polyunsaturated arachidonyl tail (Prusakiewicz *et al.*, 2002). One strategy to circumvent, or slow, the metabolism of a GlyT2 lipid inhibitor is to alter the lipid tail of the compound. Previously, our group has reported the activity of N-oleoyl glycine (NOGly) as an inhibitor of GlyT2 (Carland *et al.*, 2013). NOGly similarly contains a glycine head group and has instead an ω9 monounsaturated 18-carbon tail (Figure 3.2) which imparts a lower maximal level of inhibition at GlyT2 and may provide important clues for the future development of partial inhibitors.

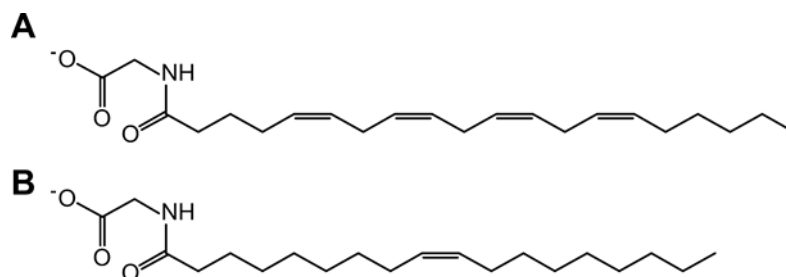


Figure 3.1. Structures of NAGly and NOGly. A. N-arachidonyl glycine (NAGly) (compound 1) and **B.** N-oleoyl glycine (NOGly) (compound 2)

It has been reported that compounds containing saturated or polyunsaturated tails are either inactive or have a much lower potency (Carland *et al.*, 2013). This is in contrast to N-acyl ethanolamine derivatives of anandamide where 3 or 4 double bonds were required to impart significant activity at CB receptors (Lin *et al.*, 1998; Sheskin *et al.*, 1997; Thomas *et al.*, 1996). The tail group of the compounds contributes to the mechanism of inhibition, but the extent of its influence is unknown. In this chapter I report the activity of synthesised glycine conjugated monounsaturated 14, 16, or 18 carbon lipids and their potency in inhibiting glycine transport by GlyT2 and the closely related GlyT1 transporter.

3.2 Results and Discussion

NOGly (Figure 3.1) is comprised of a glycine head group covalently bonded to an 18 carbon monounsaturated fatty acid (MUFA) tail bearing an ω 9 *cis*-double bond (referred to as C18 ω 9 gly). To examine the influence of double bond position on GlyT2 inhibition, a series of NOGly analogues were synthesized by Dr Tristan Rawling (UTS), in which the alkene bond was moved to the ω 11, ω 7, ω 5, or ω 3 position. Analogues with ω 12 and ω 6 double bonds were also prepared, which are common motifs in natural fatty acids, as well as both *cis* and *trans* isomers. In addition, acyl-glycine compounds with 14 and 16 carbon MUFA tails were synthesized to assess the impact of chain length on potency.

3.2.1 Inhibitory activity of acyl-glycine analogues at GlyT2 and GlyT1

Glycine transport by GlyT2 and GlyT1 is coupled to the cotransport of $3\text{Na}^+/1\text{Cl}^-$ and $2\text{Na}^+/1\text{Cl}^-$ respectively (Roux & Supplisson, 2000), creating an electrogenic process that can be measured electrophysiological techniques. Application of glycine to *Xenopus laevis* oocytes expressing GlyT2, clamped at -60 mV, results in inward currents with an EC_{50} of 21.6 ± 1.6 μM , which is consistent with previously reported values (Vandenberg *et al.*, 2007). The inhibitory profiles of each of the synthesized compounds was assayed by measuring glycine dependent (EC_{50}) currents in the presence of increasing concentrations of lipid to determine IC_{50} values at GlyT2 and GlyT1. NAGly (**1**) and NOGly (**2**) have previously been shown to be non-transportable, non-competitive inhibitors of GlyT2 with little or no activity on GlyT1 (Carland *et al.*, 2013; Edington *et al.*, 2009; Wiles *et al.*, 2006). The newly synthesized acyl-glycine analogues do not generate currents when applied to oocytes at concentrations up to 10 μM for 5 minutes, which are conditions that lead to a substantial destabilising inward current when 3 μM oleoyl L-carnitine (OLCarn) is applied (Carland *et al.*, 2013). The lack of any acyl-glycine induced current suggests that these compounds are not substrates for the transporter and also that the compounds are unlikely to induce any chaotropic effects on the cell membrane.

Application of the EC_{50} concentration of glycine produced robust inward currents (Figure 3.2), which were reduced in the presence of lipid inhibitors (representative current traces are shown for C16 ω 6 Gly (**15**) and C18 ω 8 Gly (**7**) inhibition of glycine transport). Following inhibition, glycine and inhibitor were washed from the bath by continuously perfusing ND96 buffer over the oocyte. Reapplication of glycine 5 minutes post-inhibition results in currents comparable to pre-exposure glycine transport currents, indicating that binding of the inhibitors is reversible. Concentration inhibition curves were generated for each compound with the max inhibition, and relative IC_{50} values at GlyT2 and GlyT1 presented in Table 3.1. While many compounds showed marked inhibition of transport by GlyT2, none of the compounds tested showed any appreciable inhibitory activity on the closely related glycine transporter GlyT1.

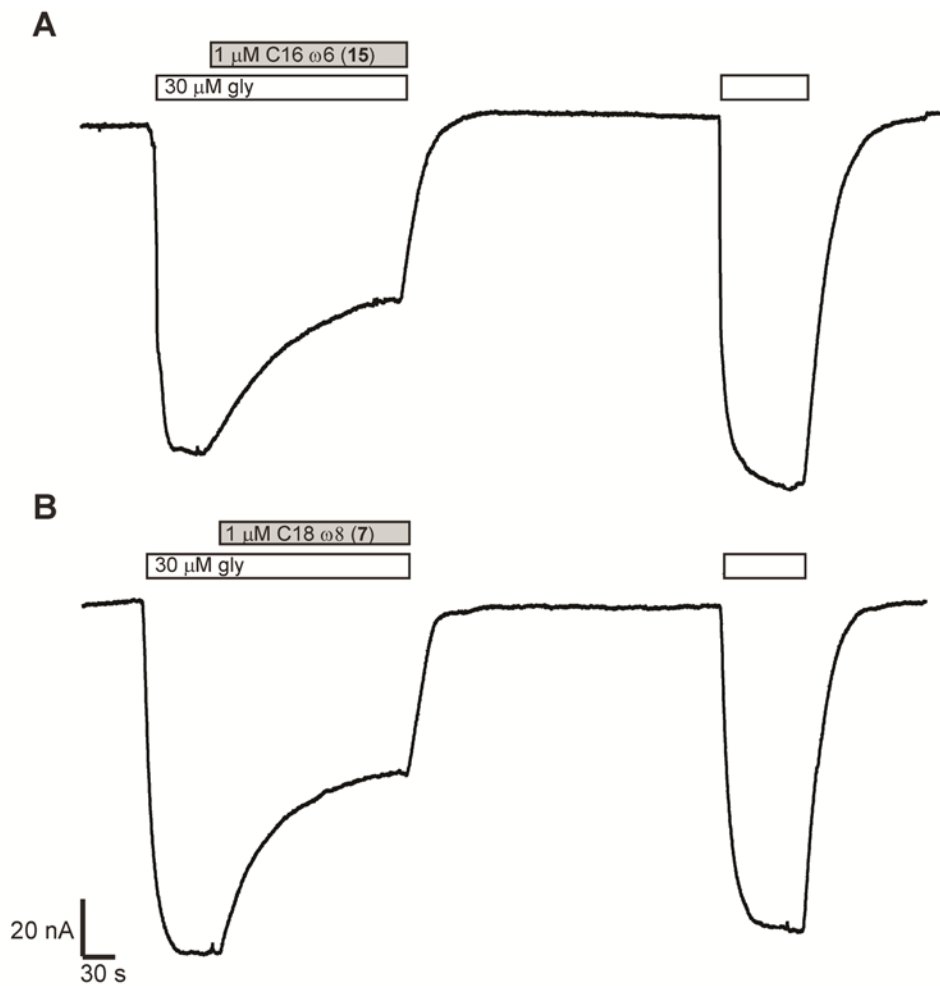


Figure 3.2. Example glycine induced transport current traces from oocytes expressing GlyT2 and clamped at -60 mV. The EC₅₀ of glycine was applied (open bars) and produced inward currents which were inhibited (closed bars) by **A.** 1 μM C16 ω6 Gly (**15**) and **B.** 1 μM C18 ω8 Gly (**7**). 5 minutes following inhibition the EC₅₀ of glycine was reapplied to show reversibility of inhibition and restoration of glycine currents to pre-exposure levels.

3.2.2 Activity of C18 acyl-glycine analogues

Maintaining the 18-carbon chain and positioning the double bond more than two bonds from the ω 9 position (in compounds ω 3- ω 7 (**3-6**), ω 11 (**9**), and ω 12 (**10**)), produced inactive compounds. To further probe this apparent strict requirement for double bond position we synthesized C18 ω 8 Gly (**7**) and C18 ω 10 Gly (**8**), in which the double bond is shifted by only one bond. Both analogues had slightly increased potencies compared to NOGly (0.32 μ M for ω 8 and 0.34 μ M for ω 10 compared to 0.50 μ M for NOGly). It is notable that shifting the position of the double bond by one further carbon (C18 ω 7 (**6**) or C18 ω 11 (**9**)) to either end of the lipid chain abolished inhibitory activity (Figure 3.3A). For the C18-compounds, it is apparent that compounds with double bonds in this “goldilocks zone” are selective for GlyT2. It is also notable that these analogues are partial inhibitors of GlyT2, with the maximal level of inhibition observed being 52–66% (Table 3.1). Flexible monounsaturated lipids can exist in a number of different conformations. If the tail is not directly interacting with GlyT2, and instead sticking in the membrane or adjacent to hydrophobic regions of the transporter, a large number of subtle binding positions could be accommodated. To further probe the importance of the double bond, *trans*-isomers of the ω 7 and ω 9 C18- compounds were synthesized and screened on GlyT2 and GlyT1. The minimum energy conformation of a hydrocarbon tail with a *cis* double bond approximately medial has a substantial kink, which has been shown to distort the packing of membrane lipids (Funari *et al.*, 2003). However, *trans* double bonds would constrain the geometry of the tail to adopt a similar conformation as saturated lipids, which have been previously shown to be inactive at GlyT2 (Carland *et al.*, 2013). In contrast to the *cis*-isomers, C18 *trans*- ω 9 gly (**12**) and C18 *trans*- ω 7 gly (**11**) were both inactive (Figure 3.3C) which suggests there is a selective pocket on GlyT2 which can only accommodate *cis* conformations of the lipid tail moiety.

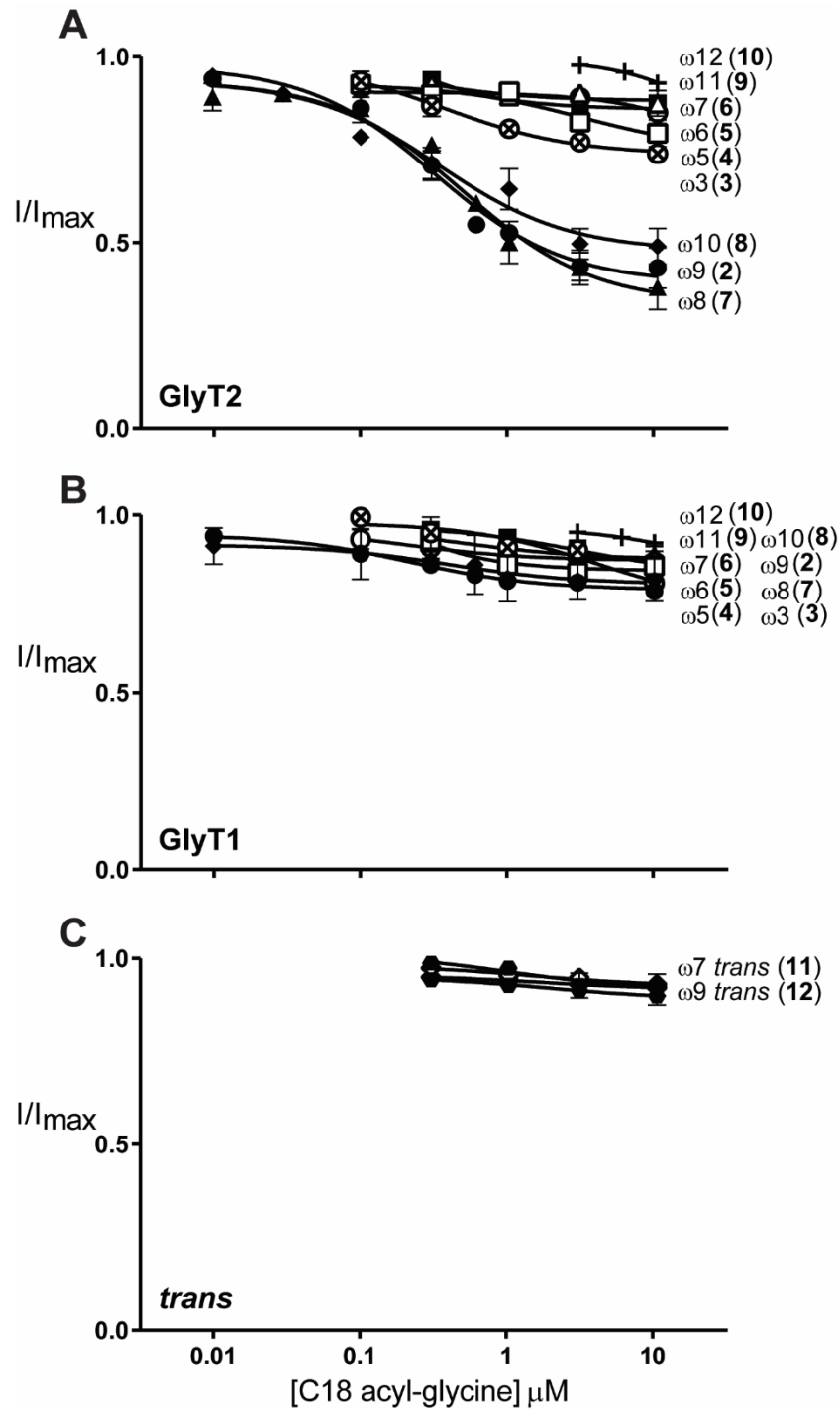


Figure 3.3. Monounsaturated C18 acyl-glycines inhibit glycine transport currents of GlyT2 and GlyT1 transporters expressed in *Xenopus laevis* oocytes. 30 μ M glycine transport currents were measured in the presence of lipids in the range of 10 nM to 10 μ M for **A.** GlyT2 and **B.** GlyT1. **C.** Concentration-dependent inhibition of GlyT2 and GlyT1 for compounds (11) and (12). The responses are normalized mean values \pm SEM ($n \geq 3$ cells) fit using least-squares analysis. \otimes C18 ω 3 \square C18 ω 5 \triangle C18 ω 6 \blacksquare C18 ω 7 \bullet C18 ω 8 \blacktriangle C18 ω 9 \blacklozenge C18 ω 10 \circ C18 ω 11 $+$ C18 ω 12 \bullet C18 ω 9 trans \blacklozenge C18 ω 7 trans

3.2.3 Activity of C16 and C14 acyl-glycine analogues

Substitution of the lipid tail in NAGly with C16-MUFAs and a double bond at any of the ω 3, ω 5, ω 6, ω 7, ω 9, ω 11, or ω 12 positions, produced compounds which were active at GlyT2 with IC_{50} values ranging from 0.81 to 3.5 μ M (Figure 3.4). As can be seen by the % max inhibition (Table 3.1), a majority of the C16 compounds inhibited glycine transport currents to a greater extent than previously reported [partial] lipid inhibitors of GlyT2. C16 compounds with double bonds in the ω 5 through ω 11 positions inhibited GlyT2 in the range of 85–98% (Table 3.1). Shortening the chain also appeared to reduce the affinity of the acyl-glycines (C14 ω 5 Gly IC_{50} 9.2 μ M).

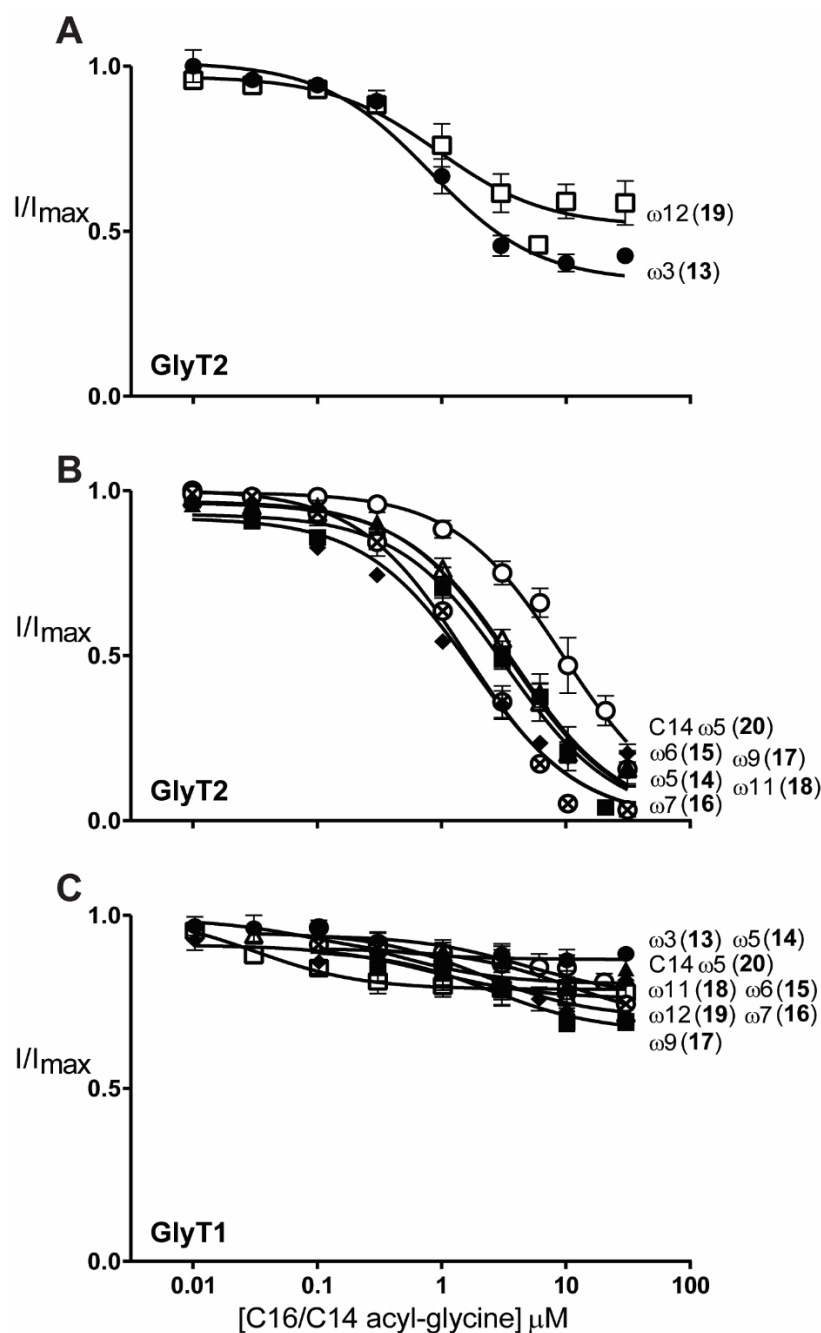
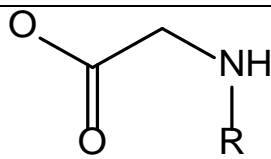


Figure 3.4. Monounsaturated C16 and C14 acyl-glycines inhibit glycine transport currents of GlyT2 and GlyT1 transporters expressed in *Xenopus laevis* oocytes. 30 μM glycine transport currents were measured in the presence of lipids in the range of 10 nM to 30 μM . **A.** Concentration–inhibition curves for partial inhibitors (compounds **13** and **19**) on GlyT2. **B.** Concentration–inhibition curves for full inhibitors (compounds **14–18** and **20**) on GlyT2. **C.** Concentration-dependent effects of compounds (**13–20**) on glycine transport currents of GlyT1. The responses are normalized mean values \pm SEM ($n \geq 3$ cells) fit using least-squares analysis. ● C16 ω_3 ▲ C16 ω_5 ◆ C16 ω_6 ⊗ C16 ω_7 ■ C16 ω_9 △ C16 ω_{11} □ C16 ω_{12} ○ C14 ω_5

Table 3.1. Structure-activity relationships of C14, C16, and C18 glycine compounds at GlyT2 and GlyT1

		IC ₅₀ (μM) (95% CI)		% max Inhibition of GlyT2 ^c
Compound	R	GlyT2a	GlyT1b	
1 NAGly ^a	C20 <i>cis</i> ω6,9,12,15	9.1 (4.5-18)	>10 ^b	79.6 ± 2.1
2 NOGly ^a	C18 <i>cis</i> ω9	0.50 (0.23-1.1)	>10	66.8 ± 2.8
3	C18 <i>cis</i> ω3	>10	>10	-
4	C18 <i>cis</i> ω5	>10	>10	-
5	C18 <i>cis</i> ω6	>10	>10	-
6	C18 <i>cis</i> ω7	>10	>10	-
7	C18 <i>cis</i> ω8	0.32 (0.18-0.57)	>10	61.3 ± 1.7
8	C18 <i>cis</i> ω10	0.34 (0.14-0.84)	>10	52.4 ± 2.2
9	C18 <i>cis</i> ω11	>10	>10	-
10	C18 <i>cis</i> ω12	>10	>10	-
11	C18 <i>trans</i> ω7	>10	>10	-
12	C18 <i>trans</i> ω9	>10	>10	-
13	C16 <i>cis</i> ω3	0.81 (0.46-1.4)	>10	65.3 ± 1.9
14	C16 <i>cis</i> ω5	3.5 (2.8-4.4)	>10	92.3 ± 2.1
15	C16 <i>cis</i> ω6	1.7 (1.4-2.2)	>10	85.2 ± 1.0
16	C16 <i>cis</i> ω7	1.5 (1.3-1.8)	>10	92.5 ± 1.6
17	C16 <i>cis</i> ω9	3.2 (2.7-3.9)	>10	88.2 ± 2.6
18	C16 <i>cis</i> ω11	3.4 (2.5-4.8)	>10	97.9 ± 2.3
19	C16 <i>cis</i> ω12	0.93 (0.41-2.2)	>10	48.5 ± 1.4
20	C14 <i>cis</i> ω5	9.2 (7.3-12)	>10	100 ± 7.2

Compounds were tested for inhibition of 30 μM glycine transport by GlyT2 and GlyT1, expressed in *Xenopus laevis* oocytes. n ≥ 3 with measurements taken from at least 2 batches of oocytes. Data presented are mean and 95 % confidence intervals or mean ± SEM.

^aCompounds are commercially available and have been previously described as GlyT2 inhibitors. ^bWhere significant inhibition was not reached, IC₅₀ are presented as greater than the maximum concentration of each compound applied.

^cWhere a plateau in concentration-inhibition did not occur at the maximal concentration used the % max response given is the inhibition at the max concentration.

3.2.4 C18 ω 8 gly and C16 ω 6 gly inhibit [3 H]-glycine uptake by oocytes expressing GlyT2

While it has been previously demonstrated that glycine-induced currents are directly related to the rate of glycine transport, I also examined the effect of representative lipids on the rate of [3 H]-glycine uptake by oocytes expressing GlyT2. A time course of [3 H]-glycine uptake was measured in the absence of inhibitors and in the presence of 10 μ M C18 ω 8 Gly and 10 μ M C16 ω 6 Gly. Both lipids caused \sim 50% reductions in the rate of [3 H]-glycine transport over 10 minutes (Figure 3.5), which is comparable to the effects observed for inhibition of glycine transport currents. It is notable that uninjected oocytes allowed \sim 15% of uptake compared to oocytes expressing GlyT2 and that this background level of uptake was not affected by the acyl-glycines. Thus, low levels of transport are likely due to an unrelated endogenous *Xenopus* oocyte amino acid transporter, which was not inhibited by acyl-glycine compounds. Additionally, the lack of any substantial change in the rate of background [3 H]-glycine uptake also confirms that there is minimal, if any, chaotropic effects of the lipids on the cell membrane.

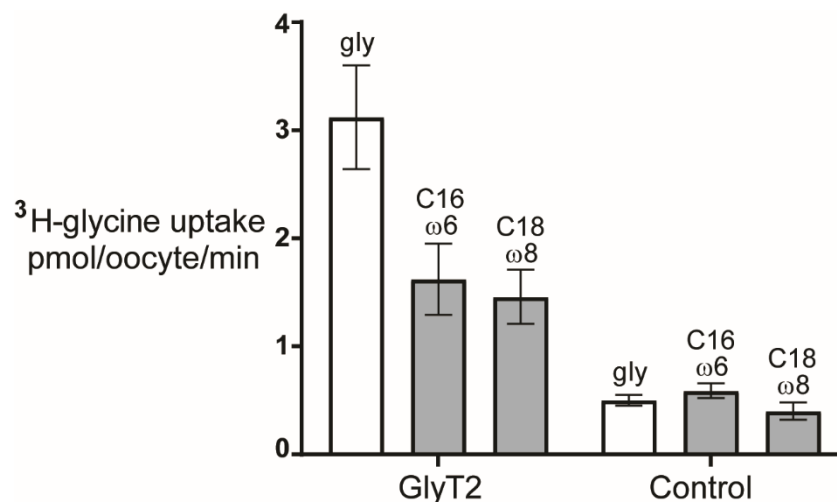


Figure 3.5. Rates of [3 H]-glycine uptake in the presence and absence of acyl-glycine inhibitors. Oocytes expressing GlyT2 and uninjected control oocytes were pre-incubated with 10 μ M C16 ω 6 Gly, 10 μ M C18 ω 8 Gly, or buffer for 2 minutes, and then the rate of 10 μ M [3 H]-glycine transport measured as described in the Methods.

3.2.5 There is a preferred double bond position and chain length for conferring affinity and extent of inhibition

It appears that when the double bond is in the centre of the carbon chain, the inhibitors are active (in the case of C18) or show a greater level of maximal inhibition (in the case of C16). However, as the properties imparted by a medial double bond differ between C16 and C18 compounds it cannot be ascertained whether the trend is connected. The order of potency was C18 > C16 > C14 for the monounsaturated compounds tested, which suggests tail length is governing activity of the inhibitors. While C18 compounds were the most potent, the placement of the double bond within the tail was limited to a stringently defined zone in the middle of the chain (from ω 8-10). The lower affinity C14 and C16 compounds were all active as GlyT2 inhibitors, with generally increased maximal level of inhibition. While the C18 compounds are more potent than their C16 counterparts, the maximal level of inhibition was reduced (52–67% for C18 ω 8, ω 9, ω 10 and 88–92% for C16 ω 5, ω 6, ω 7, ω 9, ω 11). I speculate that there is an optimal size and/or shape of the lipid tail which can be accommodated in the allosteric inhibitor binding pocket. While lipids with C14, C16, and C18 tails with glycine head group can fit into a binding pocket, lipids with larger C18 tails are likely to have the potential to form more hydrophobic interactions causing increased potency of inhibition, but also creating partial inhibitors. In the case of NAGly, its C20 polyunsaturated tail would be more condensed than the shorter monounsaturated lipids, allowing it to fit in the lipid binding site. The observed lower affinity of NAGly could be due to the number of kinks in the tail which restrict the ideal binding mode and reduce the capacity for intermolecular interactions. For inactive C18 acyl-glycine compounds, the *cis* double bond would create lateral kinks which may not be accommodated if the acyl binding pocket is at capacity.

The majority of mammalian cell membranes are composed of phosphatidylcholine, with phosphatidylethanolamine, sphingomyelin, and cholesterol also abundantly present (Funari *et al.*, 2003; van Meer *et al.*, 2008). Unsaturated [oleoyl] C18 or saturated [palmitoyl] C16 are the most common lipid chains present in phospholipids. The most efficacious of the lipid inhibitors

in this study contain similar tails and therefore may be capable of inserting into the bilayer, spanning the depth of one leaflet, and interacting with or displacing membrane lipids at the protein membrane interface. The predilection for certain tail lengths and configurations could also reflect the capacity for acyl-glycine compounds to associate with the membrane and form a lipid-bound pool.

The arachidonyl tail has multiple double bonds which allow it to exist in a number of different conformations: U-shaped, J-shaped, or in an extended conformation (Figure 3.6A) (Makriyannis, 1995). Despite the U-shape conformation possessing the lowest energy, it has been shown using solid-state NMR that anandamide exists in an extended conformation within the membrane bilayer, with the head group at the phospholipid-aqueous interface and the terminal carbon approximately half way across the membrane (Tian *et al.*, 2005). This conformation is most similar to monounsaturated lipids, where the *cis* configuration single double bond would create a small kink (Figure 3.6B) and disrupt neighbouring chains. *Trans* double bond containing acyl-glycine compounds would instead behave as unsaturated, straight, lipid tails (Figure 3.6C) which can regularly pack within membranes and restrict membrane fluidity (Stubbs & Smith, 1984). The inactivity of C18 *trans*- ω 9 Gly may therefore reflect movement within the membrane to associate with GlyT2 and cause inhibition.

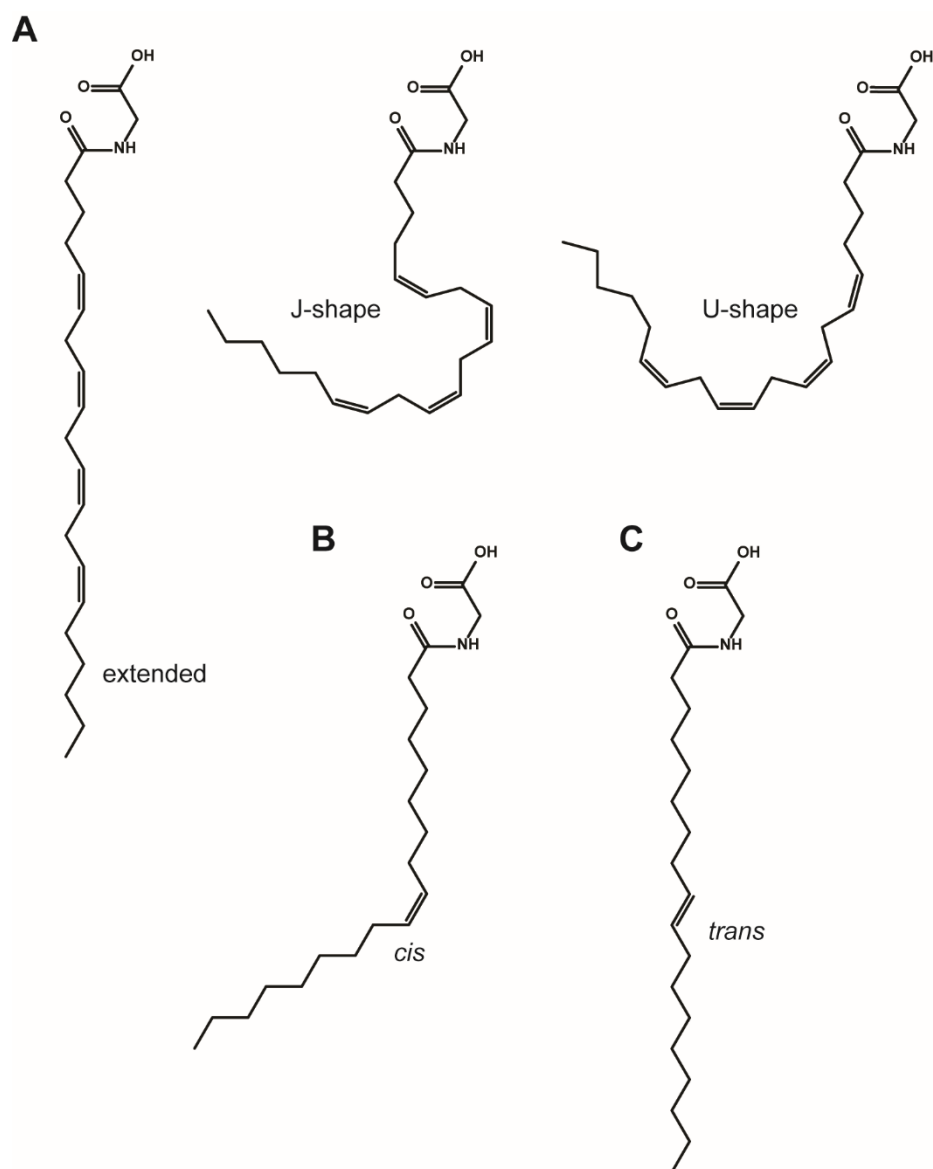


Figure 3.6. Possible conformations of acyl tails. A. N-arachidonyl glycine, **B.** N-oleoyl glycine, and **C.** C18 *trans*- ω 9 Gly.

Studies of the structure–activity relationship for lipid ligands of CB receptors have also revealed that small changes can impart inactivity (Berglund *et al.*, 1998; Lin *et al.*, 1998; Pei *et al.*, 2008; Thomas *et al.*, 1996). NAGly and anandamide differ only by a carboxylic acid in the head group and yet this difference is sufficient to prevent binding of NAGly. The acyl-glycine analogues in this study have a preferred double bond position and chain length which, in addition to the well characterized importance of the head group, establishes the coinciding influence of the tail in conferring the activity of lipid ligands.

3.2.6 Reversibility of acyl-glycine inhibitors

Following a 5 minute washout of each of the active inhibitors, glycine transport currents were comparable to pre-exposure transport currents (Figure 3.2). Despite the differences in lipid tail, and large variation in relative potency (0.32–9.2 μM), all inhibitors in this study were reversible. These observations are in contrast to OLCarn inhibition of GlyT2 which is very slowly reversible (Carland *et al.*, 2013). This data suggests that the head group is more important in determining the rate of reversibility. The IC_{50} of OLCarn is similar to the most potent acyl-glycine inhibitor (~ 320 nM) and so reversibility must be governed by a mechanism other than simple unbinding. In the case of OLCarn, application of β -cyclodextrin accelerates washout which suggests that it is a lipid membrane-mediated mechanism of inhibition (Carland *et al.*, 2013). Thus, I speculate that the head group influences the stability of the lipid in the membrane, which can influence the time course of washout of the lipid. Since neither potency at the binding site nor hydrophobic interactions of the tail in the membrane are driving reversibility, I propose that reversibility is related to how compounds can access or leave the site and therefore is another independent property of the compound that must be considered when designing an optimal GlyT2 lipid inhibitor. A carnitine head group has a positive charge and is significantly larger than the glycine head group, so perhaps the charge and/or size is capturing the compounds in a membrane reservoir, such as the negatively charged phosphate groups of the lipid bilayer, for longer periods impeding washout. In addition to full inhibition, reversibility is another potential problem which is hindering the pursuit of GlyT2 as a molecular target. The excitotoxicity of ORG-25543 is associated with both its full and irreversible inhibition (Mingorance-Le Meur *et al.*, 2013), and it has been suggested that instead a reversible inhibitor may be used to avoid adverse side effects. All inhibitors identified in this study are readily reversible within 5 minutes, and may provide insight into the future design of reversible inhibitors to circumvent side effects.

3.3 Conclusions

Crystal structures of neurotransmitter transporters with the conserved LeuT-like fold show membrane lipids binding to proteins, and these interactions have been proposed to play important regulatory roles in their function (Koshy *et al.*, 2013; Penmatsa *et al.*, 2013). I have demonstrated that the lipid constituent of acyl-glycine compounds is essential in their specific interactions and mechanism of inhibition of the LeuT-like transporter, GlyT2, and not merely a nonselective, “sticky” adjunct. The data presented here establishes there is an ideal chain length and double bond conformation, and that potency and maximal level of inhibition are influenced by the lipid tail. Conservative differences between compounds are sufficient to impart or remove inhibitory activity which validates highly specific binding to a subtype selective allosteric pocket.

In this chapter, a number of synthesised acyl-glycine compounds have been shown to inhibit GlyT2 over the closely related GlyT1. These compounds contain novel synthetic tails which may be less susceptible to enzymatic degradation than the parent compound NAGly. I have identified C18 ω 8 Gly, a relatively potent (320 nM), reversible, and partial ($61 \pm 1.7\%$) novel inhibitor of GlyT2 which has low activity on GlyT1 and is ~ 28 -fold more potent than the endogenously produced ligand, NAGly. In addition to improving the potency of GlyT2 inhibitors, there is a great need to develop effective inhibitors which are partial and reversible as to not disrupt the equilibrium cytosolic glycine concentrations, which has to date hampered the progress of GlyT2 inhibitors as therapeutics. In this chapter I have identified important structural elements which contribute to the overall activity as well as what governs the maximal level of inhibition and reversibility characteristics of lipid glycine transporter inhibitors.

Chapter 4: N-acyl amino acid inhibitors of GlyT2 for the treatment of neuropathic pain

4.1 Introduction

Disease or injury to the somatosensory nervous system can cause long-term neuropathic pain, characterised by associated hyperalgesia (amplified pain sensation) and allodynia (pain response to innocuous stimuli), which produce distinctive symptoms of numbness, burning, shooting, and electric-like pain in sufferers (Constigan *et al.*, 2009). A large number of cases are refractory to conventional analgesics, perhaps due to adaptations within the CNS (Latremoliere & Woolf, 2009). There is therefore a great need to develop new drugs with novel targets to treat neuropathic pain.

A number of GlyT2 inhibitors have been developed which have been shown to be analgesic in a number of models of neuropathic pain (Haranishi *et al.*, 2010; Mingorance-Le Meur *et al.*, 2013; Morita *et al.*, 2008; Omori *et al.*, 2015; Xu *et al.*, 2005), however, many cause significant excitotoxic symptoms (Hermanns *et al.*, 2008; Mingorance-Le Meur *et al.*, 2013). Endogenous lipid compounds have also been identified as novel agents capable of inhibiting glycine transporters. NAGly is a partial, reversible, non-competitive inhibitor of GlyT2 ($IC_{50} \sim 9 \mu M$) with little activity at GlyT1 (Wiles *et al.*, 2006). Other endogenous acyl compounds also inhibit the GlyT2 transporter; with an order of potency of OLCarn (340 nM) > NOGly (500 nM) > palmitoyl L-carnitine (600 nM) > NAGly > N-arachidonyl alanine (9 μM) > N-arachidonyl GABA (12 μM) (Carland *et al.*, 2013; Wiles *et al.*, 2006). These lipid inhibitors of GlyT2 are amphipathic; comprised of a long flexible lipid tail conjugated to a charged or polar head group.

Previous attempts to improve potency and stability led to the synthesis of a series of acyl-glycine analogues, presented in Chapter 3. It was shown that the lipid tail constituent was critical in their activity as inhibitors of GlyT2, and that there was an ideal chain length and double bond conformation. C16 *cis*- $\omega 3$ Gly was shown to be a relatively potent (IC_{50} 810 nM), partial inhibitor (65% maximal inhibition), while shifting the double bond to the $\omega 7$ position

produced an inhibitor with a larger maximal level of inhibition (93% maximal inhibition). I propose that a reversible, partial GlyT2 inhibitor will allow for sufficient glycine re-uptake into presynaptic terminals for loading of vesicles, but will slow the removal of glycine to increase transient concentrations at inhibitory glycinergic synapses while minimising spill-over into excitatory glutamatergic synapses.

Lipid GlyT2 inhibitors resemble bioactive lipid molecules, which are long chain fatty chains often conjugated to amino acids or neurotransmitters, including acyl-serines, acyl-aurines, and acyl-dopamines. These compounds activate specific signalling pathways, and have to date been identified within the CNS, immune system, and cardiovascular system (Evans & Hutchinson, 2010). The availability of the precursor fatty acids and amino acids suggest that there may be other lipids whose role are yet to be determined. In 2010, Tan and colleagues identified 50 novel acyl-amino acids present in the rat brain or bovine spinal cord (Tan *et al.*, 2010). It is proposed there are a number of unknown targets for bioactive lipids, and that acyl-amino acids are ubiquitous within the CNS. Lipid based drugs may therefore be stable and tolerated, however off target side effects will need to be investigated as they have the potential to activate other receptors and signalling pathways.

In Chapter 3, I demonstrated that the lipid tail constituent is critical in the activity of lipid inhibitors at GlyT2, and that the most potent chain is 18 carbons in length with a *cis*-double bond in the ω 8, ω 9, or ω 10 positions. To further investigate the structure activity relationship of lipid inhibitors, an additional series of lipid analogues were synthesised by Dr Tristan Rawling (UTS), in which the optimal oleic [C18 *cis*- ω 9] tail was conjugated to a number of amino acid head groups. A range of aliphatic, aromatic, polar, negatively charged, and positively charged acyl-amino acids were prepared. The configuration of the amino acids was also explored through L- and D- isomers. In this chapter, I report the inhibitory activity of N-acyl amino acids at GlyT1 and GlyT2. Select compounds were also screened for metabolic stability, with the most potent, stable compound, oleoyl [C18 *cis*- ω 9] D-Lys tested for BBB

permeability, and ability to reduce allodynia nerve ligation rat model of neuropathic pain, which was conducted by Dr Sarasa Mohammadi (USYD).

4.2 Results and Discussion

4.2.1 Activity of N-acyl amino acid analogues on GlyT2 and GlyT1

As previously reported, inward currents were produced following the application of the EC₅₀ concentration of glycine to oocytes expressing GlyT1 or GlyT2. For GlyT2, these currents were reduced or abolished in the presence of acyl-amino acids, while none of the compounds displayed considerable inhibition at GlyT1 at concentrations up to 3-10 μ M (example traces Figure 4.1; Table 4.1). While glycine activated currents are relatively rapid following its administration, N-acyl amino acids slowly reduce currents, suggesting the binding site is not immediately accessible. Subsequent re-application of glycine 5 minutes following washout of the inhibitor results in reduced currents compared to pre-exposure levels, indicative of irreversible or slowly reversible inhibition. Concentration-inhibition curves were thus generated by applying increasing concentrations of N-acyl amino acid, producing a cumulative inhibition response (representative trace shown, Figure 4.1C), with % max inhibition and apparent IC₅₀ values at GlyT1 and GlyT2 shown in Table 4.1.

Prolonged application of >10 μ M N-acyl amino acids to either transporter expressing, or uninjected oocytes, did not produce any currents, with the exception of acyl-serine and positively charged N-acyl amino acid compounds. Concentration response curves for these inhibitors were therefore limited to 3 μ M to circumvent non-specific membrane effects.

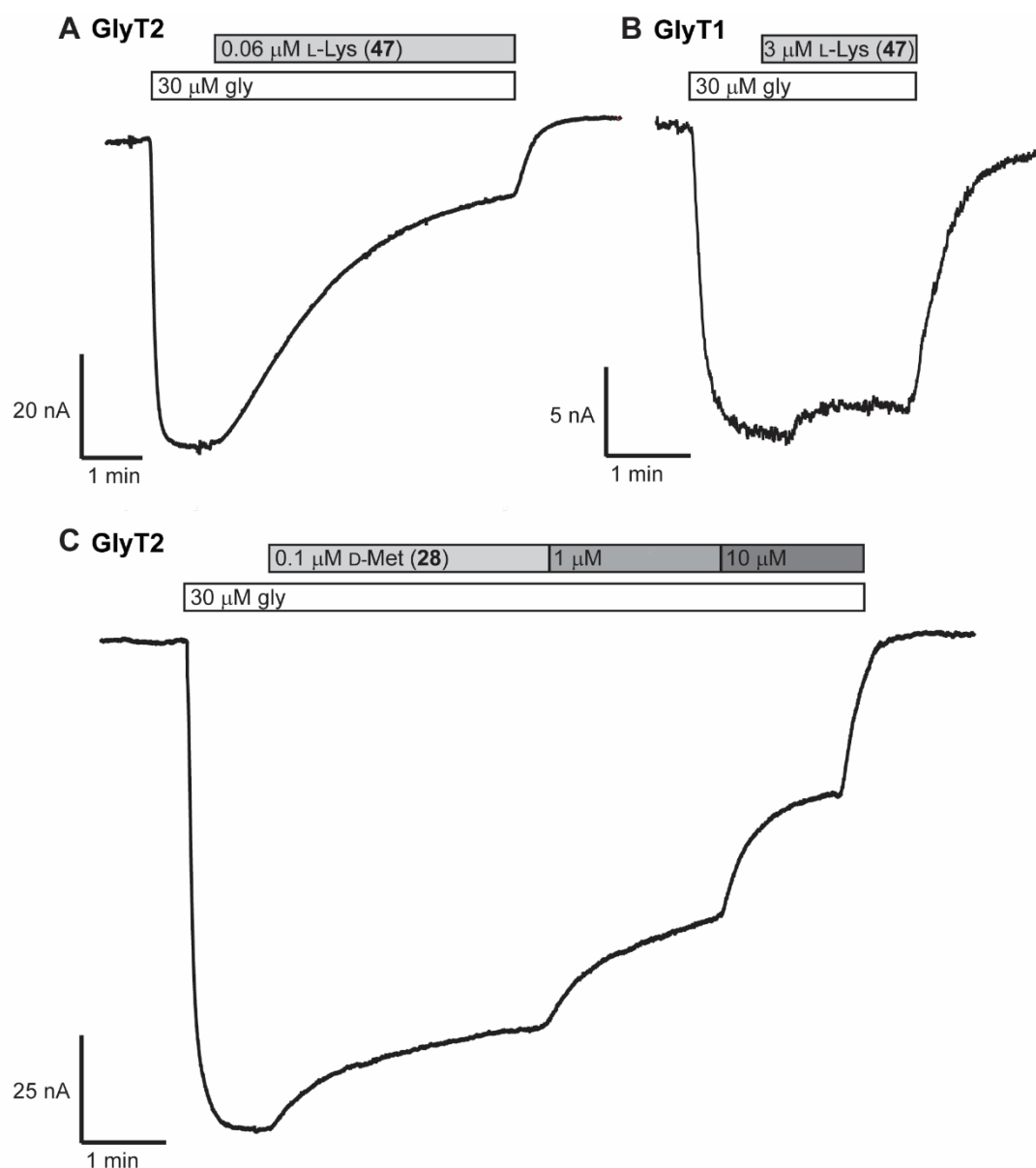


Figure 4.1. Representative current traces from oocytes expressing glycine transporters, clamped at -60 mV. A. the EC₅₀ concentration of glycine (30 μM) was applied (open bar) to produce inward currents, which was reduced by application of oleoyl L-Lys (**47**) (grey bar). **B.** GlyT1 mediated glycine currents were not reduced by (**47**), even at high concentrations. **C.** Cumulative concentration response curves were generated by applying increasing concentrations of acyl inhibitor (**28** in this example, grey segmented bar) to reduce glycine induced currents at GlyT2.

4.2.2 Activity of N-acyl L-amino acids

Conjugation of the oleoyl tail to an amino acid head group in the L- configuration produced compounds which all reduced GlyT2 transport currents, with IC₅₀ values ranging from 25.5 nM – 4.35 μM (Table 4.1). For compounds containing small aliphatic side chains (L-Ala (**21**) and L-Val (**23**)) weaker inhibition was observed (IC₅₀ values > 1 μM) (Figure 4.2A) compared to compounds with a larger, bulkier side chain (e.g. L-Leu (**25**) IC₅₀ 143 nM) (Figure 4.2B).

While methionine is often grouped with aliphatic amino acids, the L-Met analogue (**27**) is a potent, near full inhibitor (29.2 nM, 91.2%) which suggests it may have more than just hydrophobic interactions at the binding site. In order to further understand these interactions, an N-acyl amino acid was synthesised containing the head group L-NorLeu (**29**), a straight chained isomer of leucine containing a carbon atom in place of the sulfur in methionine. This compounds was *~9-fold* less potent, indicating the sulfur atom in the L-Met analogue is providing additional interactions with GlyT2. This sulfur may also behave as an electrophile; the σ-hole of the S possibly interacting with an oxygen atom, or with aromatic π electrons in the binding site (Beno *et al.*, 2015; Pal & Chakrabarti, 2001).

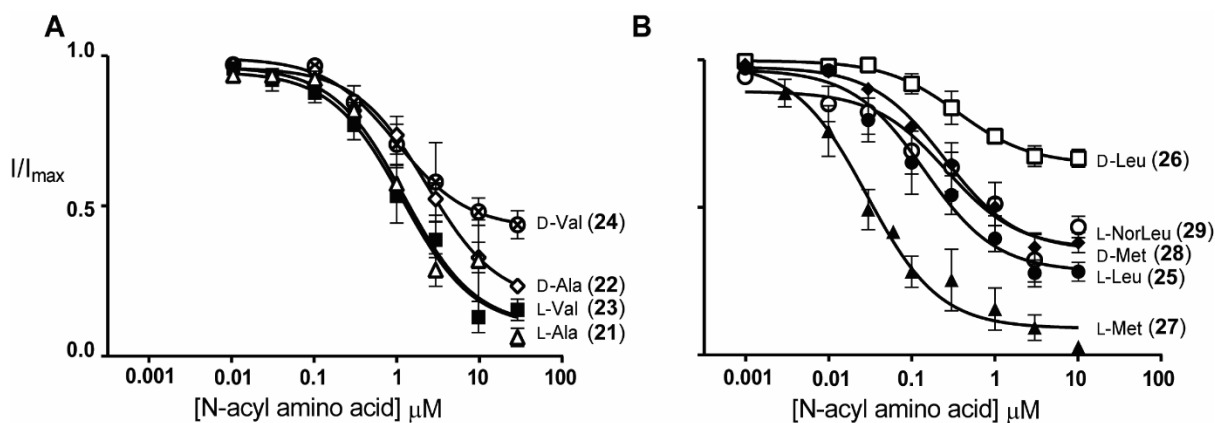


Figure 4.2. Aliphatic acyl amino acids inhibit glycine transport currents of GlyT2 transporters expressed in *Xenopus laevis* oocytes. 30 μM glycine transport currents were measured in the presence of lipids in the range of 1 nM to 10 μM . **A.** Concentration–inhibition curves for compounds (21–24). **B.** Concentration–inhibition curves for compounds (25–29). The responses are normalized mean values \pm SEM ($n \geq 3$ cells) fit using least-squares analysis. Δ L-Ala \diamond D-Ala \blacksquare L-Val \otimes D-Val \bullet L-Leu \square D-Leu \blacktriangle L-Met \circ D-Met \blacklozenge L-NorLeu

For acidic amino acids where their side chains would be negatively-charged at both assay conditions and physiological pH, conjugation to the oleic tail produces active inhibitors of GlyT2 (Figure 4.3B). However, these compounds possess relatively low affinity (L-Asp (32) 865 nM; and L-Glu (34) 4.35 μM), and do not appear to provide any additional activity compared to an aliphatic side chain. The L-Asn (36) analogue is similar to L-Asp but instead contains a primary amide side chain which is uncharged. The IC_{50} is largely unchanged (613 nM) compared to L-Asp which suggests the negative charge is not providing any significant binding or repulsive interactions with GlyT2.

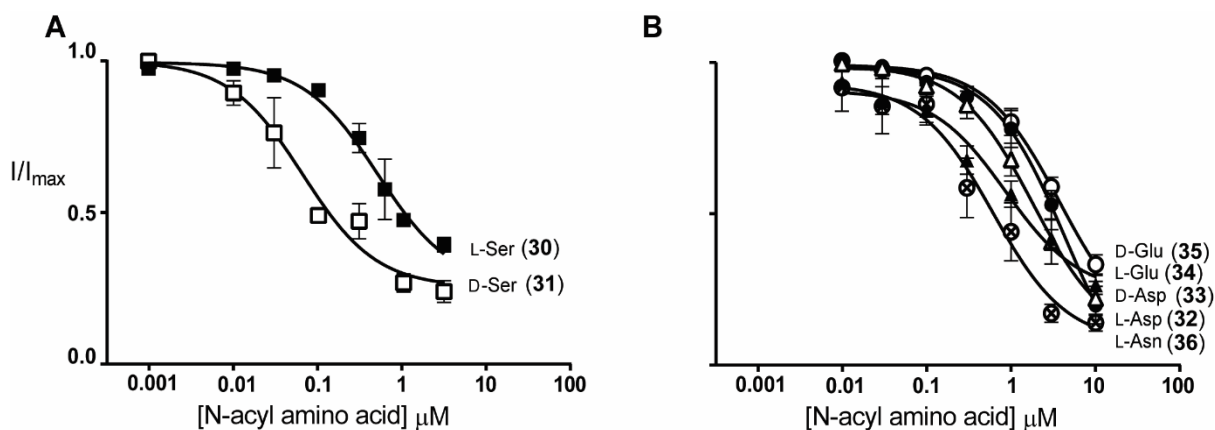


Figure 4.3. Polar and negatively charged acyl amino acids inhibit glycine transport currents of GlyT2 transporters expressed in *Xenopus laevis* oocytes. 30 μM glycine transport currents were measured in the presence of lipids in the range of 1 nM to 10 μM . Concentration–inhibition curves for **A**. Compounds (30) and (31). **B**. Compounds 32-36. The responses are normalized mean values \pm SEM ($n \geq 3$ cells) fit using least-squares analysis.

■ L-Ser □ D-Ser ● L-Glu ○ D-Glu ▲ L-Asp △ D-Asp ⊗ L-Asn

The N-acyl L-amino acids with aromatic side chains are all relatively potent inhibitors of GlyT2 (Figure 4.4A). The L-Phe analogue (37) inhibited GlyT2 with an IC_{50} of 214 nM, and extension of the alkyl chain between the aromatic ring and amino acid back bone further improved potency (L-C2-Phe (39) IC_{50} 151 nM). The benzene ring of the indole group in L-Trp (41) is also 3 bonds from the head group α -carbon and conferred a high potency (IC_{50} 54.6 nM), which suggests there is an optimum distance from the amino acid backbone to the aromatic group.

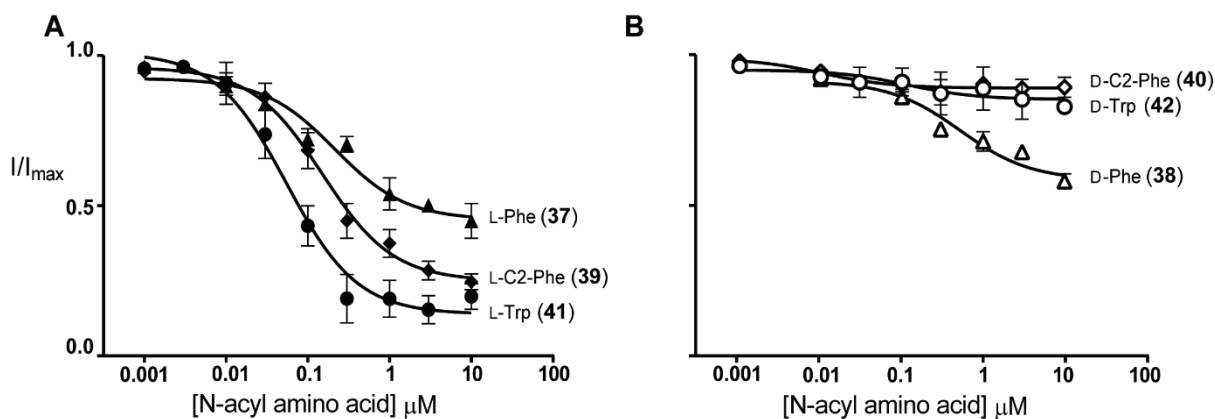


Figure 4.4. Aromatic acyl amino acids inhibit glycine transport currents of GlyT2 transporters expressed in *Xenopus laevis* oocytes. 30 μM glycine transport currents were measured in the presence of lipids in the range of 1 nM to 10 μM . Concentration–inhibition curves for **A.** Compounds (37, 39, and 41) and **B.** Compounds (38, 40, and 40). The responses are normalized mean values \pm SEM ($n \geq 3$ cells) fit using least-squares analysis. \blacktriangle L-Phe \blacklozenge L-C2-Phe \bullet L-Trp \triangle D-Phe \diamond D-C2-Phe \circ D-Trp

Conjugation of a positively charged L-amino acid to the oleic tail produced analogues which were the most potent inhibitors in the N-acyl amino acid series (L-His (43) 130 nM; L-Arg (45) 47.9 nM; L-Lys (47) 25.5 nM) (Figure 4.5A). Because the L-Lys head group produced the most potent inhibitor, 3 compounds were prepared with “lysine-like” side chains, with 1, 2, or 3 carbons linking the NH_3^+ to the amino acid backbone (23–25). Shortening the length of this linker reduced activity in the order of C4 (L-Lys) = C3 > C2 > C1 (Figure 4.5C). The importance of the backbone carboxylic acid was also examined through lysine derivatives; C5- NH_3^+ (52) where the carboxylic acid is removed; and L-Lys-OMe (53) which instead contains a methyl ester. In both cases, the compounds were less active than L-Lys (IC_{50} 560 nM and 91.3 nM respectively), with complete removal of the carboxylic acid reducing potency by ~ 22 -fold.

The importance of the tail group was similarly explored with 4 additional compounds synthesised with either L- or D- Lys conjugated to a C16- or C18- monounsaturated tail (54–57). All compounds were active GlyT2 inhibitors (Figure 4.5D) with C16 $\omega 3$ L-Lys (56) the most

potent (10.7 nM). Interestingly, altering the tail group in this case did not follow the same trend as in Chapter 3, where conjugation to the C18 ω 5 tail or C16 ω 3 tail produced inactive or partial inhibitors respectively.

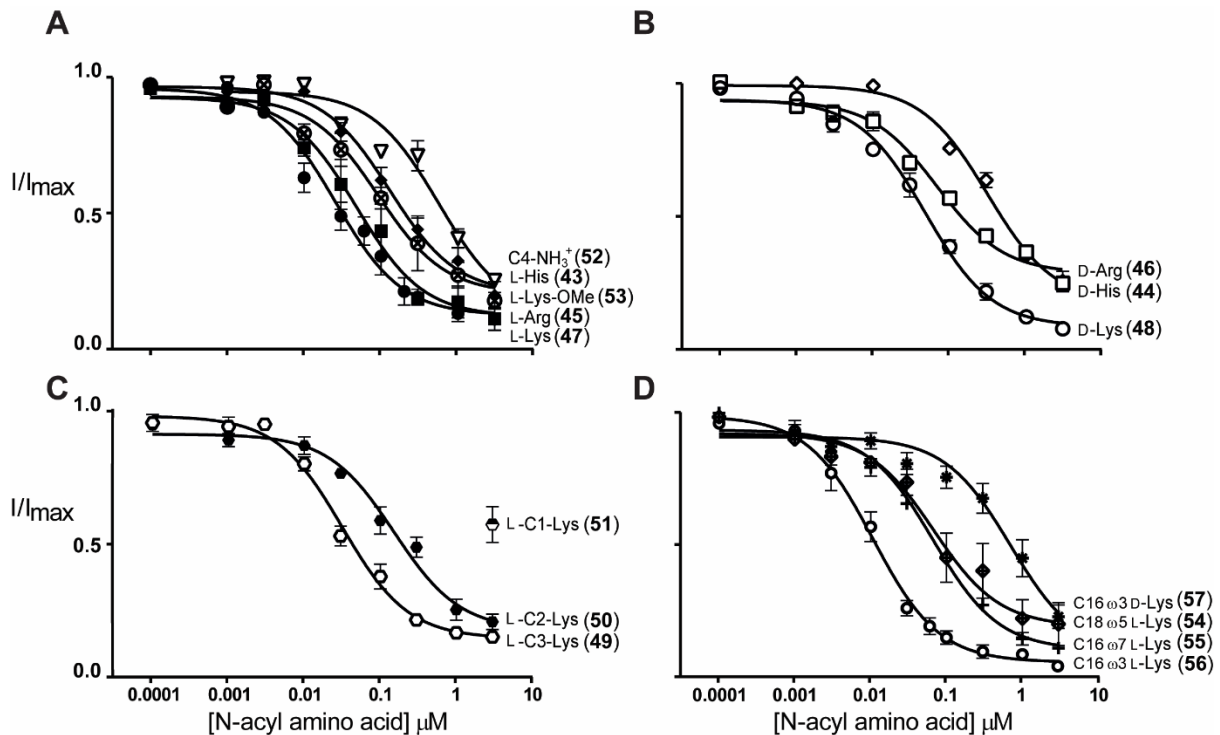


Figure 4.5. Positively charged acyl amino acids inhibit glycine transport currents of GlyT2 transporters expressed in *Xenopus laevis* oocytes. 30 μ M glycine transport currents were measured in the presence of lipids in the range of 100 pM to 3 μ M. Concentration-inhibition curves for **A.** Compounds (43, 45, 47, 53, and 53), **B.** Compounds (44, 46, and 48), **C.** Compounds (49-51). Only 1 data point is presented for (31) at the maximal concentration (3 μ M) as the data could not be reliably fit. **D.** L- or D- Lys analogues (54-57) with differing acyl tails. The responses are normalized mean values \pm SEM ($n \geq 3$ cells) fit using least-squares analysis. \diamond L-His \blacklozenge D-His \blacksquare L-Arg \square D-Arg \bullet L-Lys \circ D-Lys \circ L-C1-Lys \bullet L-C2-Lys \circ L-C3-Lys ∇ C4-NH₃⁺ \otimes L-Lys-OMe \blacklozenge C18 ω 5 L-Lys \dagger C16 ω 7 L-Lys \circ C16 ω 3 L-Lys $*$ C16 ω 3 D-Lys

4.2.3 Activity of N-acyl D-amino acids

Comparison of D- and L- enantiomers revealed, with the exception of serine analogues (**30** and **31**), the L-enantiomers had equal or greater potency as GlyT2 inhibitors. For compounds with a small or flexible side chain, IC₅₀ values for N-acyl D-amino acids were only 2-9-fold lower than the corresponding L- isomer. For example, D-Lys (**48**) is only marginally less potent than L-Lys (48.3 nM compared with 25.5 nM). Conversely, N-acyl D-amino acids with a large aliphatic or aromatic side chain had significantly reduced activity, particularly for D-C2-Phe (**40**) and D-Trp (**42**) analogues where negligible inhibition was reached even at maximal concentrations (10 μM) (Figure 4.4B), while L- isomers are potent nanomolar inhibitors.

4.2.4 Structure activity of acyl inhibitors on GlyT2

The chemical nature of the binding site can also be inferred through structure activity data. A methionine- π interaction produces ~4 – 6 kJ/mol (Valley *et al.*, 2012) while a cation- π interaction has a value of ~4 kJ/mol; contacts with aromatic residues at the binding site may therefore explain the similar affinities between a lysine and methionine containing acyl inhibitors. I propose that the head group binding site is likely to be comprised of aromatic residues which would provide π -electrons for cation- π (positive amino acids), methionine- π (methionine), and π - π (aromatic amino acids) interactions for the most potent acyl inhibitors. The side chain binding region is likely to be distant from the backbone carboxylate binding site as longer side chains promote greater activity, and orientated in a direction preferred by the L-enantiomers. Given the wide range of head groups that are allowed, the binding site must also be large and/or flexible to accommodate a number of different chemical groups and conformations.

For the G- protein-coupled receptor family, lysophosphatidic acid (LPA) and sphingosine-1-phosphate lipid ligands contain larger head groups than the endocannabinoids, and yet are proposed to fit into a similar pocket. The LPA receptor ligand pocket has head group specificity but promiscuous acyl tail binding (Chrencik *et al.*, 2015). This is proposed to be due to two

tryptophan residues which in the presence of a lipid, change rotameric states to accommodate the ligand and stack their π -electrons towards the tail (Chrencik *et al.*, 2015). Despite the GlyT2 substrate site having strict requirements for binding, the allosteric lipid inhibitor binding site may lie at a region of the transporter with high flexibility which would allow N-acyl amino acids to wiggle into their final binding site, and interact through a number of conformations and binding modes.

The apparent affinity of compounds may also be a reflection of how well N-acyl amino acids are able to interact with membranes. The most potent inhibitors have head groups known to intercalate with membrane phospholipids. Lysine residues can snorkel below the aqueous: bilayer interface to bury its aliphatic region within the oily core of the lipid bilayer, while the charged amino group can interact at the polar phospholipid head groups. Similarly, tryptophan residues prefer to orient themselves towards the polar head group: acyl tail interface of membranes (Yau *et al.*, 1998). Most known lipid ligands of membrane proteins must interact with the cell membrane to reach their protein binding site. An acyl-amino acid which can navigate the membrane more easily may therefore possess a higher apparent affinity.

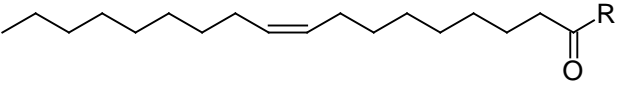
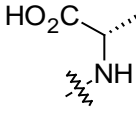
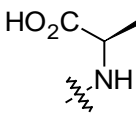
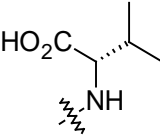
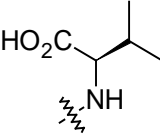
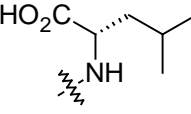
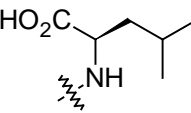
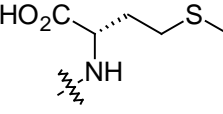
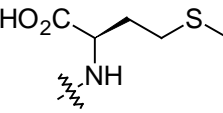
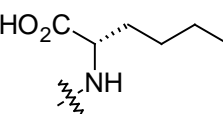
4.2.5 Maximal level of inhibition

Positively charged N-acyl amino acids all inhibited glycine transport in the range 71 – 93% (Table 4.1). Similarly, all negatively charged N-acyl amino acids produced a high % max inhibition (77 – 100%). For aliphatic and aromatic acyl-amino acids, however, the level of inhibition was influenced by the size and configuration of the side chain. For these compounds, the L- isomer possessed a higher % max inhibition compared to the D- for all cases (for example (L-Val) and (D-Val) inhibited 90.1 ± 5.9 and 56.7 ± 5.1 , respectively). This was particularly apparent for aromatic N-acyl amino acids, where all of the D- compounds displayed low level or no inhibition at GlyT2.

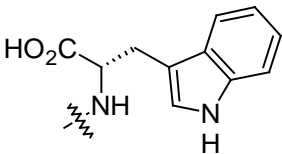
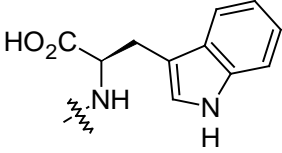
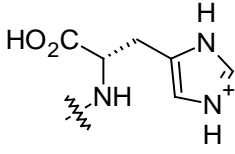
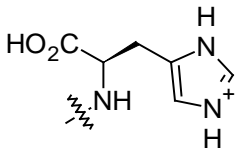
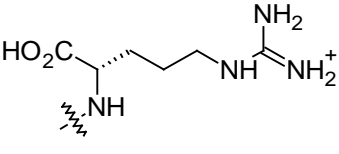
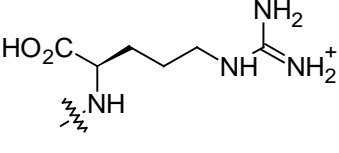
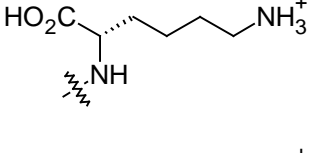
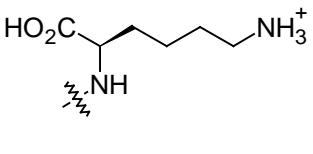
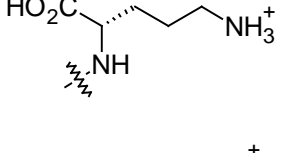
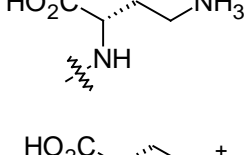
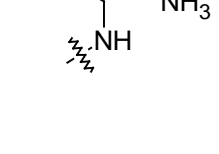
N-acyl amino acids are large and flexible and could bind in somewhat different overlapping conformations in the same binding site. These differences in binding may account for the variance in level of inhibition observed for each compound and may be a reflection of the stability of inhibitor-bound GlyT2, with some glycine transport still permitted in certain conformations.

It is known that full (100%), irreversible inhibition of GlyT2 produces severe neuromotor and respiratory side effects in animal models (Mingorance-Le Meur *et al.*, 2013). While a partial inhibitor would preserve vesicle refilling and recycling of glycine, it is unclear how much transport should remain for a balance between recycling and efficacious GlyT2 inhibition. siRNA targeting the GlyT2 gene reduces protein expression to 30% WT levels with no observable adverse effects (Morita *et al.*, 2008); significant reduction (70%) of GlyT2 activity should therefore be both safe and efficacious in treating pain. To determine optimal levels of inhibition, acyl inhibitors can be tested at *ex vivo* or *in vivo* inhibitory glycinergic synapses where glycine receptors and transporters are both present.

Table 4.1. Structure-activity relationships of amino acid conjugated lipid compounds at GlyT2 and GlyT1*

					
Compound	Head group	R	GlyT2 IC ₅₀ (nM)	GlyT1 IC ₅₀ (μM)	GlyT2 % max inhibition
21	L-Ala		1230 (649 – 2340)	>30 ^a	89.8 ± 5.8
22	D-Ala		2330 (1.26 – 4.34)	>30	81.7 ± 6.2
23	L-Val		1170 (643 – 2120)	>30	90.1 ± 5.9
24	D-Val		1000 (448 – 2570)	>30	56.7 ± 5.1
25	L-Leu		143 (70.7 – 287)	>10	72.2 ± 3.8
26	D-Leu		>30 μM ^a	>30	35.6 ± 2.6
27	L-Met		29.2 (18.6 – 45.7)	>3	91.2 ± 2.7
28	D-Met		259 (79.6 – 845)	>3	68.6 ± 8.1
29	L-NorLeu		259 (166 – 372)	>10	64.5 ± 6.9

30	L-Ser		496 (308 – 799)	>3	73.1 ± 5.1
31	D-Ser		64.8 (31.1 – 135)	>3	73.6 ± 4.4
32	L-Asp		865 (468 – 1600)	>10	76.7 ± 5.3
33	D-Asp		1810 (1050 – 3140)	>10	92.5 ± 6.9
34	L-Glu		4350 (2350 – 8070)	>10	100 ± 14.0
35	D-Glu		3750 (2240 – 6260)	>10	91.6 ± 7.9
36	L-Asn		613 (265 – 1420)	>10	92.7 ± 7.2
37	L-Phe		214 (86.4 – 530)	>10	54.7 ± 3.8
38	D-Phe		>10 μM ^a	>10	42.3 ± 2.8
39	L-C2-Phe		151 (88.8 – 257)	>10	75.1 ± 2.9
40	D-C2-Phe		>10 μM ^a	>10	10.2 ± 1.2

41	L-Trp		54.6 (31.4 – 95.8)	>10	86.2 ± 3.8
42	D-Trp		>10 μM ^a	>10	14.2 ± 3.5
43	L-His		130 (84.4 - 199)	>3	78.4 ± 3.4
44	D-His		313 (229 – 889)	>3	82.1 ± 3.3
45	L-Arg		47.9 (27.2 – 84.2)	>3	87.2 ± 3.7
46	D-Arg		69.2 (48.0 – 99.9)	>3	70.9 ± 2.2
47	L-Lys		25.5 (17.2 – 37.7)	>3	86.8 ± 2.4
48	D-Lys		48.3 (37.2 – 62.7)	>3	91.0 ± 1.9
49	L-C3-Lys		31.6 (23.1 – 43.3)	>3	86.0 ± 2.2
50	L-C2-Lys		152 (100 - 231)	>3	82.7 ± 3.3
51	L-C1-Lys		182 ^b (27.3 – 1210)	>3	58.2 ± 7.6

52	C5-NH ₃		560 (312 – 1010)	>3	86.7 ± 7.2
53	L-Lys- OMe		91.3 (37.5 - 222)	>3	78.8 ± 5.8
Compound	Tail group	R L-Lys or D-Lys	GlyT2 IC ₅₀ (nM)	GlyT1 IC ₅₀ (μM)	GlyT2 % max inhibition
54	C18 ω5		67.5 (32.6 - 140)	>3 μM	81.3 ± 5.1
55	C16 ω7		66.6 (51.1 – 86.8)	>3 μM	90.2 ± 2.1
56	C16 ω3		10.7 (8.32 – 13.9)	>3 μM	94.9 ± 1.6
57	C16 ω3		699 (367 – 1330)	>3 μM	91.8 ± 8.2

*Compounds were tested for inhibition of 30 μM glycine transport by GlyT2 and GlyT1, expressed in oocytes. n ≥ 3 with measurements taken from at least 2 batches of oocytes. Data presented are mean and 95% confidence intervals or mean ± SEM.

a. Where significant inhibition was not reached, IC₅₀ are presented as greater than the maximum concentration of each compound applied.

b. Curve could not reliably be fit from the data

4.2.6 Oleoyl L-Lys reduces radiolabelled uptake of GlyT2 expressing oocytes in a dose dependent manner

Lipids are able to exert their effects on membrane proteins through either specific interactions with select amino acid residues, or non-specific mechanisms, such as influencing the cell membrane. In order to demonstrate that a reduction in glycine-induced currents is directly related to the reduced transport by GlyT2 and not GlyT1, [³H]-glycine uptake was performed on oocytes expressing either transporter in the presence and absence of oleoyl L-Lys. There

was a dose-dependent reduction of [³H]-glycine uptake by GlyT2, and no change of glycine uptake by GlyT1, even at high concentrations of oleoyl L-Lys (Figure 4.6). This confirms N-acyl amino acid compounds are acting through inhibition of GlyT2 mediated glycine transport.

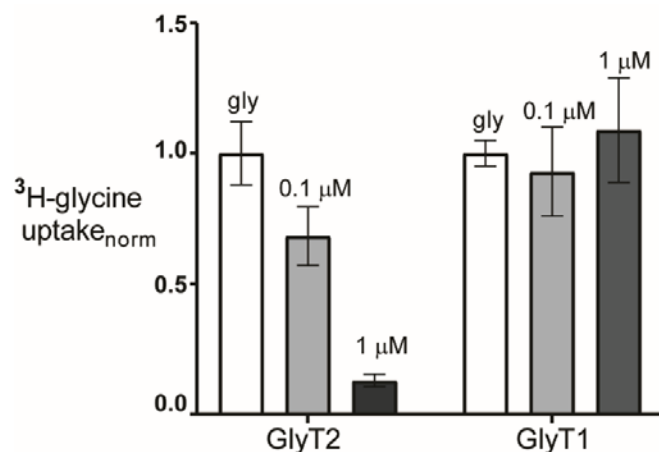


Figure 4.6. Radiolabelled uptake of [³H]-Glycine by GlyT2 but not GlyT1 is inhibited by oleoyl L-Lys. Oocytes expressing either transporter or uninjected control oocytes were pre-incubated for 2 minutes with either 100 nM or 1 μM oleoyl L-Lys (47), followed by measurement of 10 μM [³H]-Glycine uptake as described in methods.

4.2.7 Reversibility of N-acyl amino acid inhibitors

The reversibility of N-acyl amino acid inhibition was investigated by first applying an IC₅₀ concentration of inhibitor and once a stable level of inhibition was observed, washing the recording chamber with buffer. 30 μM glycine was then reapplied at 5 minute intervals throughout the wash time course to determine transport recovery, which is indicative of the reversibility of an inhibitor (Figure 4.7). For some cells, baselines were observed to drift over the course of the assay (Figure 4.8), which is a phenomenon observed both in the presence and absence of inhibitor dependent on the health and longevity of the cell. Current values were thus adjusted for the shifting baseline.

At 5 minutes post-inhibition by oleoyl L-Val and oleoyl L-Asp glycine currents were 77.7 ± 2.6% and 92.4 ± 3.2% respectively, signifying relatively fast reversibility (Figure 4.8A,

B). For L- and D- Lys analogues, recovery was slower, but steady, with most transport restored by 30 minutes (Figure 4.8D, E). Transport currents following oleoyl L-Trp application, however, did not recover at all throughout the time of the assay (Figure 4.8C), with currents at 30 minutes no greater than time 0 ($43.0 \pm 3.1\%$ and $36.7 \pm 5.1\%$ respectively). As each inhibitor was assayed at its own IC_{50} , washout rates of compounds with similar potencies should have been comparable if it was a simple binding and unbinding reaction. Instead, reversibility was shown to be dependent on the head group, but this effect was not directly correlated with potency. Oleoyl L-Trp (IC_{50} 54.6 nM) showed no recovery whilst oleoyl L-Lys (IC_{50} 25.5 nM) displayed considerable recovery after 30 minutes. The time taken to reach a stable level of inhibition also differed for each N-acyl amino acid. While application of glycine results in rapid inward currents, inhibition of this current by lipid inhibitors is comparably slow. Inhibition by L-Val and L-Asp analogues was faster than L-Lys and D-Lys, and L-Trp took ~10 minutes to reach a plateau of inhibition (Figure 4.8). Lipid ligands of membrane proteins are often proposed to first diffuse into the membrane before activating or inhibiting their targets. The slow rate of onset may therefore be a reflection of membrane insertion.

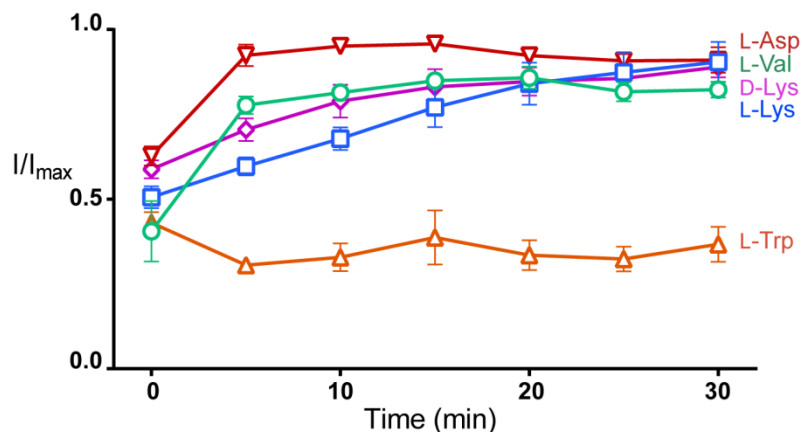


Figure 4.7. Reversibility time course for N-acyl amino inhibition of GlyT2. The EC_{50} concentration of glycine was applied to GlyT2 expressing oocytes to determine the maximal current at this dose. Acyl inhibitors were then co-applied with glycine at time 0, and then washed from the recording chamber. EC_{50} glycine was then reapplied at 5 minute intervals over a 30 minute period. Transport recovery for each compound is presented as I/I_{max} .

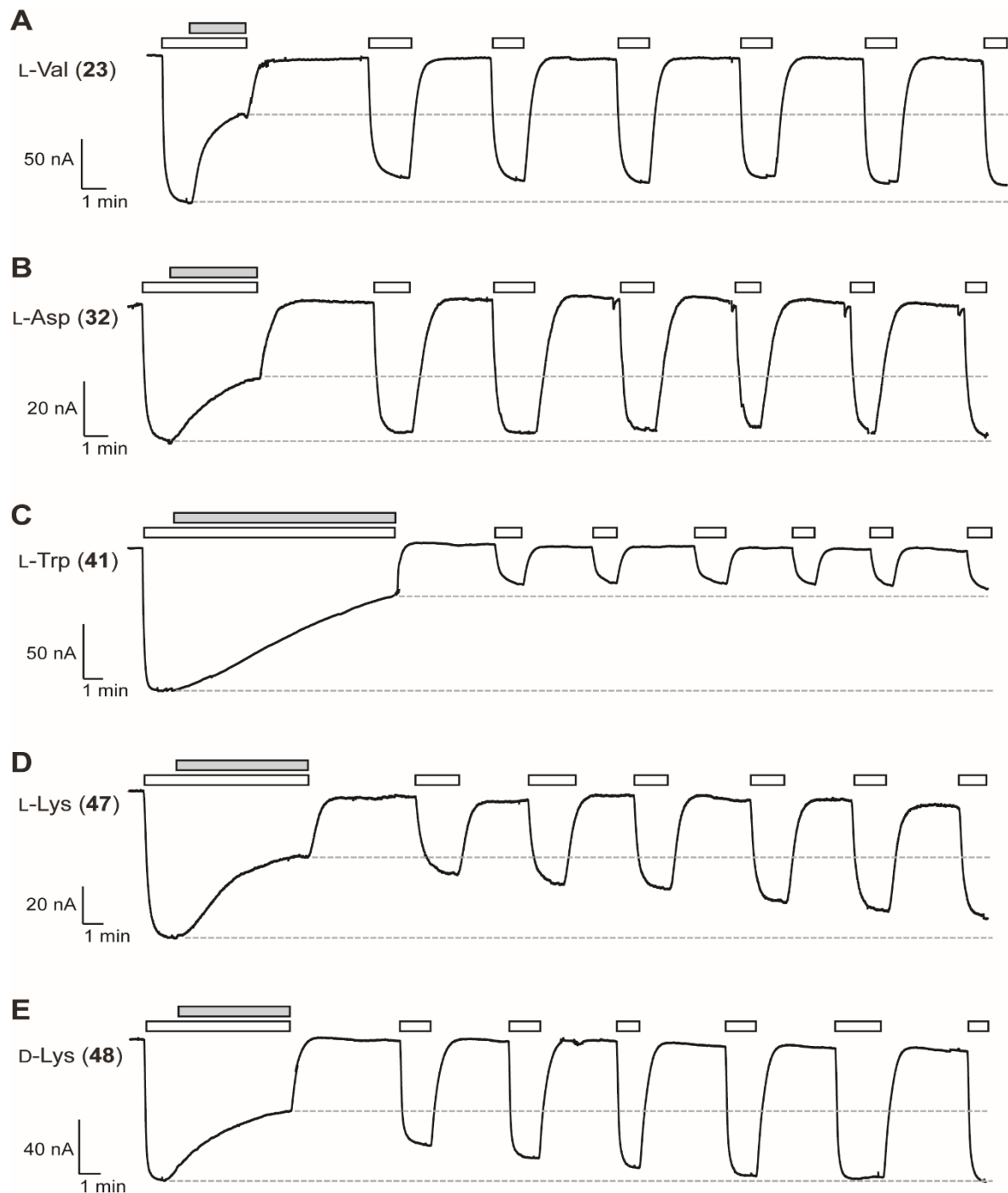


Figure 4.8. Representative traces for reversibility of select N-acyl amino acids. Glycine EC_{50} (open bars) was applied to GlyT2 expressing oocytes until stable transport was reached. The IC_{50} concentration of N-acyl amino acids was then co-applied (grey bars) until inhibition reached a plateau. Buffer was subsequently perfused over the oocytes for 30 minutes with the EC_{50} concentration of glycine reapplied at 5 minute intervals to check the transport recovery. **A.** oleoyl L-Val **B.** oleoyl L-Asp **C.** oleoyl L-Trp **D.** oleoyl L-Lys **E.** oleoyl D-Lys. Dashed lines are indicated for I_{max} and level of inhibition.

The GlyT2 lipid inhibitor OLCarn shows partial recovery after 30 minute washout, but the level and rate of recovery can be enhanced with the lipid extruding compound β -cyclodextrin (Carland et al., 2013). A tryptophan head group may increase the affinity for cell membranes by burying at the phospholipid head group:acyl tail interface (Yau *et al.*, 1998). This membrane affinity may contribute to the irreversibility of oleoyl L-Trp and slow reversibility of other acyl amino acids.

The apparent irreversibility of the L-Trp analogue could also simply be a reflection on the large size of the head group. Perhaps once the compound is lodged within its GlyT2 binding site there is much less protein flexibility and freedom for the N-acyl amino acid to be removed. The other amino acid head groups are considerably more flexible, which may explain their reversibility.

4.2.8 Metabolism of oleoyl L-Lys and oleoyl D-Lys

N-acyl amino acids may be metabolised through several pathways that can limit their in vivo half-lives and therapeutic potential. The amide bonds in N-acyl amino acids are likely to be cleaved by hydrolytic enzymes, such as fatty acid amide hydrolase (FAAH) (Giang & Cravatt, 1997), and may also be susceptible to oxidative metabolism, including cytochrome P450 hydrolates (Bornheim *et al.*, 1995) and lipoxygenases (Ueda *et al.*, 1995). Thus, the stability of L-Lys and its D-enantiomer towards hydrolysis in plasma and cytochrome P450-mediated oxidation in liver microsomes were assessed (Table 4.2). Stability assays were performed by the Centre for Drug Candidate Optimisation (CDCO) at Monash University.

Table 4.2. Degradation half-lives of N-acyl amino acids in rat plasma and liver microsomes

Head group	Degradation half-life ($t_{1/2}$; min)	
	Plasma	Liver microsomes
L-Lys	86	54
D-Lys	> 1022 ^a	> 255 ^a

a. Minimal degradation (<15%) was observed over the course of the plasma (240 minute) or liver microsome (60 minute) incubation period.

The L-Lys analogue displayed degradation half-lives of 86 minutes and 54 minutes in the rat plasma and liver microsome assays respectively. Interestingly D-Lys did not exhibit measurable degradation in either assay. It is likely that the unnatural head group orientation hinders its ability to fit within the active site of the hydrolytic enzyme/s. It is important to note that hydrolysis studies in plasma do not take into account degradation by FAAH, an important hydrolytic regulator of anandamide (N-arachidonyl ethanolamide) activity (Giang & Cravatt, 1997). FAAH is a membrane bound enzyme and as such will not be present in plasma. However, the observed stability of D-Lys *in vivo* demonstrates that incorporation of an unnatural head group configuration can improve stability to N-acyl amino acids, and that D-Lys may be sufficiently stable to achieve therapeutic effect.

4.2.9 Blood brain barrier permeability of oleoyl D-Lys

GlyT2 is expressed within the dorsal horn of the spinal cord and for GlyT2 inhibitors to show *in vivo* efficacy they must cross the blood brain barrier. Structurally similar lipids including anandamide (Maccarrone *et al.*, 2005) and DHA-dopamine (Shashoua & Hesse, 1996) are both able to cross the blood brain barrier and it was anticipated that oleoyl D-Lys would display similar permeability. This was tested directly by studying the pharmacokinetics and brain penetration *in vivo* following intraperitoneal bolus injection into rats, with the C_{max} , T_{max} , terminal half-life ($t_{1/2}$), AUC_{0-24h} , and total brain-to-plasma ratio (B/P) presented in Table 4.3. This service was also performed by CDCO.

Following administration oleoyl D-Lys was rapidly adsorbed with maximum plasma concentrations observed at the first time point (1 hour). It was then slowly cleared from plasma with a terminal half-life ($T_{1/2}$) of 10 hours. Conversely, oleoyl D-Lys concentrations in the brain were steady for the length of the sampling period. The C_{max} in the brain was 1854 ng/g (approximately 4.5 μ M), which is well above the IC_{50} value at GlyT2 (48.3 nM). The B/P ratio increased over the sampling period from 0.08 at 1 hour to 1.1 at 24 hours, and a time averaged B/P ratio of 0.31 was calculated from the AUC_{0-24h} values. Collectively, these results show that oleoyl D-Lys is stable *in vivo* and can cross the BBB.

Table 4.3. Pharmacokinetic parameters of 28 after intraperitoneal administration of a single 27.5 mg/kg dose in Sprague Dawley rats.

Parameter	Plasma	Brain
C_{max} (ng, mL, ng/g)	16690	1854
T_{max} (h)	1	24
$t_{1/2}$ (h)	10	c.n.c.
AUC_{0-24} (ng*h/mL, ng*h/g)	122473	38479
Time averaged B/P ratio	0.31	

Male Sprague Dawley rats received a single intraperitoneal dose of oleoyl D-Lys (27.5 mg/kg) and plasma and brain concentrations were measured over a 24-hour period. Concentration max (C_{max}), time at max concentration (T_{max}), half-life ($t_{1/2}$), and area under the curve (AUC) was calculated from the data.

c.n.c – Could not calculate as the flat profile precluded an estimation of half life

4.2.10 Analgesic activity of oleoyl D-Lys on a partial nerve ligation rat model of neuropathic pain

Encouraged by the stability of oleoyl D-Lys and its ability to cross the BBB, male Sprague Dawley rats with a partial nerve ligation injury were tested for allodynia following an intraperitoneal injection at varying concentrations of oleoyl D-Lys (Figure 4.9). Healthy rats tolerated pressures of 12.3 ± 1.6 g (low dose group) and 14.2 ± 0.84 g (high dose group) Von Frey filaments. This tolerance was markedly reduced following partial nerve ligation surgery which induces a neuropathic pain phenotype in rats (low dose 0.20 ± 0.0 g; and high dose 0.93 ± 0.73 g). Intraperitoneal injection of either 3 mg/kg or 30 mg/kg of oleoyl D- Lys;

increased the paw withdrawal threshold to a peak pressure of 3.1 ± 1.0 g and 8.5 ± 3.2 g respectively, 15 minutes following administration, which were then reduced for the length of the testing period. Overall, there was a dose dependent reduction in allodynia experienced by partial nerve ligation injured rats following intraperitoneal injection of oleoyl D-Lys; this inhibitor is therefore likely to cross the BBB to achieve on target effects at glycinergic inhibitory synapses in the dorsal horn of the spinal cord.

Any treatment for chronic pain will be ongoing, and further studies on the long-term application of oleoyl D-Lys should be performed. Oleoyl D-Lys persists in brain tissue and is degraded slowly which may allow for accumulation in the CNS. N-acyl amino acids which are not full inhibitors will still allow for vesicular recycling of glycine, and in this case long-term stability of compounds may prove beneficial for long term efficacy, and may circumvent adverse side effects associated with full, irreversible inhibition.

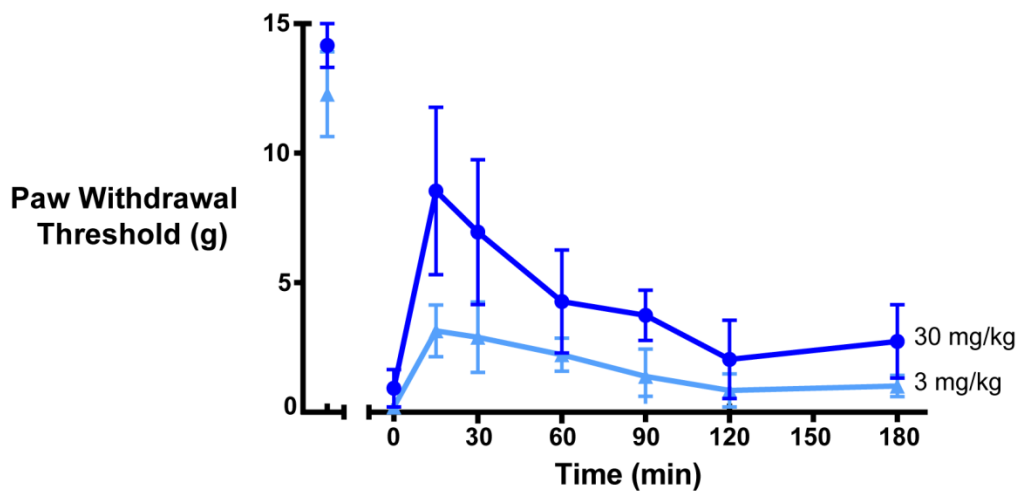


Figure 4.9. Von Frey threshold for partial nerve ligation injured rats following injection of oleoyl D-Lys. Male Sprague Dawley rats were tested for allodynia using the Von Frey test. Paw withdrawal was measured prior to and following a partial nerve ligation surgery (time 0). Following low dose (3 mg/kg) or high dose (30 mg/kg) bolus intraperitoneal injections of oleoyl D-Lys, paw withdrawal was again measured over the course of 180 minutes. Data are averages \pm SEM from $n=3$. Performed by Dr Sarasa Mohammadi (USYD).

4.3 Conclusions

By conjugating a broad range of amino acids to the [C18 *cis*- ω 9] oleoyl tail, a large pool of inhibitors of GlyT2 have been identified, most of which have similar or improved potency compared with NAGly and other acyl-glycine compounds. It has been determined that N-acyl amino acids are active with the order of potency: positively charged > aromatic >> aliphatic > negatively charged, and that L- isomers are more active than D-isomers in majority of cases. Although both positive and negative side chains are accommodated, a positively charged side chain confers a much higher (~85-fold) apparent affinity, which implies information about molecular determinants of the binding site. I propose that the binding site is comprised of aromatic amino acids to coordinate the head group, and a structurally defined aliphatic cavity to cradle the ideal [oleoyl] acyl tail.

While oleoyl L-Lys (IC₅₀ 25.5 nM), has an apparent affinity ~353-fold higher than NAGly, it is limited by its metabolic instability. The D-enantiomer is also a potent GlyT2 inhibitor (IC₅₀ 48.3 nM), is metabolically stable, and is rapidly absorbed into the CNS following IP administration. It has also been demonstrated that oleoyl D-Lys is antiallodynic in preliminary pain studies of PNL rats. In this chapter I have expanded the pool of GlyT2 lipid inhibitors to include a broad range of lipids with different properties. I have revealed important moieties which confer faster or slower rates of reversibility, different levels of inhibition (57 – 100%), and identified 12 inhibitors with an IC₅₀ value below 100 nM. GlyT2 is a challenging drug target as many compounds which have been developed to target GlyT2 display undesirable inhibitory properties (irreversibility, full inhibition). It is presently unknown which attributes are ideal *in vivo*, and perhaps by testing a range of different inhibitors optimal properties can be resolved.

Chapter 5: Molecular determinants for acyl amino acid inhibition of GlyT2

5.1 Introduction

Structure-activity studies of acyl inhibitors provide insight into binding, but, it is still unknown how they interact with GlyT2 to cause inhibition. At present there are no crystal structures of glycine transporters, however crystal structures of related transporters in different conformational states can help to infer regions of GlyT2 that may influence lipid interactions and be involved in the mechanism of inhibition by acyl amino acids. Crystal structures of the dopamine (DAT), serotonin (SERT), and bacterial leucine (LeuT) transporters, suggest a common transport mechanism where; substrate and co-transported ions enter the aqueously accessible extracellular facing vestibule; large movements of extracellular loop 4 (EL4) close the extracellular gate; and rearrangement of core transmembrane (TM) helices allow TM1a to swing open and release substrate into the cytoplasm (Coleman *et al.*, 2016; Krishnamurthy & Gouaux, 2012; Penmatsa *et al.*, 2013, 2015; Wang *et al.*, 2015; Yamashita *et al.*, 2005). While members of this family share a common transport mechanism, they differ in the population of co-transported ions, and molecular determinants of the substrate binding sites. GlyT2 possesses the smallest substrate binding site and only permits the binding of the simplest amino acid, glycine. We have shown previously that mutation of the substrate site allows for transport of larger amino acids (Carland *et al.*, 2018), but that these mutant transporters are not differentially inhibited by NAGly and OLCarn (unpublished data). Additionally, it has been demonstrated that NAGly and OLCarn do not competitively inhibit transport of glycine (Carland *et al.*, 2013; Wiles *et al.*, 2006). It appears that lipid inhibitors bind allosterically to GlyT2, but this site remains elusive.

In addition to substrate bound crystal structures of neurotransmitter transporters, there are a number of inhibitor bound structures which can give insight into transport-unfavourable conformations. In each of the inhibitor bound structures of *Drosophila* DAT (dDAT) and human SERT (hSERT), the transporters are in outward-open conformations with core TM helices in

positions incongruous with the occlusion of the binding site. In the nortriptyline bound dDAT structure (Penmatsa *et al.*, 2013) there is a 10 Å opening compared to the occluded substrate bound structure of LeuT (Yamashita *et al.*, 2005), which suggests inhibitors that bind in the primary site stop transport by preventing the closure of the extracellular gate. Additionally, LeuT has been shown to favour the outward-open conformation in the presence of β -octyl glucoside, even when Na^+ and leucine are present (Kazmier *et al.*, 2014). It is apparent that stabilisation of the outward-open conformation is a common mechanism for inhibitors of the NSS transporters which prevent transport even in otherwise transport-favourable conditions.

In addition to structures of classical NSS inhibitors bound within the central cavity of these transporters, a structure of dDAT has been elucidated which has a cholesterol molecule bound to a membrane-exposed surface of the transporter, between helices TM1a, TM5, and TM7 (Penmatsa *et al.*, 2013). It has been suggested that cholesterol may be an allosteric modulator of dopamine transport; its presence in this membrane exposed cavity may inhibit important conformational changes of TM1a required for transport (Zeppellin *et al.*, 2018). While glycine transporters do not appear to be modulated by membrane cholesterol (Liu *et al.*, 2009), this site may be conserved within GlyT2, as it is proposed to similarly inhibit serotonin and noradrenaline transporters (Zeppellin *et al.*, 2018). It has also been demonstrated in our lab that mutation of the equivalent TM1a residues in GlyT2 does not abolish inhibition by lipid inhibitors (unpublished data); however it is possible that there are a number of similar lipid binding sites on GlyT2. Rates of OLCarn reversibility are slow, and this can be accelerated using the membrane lipid extruding compound, β -cyclodextrin, which suggests lipid inhibitors may interact at membrane exposed region of GlyT2 (Carland *et al.*, 2013).

While intracellular hinging of TM1a is necessary for substrate release into the cytoplasm, large extracellular movements of EL4 are required to occlude the substrate and close the extracellular gate. Lipid inhibitors could similarly target any region which must undergo substantial conformational changes. EL4 is essential for the inhibition of GlyT2 by the inhibitors NAGly and OLCarn; chimeric GlyT2 transporters containing an EL4 region from GlyT1

(GlyT2(GlyT1-EL4)) are insensitive to inhibition (Carland *et al.*, 2013; Edington *et al.*, 2009). Furthermore, a single point mutation in EL4, I545L, results in transporters with reduced sensitivity to lipid inhibitors. These compounds may inhibit GlyT2 by obstructing the movements of EL4, locking it in a conformation that is not conducive to transport.

The membrane exposed transmembrane domains TM7 and TM8 flank EL4 (Figure 5.1) and guide its movements. For example, TM7 tilts 17° from the core of the transporter to allow EL4 to plug the vestibule (Kazmier *et al.*, 2014; Krishnamurthy & Gouaux, 2012). TM7 and TM8 are both membrane exposed helices that could provide a point of interaction between protein and membrane for GlyT2 lipid inhibitors, which may greatly influence the movements of EL4 to stall transport of glycine. In this chapter, I generated 14 mutant glycine transporters with changes to EL4, TM7, and TM8, as well as the adjacent helices TM1, TM3, and TM5, to tease out the mechanism of inhibition by different acyl-glycine and acyl amino acid inhibitors presented in the previous chapters.

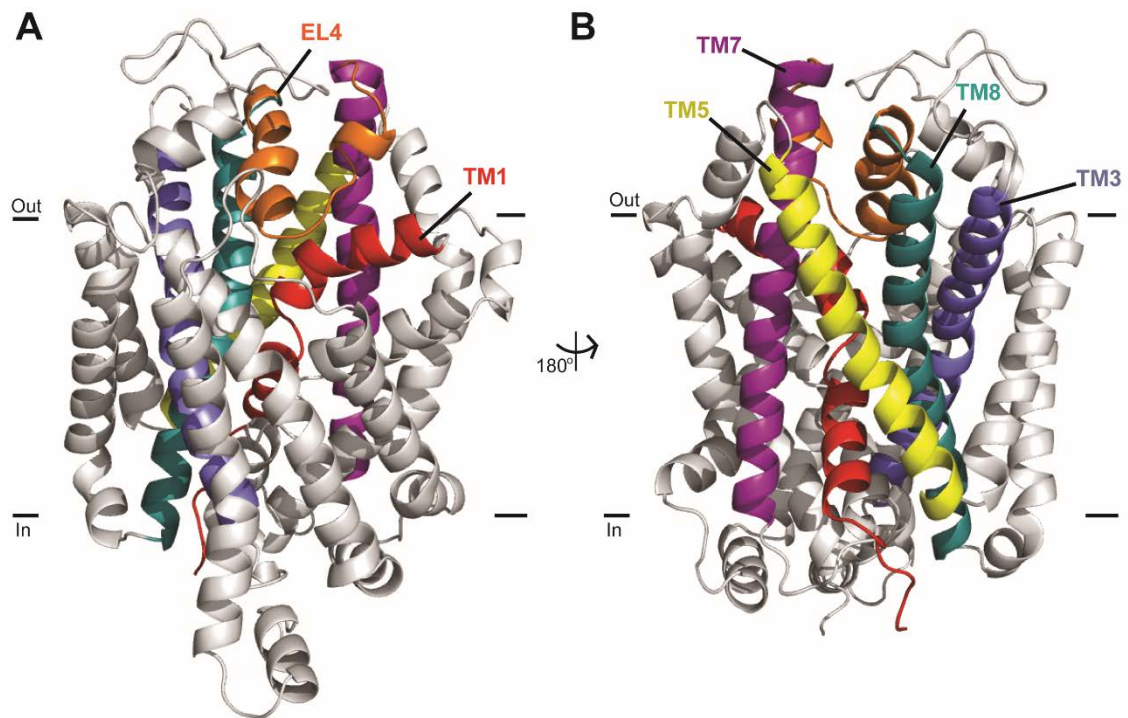


Figure 5.1. Homology model of GlyT2 shown in plane of the membrane. A. front face and **B.** reverse face. Mutated helices and loops are coloured, EL4 (orange), TM1 (red), TM3 (blue), TM5 (yellow), TM7 (purple), and TM8 (teal).

5.2 Results and Discussion

5.2.1 Oleoyl L-Lys is not a competitive inhibitor of GlyT2

GlyT2 possesses the smallest substrate binding site of the NSS family and is only able to transport the smallest amino acid, glycine (Carland *et al.*, 2018). While NAGly contains a glycine head group, it is conjugated to a large polyunsaturated lipid tail via its backbone nitrogen. This adds considerable bulk to the compound, and removes the capacity for the amine to form important interactions in the glycine binding site. NAGly has also been previously shown to be a non-competitive GlyT2 inhibitor (Wiles *et al.*, 2006), and is therefore unlikely to bind at a site overlapping the substrate binding site. Similarly, it has been demonstrated that OLCarn displays a mixed mechanism of inhibition at GlyT2 (Carland *et al.*, 2013).

The synthesised N-acyl amino acids presented in Chapter 4 contain side-chains that add additional bulk to the head group, making them larger and chemically different to the glycine head group of NAGly. To ascertain whether these N-acyl amino acids are likely to possess a similar mechanism of inhibition, glycine concentration responses were measured in the presence of increasing concentrations of oleoyl L-Lys (Figure 5.2A). The apparent affinities for glycine at each concentration of inhibitor (EC_{50} [10 nM inhibitor] = $14.0 \pm 2.7 \mu\text{M}$; [30 nM inhibitor] = $23.5 \pm 8.0 \mu\text{M}$; [1 μM inhibitor] = $12.8 \pm 7.6 \mu\text{M}$) were not significantly different to the EC_{50} for glycine transport in the absence of any inhibitor ($15.8 \pm 1.3 \mu\text{M}$). Conversely, the I_{max} was significantly reduced for all concentrations of C18 ω 9 L-Lys (% I_{max} [10 nM] = $82.8 \pm 4.0\%$ *; [30 nM] = $62.4 \pm 5.8\%$ ***; [1 μM] = $30.2 \pm 4.4\%$ ***). This indicates that oleoyl L-Lys acts as a non-competitive inhibitor of GlyT2, however an Eadie-Hofstee plot of the data suggests that the mechanism may not be purely non-competitive (Figure 5.2B). Lipid inhibitors may display a mixed mechanism of action where the allosteric inhibitor site greatly influences glycine binding at the substrate site. It has previously been shown that residues at the substrate binding site are not important for the mechanism of inhibition (unpublished data). It is unlikely that large bulky acyl inhibitors bind in the narrow substrate binding cavity at the base of the extracellular vestibule, and rather cause inhibition through action at another allosteric site, which is the focus of this thesis chapter.

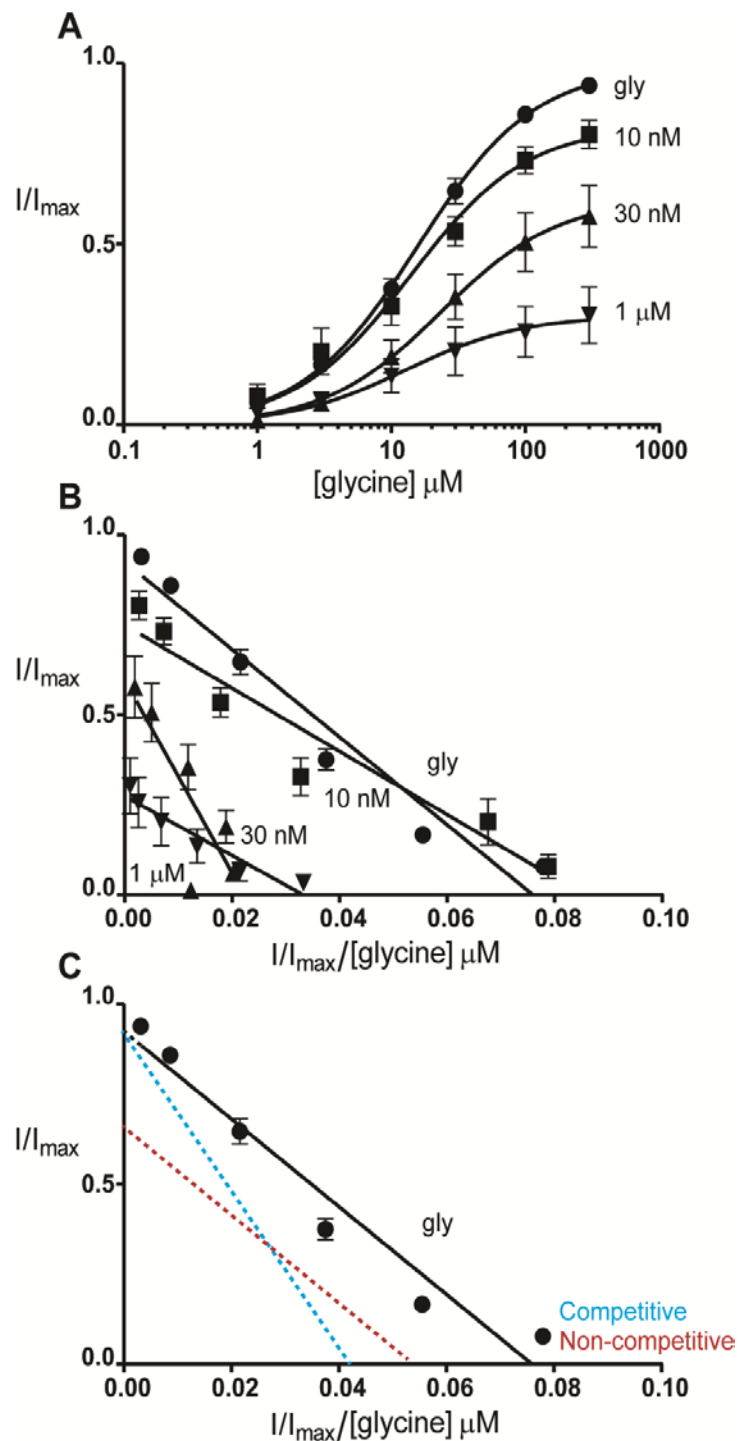


Figure 5.2. Oleoyl L-Lys reduces concentration-dependent glycine currents. A.

Concentration-dependent glycine transport currents with increasing concentrations of oleoyl L-Lys. ANOVA tests were performed for EC_{50} and I_{max} values **B**. Eadie-Hofstee plot of data from A. **C**. Representative linear fit of hypothetical competitive (blue) or non-competitive (red) inhibitors using an Eadie-Hofstee transformation. The data in panels A and B do not fit either

case. ● gly ■ 10 nM ▲ 30 nM ▼ 1 μM

5.2.2 Screening of residues which may be involved in the mechanism of inhibition by lipid inhibitors

To locate the allosteric binding site of lipid GlyT2 inhibitors, a selection of mutations were made (Figure 5.3, Figure 5.4) which were either in close proximity to EL4 (TM1: A221C/F222Y/Q223R; TM3: F302A and S304A; TM5: R439L; TM8: P561S, F562L, and W563L; EL4: Y550L and E552A), or in membrane exposed regions which may influence the movements of EL4 (TM5: F428A; TM7: C507I and F515Y; TM8: L569F). GlyT1 is 48% identical to GlyT2 (Morrow *et al.*, 1998) and yet it is insensitive to acyl inhibition. This differential sensitivity was used to identify potential residues for mutation and where aligned residues in each of the TM domains differed between GlyT1 and GlyT2, the GlyT2 residue was mutated to the corresponding residue in GlyT1. Mutations were also selected using structure activity data presented in previous chapters which suggests that aromatic residues may play a role in coordinating the head group of acyl amino acids.

	TM1a														TM1b														
GlyT2	L	D	F	I	L	S	M	V	G	Y	A	V	G	L	G	N	V	W	R	F	P	Y	L	A	F	Q	223		
GlyT1	Q	I	E	F	V	L	T	S	V	G	Y	A	V	G	L	G	N	V	W	R	F	P	Y	L	C	Y	R		
DAT			D	F	L	L	S	V	I	G	F	A	V	D	L	A	N	V	W	R	F	P	Y	L	C	Y	K		
LeuT	R	L	G	L	I	L	A	M	A	G	N	A	V	G	L	G	N	F	L	R	F	P	V	Q	A	A	E		

	TM3																																						
GlyT2	P	A	L	Q	G	C	G	I	A	M	L	I	I	S	V	L	I	A	I	Y	Y	N	V	I	I	C	Y	T	L	F	Y	L	F	A	S	F	V	S	304
GlyT1	P	M	F	K	G	V	G	Y	G	M	M	V	V	S	T	Y	I	G	I	Y	Y	N	V	V	I	C	I	A	F	Y	Y	F	F	S	S	M	T	H	
DAT	P	I	L	K	G	V	G	F	T	V	I	L	I	S	L	Y	V	G	F	F	Y	N	V	I	I	A	W	A	L	H	Y	L	F	S	S	F	T	T	
LeuT	R	F	A	K	I	L	G	V	F	G	L	W	I	P	L	V	V	A	I	Y	Y	V	Y	I	E	S	W	T	L	G	F	A	I	K	F	L	V	G	

	TM5																									
GlyT2	I	K	T	S	G	K	V	V	Y	F	T	A	T	F	P	Y	V	V	L	V	I	L	L	I	R	439
GlyT1	V	K	S	S	G	K	V	V	Y	F	T	A	T	F	P	Y	V	V	L	T	I	L	F	V	R	
DAT	V	K	T	S	G	K	V	V	W	I	T	A	T	M	P	Y	V	V	L	T	A	L	L	L	R	
LeuT	I	E	R	F	A	K	I	A	M	P	T	L	F	I	L	A	V	F	L	V	I	R	V	F	L	

	TM7																																
GlyT2	C	Y	R	D	T	L	I	V	T	C	T	N	S	A	T	S	I	F	A	G	F	V	I	F	S	V	I	G	F	M	A	N	529
GlyT1	C	Y	R	D	S	V	I	I	S	I	T	N	C	A	T	S	V	Y	A	G	F	V	I	F	S	I	L	G	F	M	A	N	
DAT	C	Y	R	D	A	I	V	T	T	S	I	N	S	L	T	S	F	S	S	G	F	V	V	F	S	F	L	G	Y	M	A	Q	
LeuT	I	V	L	S	G	L	T	A	A	T	L	N	E	K	A	E	V	I	L	G	G	S	I	S	I	P	A	A	V	A	F	F	

	EL4																														
GlyT2	E	R	K	V	N	I	E	N	V	A	D	Q	G	P	G	I	A	F	V	V	Y	P	E	A	L	T	R	L	P	L	559
GlyT1	H	L	G	V	D	V	S	R	V	A	D	H	G	P	G	L	A	F	V	A	Y	P	E	A	L	T	L	L	P	I	
DAT	K	H	S	V	P	I	G	D	V	A	K	D	G	P	G	L	I	F	I	I	Y	P	E	A	I	A	T	L	P	L	
LeuT	G	V	A	N	A	V	A	I	A	K	A	G	A	F	N	L	G	F	I	T	L	P	A	I	F	S	Q	T	A	G	

	TM8																														
GlyT2	S	P	F	W	A	I	I	F	F	L	M	L	L	T	L	G	L	D	T	M	F	A	T	I	E	T	I	V	T	S	589
GlyT1	S	P	L	W	S	L	L	F	F	F	M	L	I	L	L	G	L	G	T	Q	F	C	L	L	E	T	L	V	T	A	
DAT	S	S	A	W	A	V	V	F	F	I	M	L	L	T	L	G	I	D	S	A	M	G	G	M	E	S	V	I	T	G	
LeuT	G	T	F	L	G	F	L	W	F	F	L	L	F	F	A	G	L	T	S	S	I	A	I	M	Q	P	M	I	A	F	

Figure 5.3. Sequence alignment of GlyT2, GlyT1, DAT, and LeuT. Regions of interest are coloured TM1 (red), TM3 (blue), TM5 (yellow), TM7 (purple), EL4 (orange), and TM8 (teal) corresponding to Figure 5.1. Conserved residues are coloured grey. I545 is indicated with a green box, and residues which were mutated are indicated with cyan boxes.

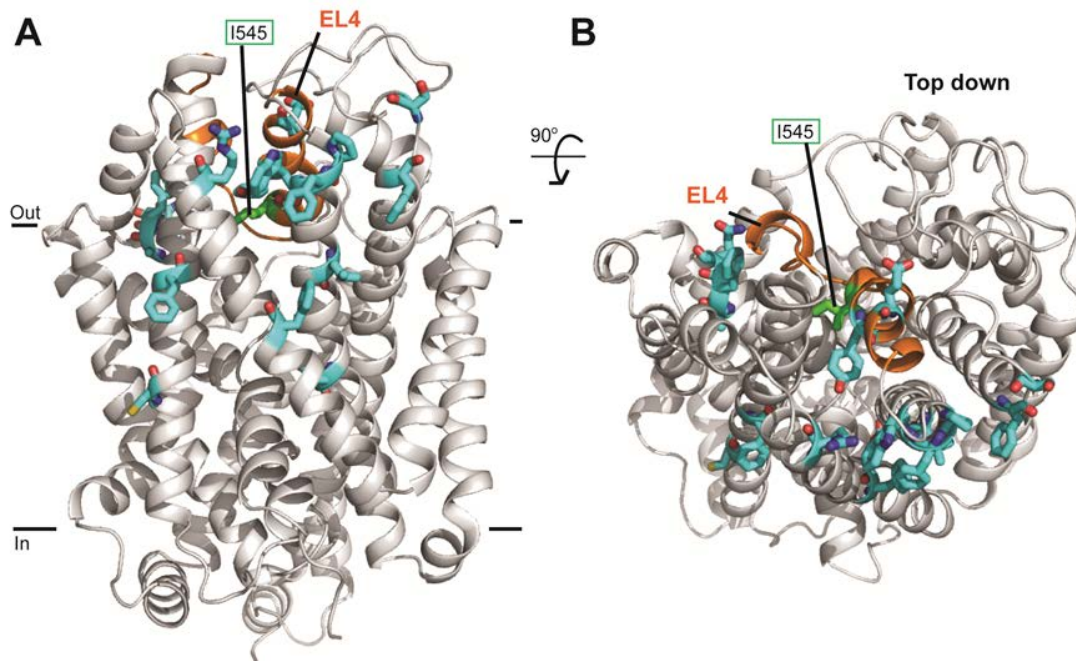


Figure 5.4. Location of mutated residues on GlyT2. A. Reverse face **B.** Top down. Residues which were mutated are shown in sticks and coloured cyan (carbon), red (oxygen), blue (nitrogen). I545 is also shown in green sticks. EL4 is coloured orange.

For WT GlyT2, co-application of 1 μM OLCarn with the EC_{50} concentration of glycine reduces currents by $60.3 \pm 2.8\%$ (Figure 5.5); this dose is sufficient to observe any changes in OLCarn sensitivity. Therefore, in order to determine differential inhibition by mutant transporters, this dose was applied as an initial screen. None of the mutants in TM1 or TM3 displayed any change in inhibition compared to WT (Figure 5.5). Similarly, inhibition of R439L, C507I, E552A, and F562L transporters were comparable to WT.

F428A, Y550L, P561S, W563L, and L569F transporters were less sensitive to inhibition by OLCarn with inhibition only reaching 14.9 – 29.0%. Conversely, the TM7 mutant F515W increased the inhibitory effect, with transport inhibited $93.8 \pm 3.7\%$. For each of the mutants with differential sensitivity at the screening dose, concentration response curves for select lipid inhibitors were performed. Additionally, I545L (Carland *et al.*, 2013; Edington *et al.*, 2009) was re-examined to determine its importance with the new group of synthesised N-acyl amino acid inhibitors.

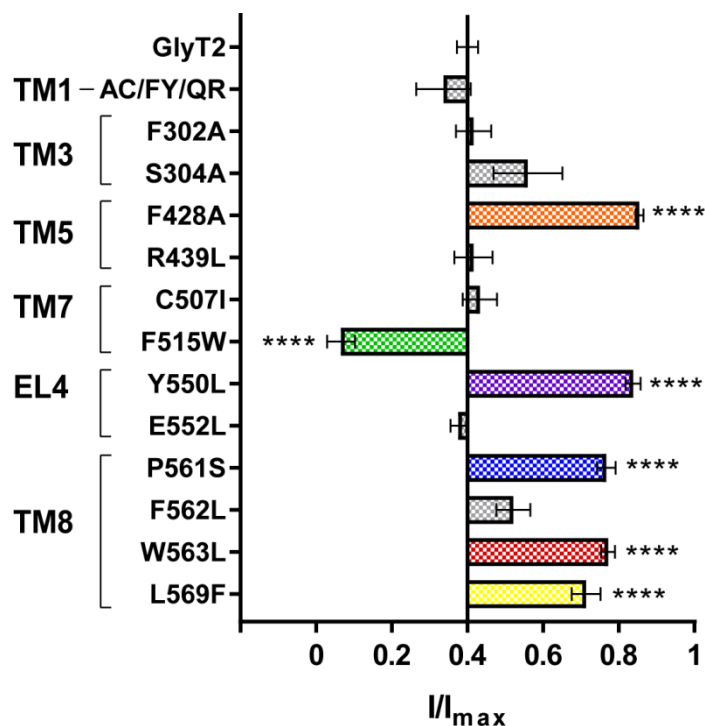


Figure 5.5. Inhibition of WT and mutant GlyT2 transporters by 1 μ M OLCarn. Glycine was applied to transporters followed by co-application of glycine and OLCarn until a plateau in inhibition was reached. The reduced glycine transport currents were normalised to the current elicited by the initial glycine application. Data represented are means \pm SEM ($n \geq 3$) with **** $p < 0.001$ following a one way ANOVA.

5.2.3 Glycine affinity of mutant transporters

The function of mutant transporters was tested to ensure any small changes in the protein did not greatly affect glycine transport. Although the mechanism of inhibition does not appear to be affected by glycine concentrations, some residues which were mutated are important in the mechanism of transport, particularly residues in TM8 which partially form the glycine and one of the Na^+ binding sites. For GlyT2 and GlyT1 WT transporters, the obtained EC_{50} values are consistent with published values (12 μM and 20 μM respectively; Vandenberg *et al.*, 2007). All mutants tested were functional glycine transporters, with small but non-significant deviations in EC_{50} compared to WT GlyT2 or GlyT1 (Figure 5.6, Table 5.1). The EL4 mutations in both GlyT2 and GlyT1 (Y550L and L425I respectively) have reduced glycine affinities compared to WT. EL4 plays an important role in extracellular gating which may explain these differences.

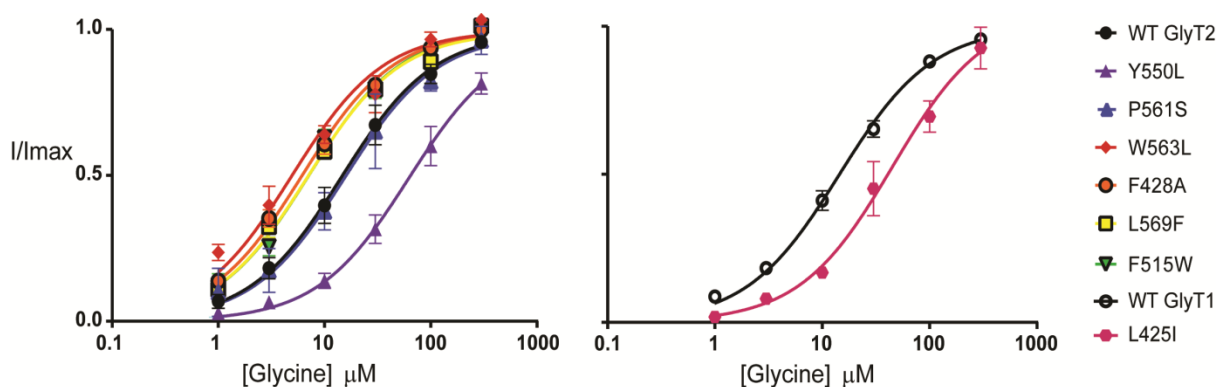


Figure 5.6. Glycine dependent transport currents for WT and mutant transporters. A. GlyT2 and **B.** GlyT1. Transport currents were measured in the presence of increasing concentrations of glycine (1 – 300 μM). Currents were fit to the modified Michaelis-Menten equation (see methods) and normalised to the calculated I_{max} . Data shown represents mean \pm SEM ($n \geq 3$).

Table 5.1. EC_{50} values for glycine transport of WT and mutant GlyT2 and GlyT1 transporters.

Region	Mutation	Glycine EC_{50} (μM)
GlyT2		
GlyT2 WT		14.5 ± 2.6
EL4	Y550L	62.2 ± 11.4
TM8	P561S	15.5 ± 4.1
	W563L	4.9 ± 0.8
	L569F	7.0 ± 0.6
TM5	F428A	6.2 ± 0.4
TM7	F515W	7.1 ± 0.7
GlyT1		
GlyT1 WT		14.4 ± 1.2
EL4	I425L	45.1 ± 9.6

Glycine concentration response curves were performed on WT and mutant transporters to generate EC_{50} values. A one-way ANOVA determined any difference in mutant GlyT2 affinity compared to WT GlyT2. A two-tailed t test compared mutant (L425I) GlyT1 with WT GlyT1. No EC_{50} values were considered significantly different than WT.

5.2.4 Differential selectivity of GlyT1 and GlyT2

It has been suggested that a single amino acid residue difference at the tip of EL4 (Figure 5.4) between GlyT1 and GlyT2 is responsible for the differential selectivity of OLCarn. Substitution of I545 with a leucine residue reduces GlyT2 inhibitor sensitivity to that of GlyT1 (Carland *et al.*, 2013). To determine whether I545 is as critical to inhibition by the newly synthesised compounds in Chapter 4, a selection of N-acyl amino acids were applied to the I545 mutant (Figure 5.7). It was shown that acyl compounds with a diverse range of head groups (L-Val, L-Asp, or L-Trp) have a drastically reduced apparent affinity and maximal level of inhibition (Table 5.2). For the L-Lys compound however, while the IC_{50} is ~17-fold higher, 80.7% inhibition could still be attained, which is significantly greater than the activity at WT GlyT1. Though clearly important, I545 is not the only molecular determinant for specificity of lipid GlyT2 inhibitors.

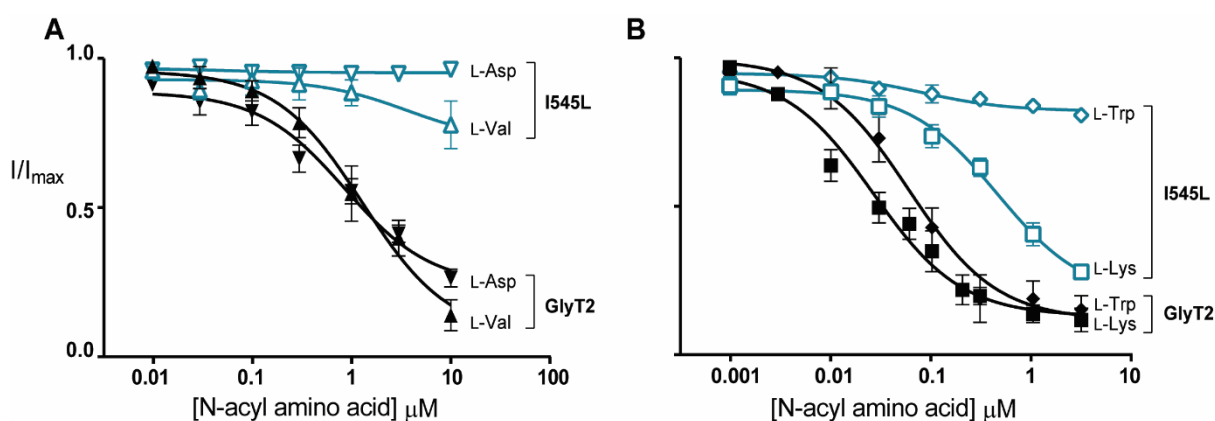


Figure 5.7. Acyl amino acids inhibit glycine transport currents of I545L mutant GlyT2 transporters expressed in *Xenopus laevis* oocytes. Glycine transport currents were measured in the presence of lipids. **A.** Concentration–inhibition curves for compounds **23** and **32**. **B.** Concentration–inhibition curves for compounds **41** and **47**. The responses are normalized mean values \pm SEM ($n \geq 3$ cells) fit using least-squares analysis. WT GlyT2 data has been shown in the previous chapters but is included for comparison (black curves). I545L is shown in teal. Δ L-Val ∇ L-Asp \diamond L-Trp \square L-Lys

While inhibition of the GlyT2(GlyT1-EL4) chimera is comparable to GlyT1, the reverse GlyT1(GlyT2-EL4) chimera remains insensitive to NAGly but has increased sensitivity to N-arachidonyl L-alanine (Edington *et al.*, 2009). To further investigate the selectivity, I created the corresponding reverse GlyT1 single point mutation, L425I. For lipid inhibitors with a Gly head group, L425I is insensitive, similar to the GlyT1 response; but inhibition of L425I by OLCarn is comparable to WT GlyT2 (IC₅₀ 195 nM; max. inhibition 74.6%). It is striking that such a conservative mutation is sufficient to impart the OLCarn GlyT2 inhibitory phenotype into GlyT1. Thus it appears that the binding site must be mostly formed in GlyT1, and the selectivity for the compounds may lie in the mechanism of inhibition rather than the binding itself.

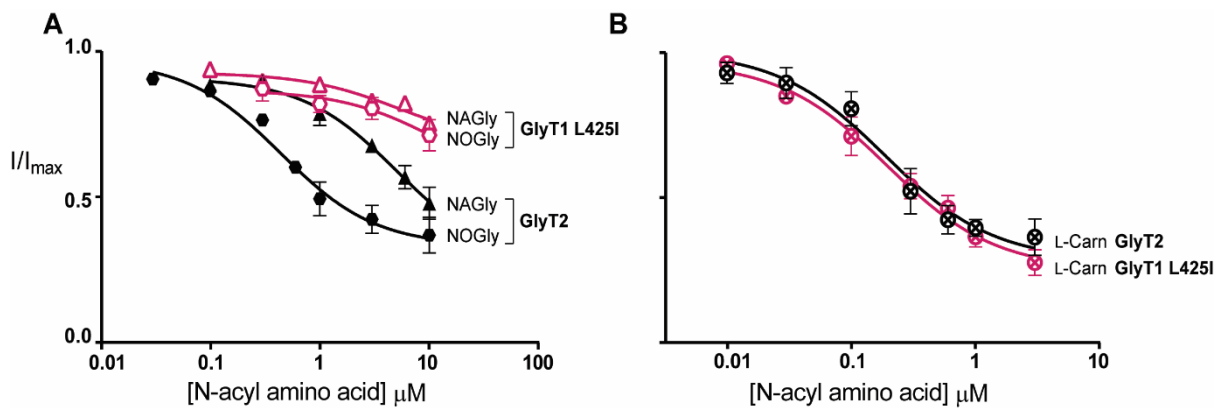


Figure 5.8. Acyl amino acids inhibit glycine transport currents of L425I mutant GlyT1 transporters expressed in *Xenopus laevis* oocytes. Glycine transport currents were measured in the presence of lipids. **A.** Concentration–inhibition curves for compounds **1** and **2**. **B.** Concentration–inhibition curves for OLCarn. The responses are normalized mean values \pm SEM ($n \geq 3$ cells) fit using least-squares analysis. WT GlyT2 data has been shown in the previous chapters but is included for comparison (black curves). GlyT1 L425I is shown in pink. Δ NAGly \circ NOGly \otimes L-Carn

5.2.5 Y550 is important in the mechanism of inhibition by lipid GlyT2 inhibitors

EL4 is important in conferring selectivity for GlyT2 over GlyT1, but little is understood about the binding site of lipid inhibitors. Previous investigation of EL4 involved the creation of single point mutations of residues that differ between GlyT1 and GlyT2. As I propose the binding site is partially formed in GlyT1, residues which are conserved between the two may also be important for binding. Y550 (Y430 in GlyT1, Figure 5.3) lies approximately one turn of the helix up from I545 and, in our homology model, points into what may be a substantial cavity between EL4, TM5, TM7, and TM8 (Figure 5.9).

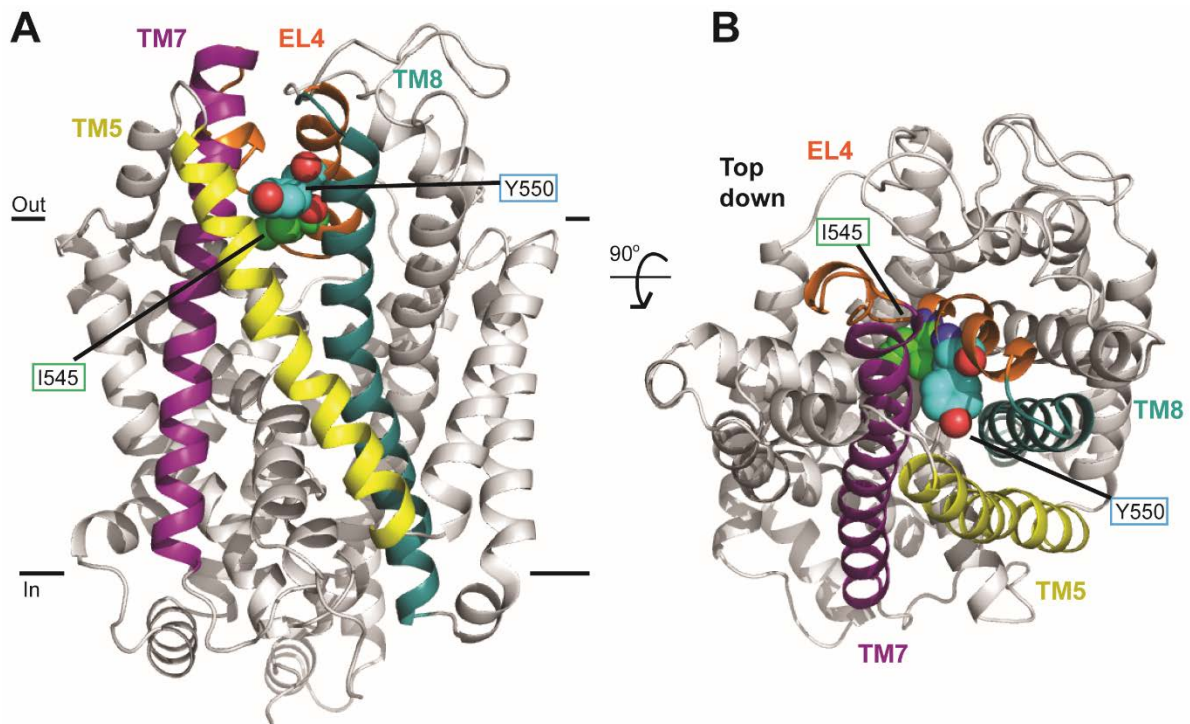


Figure 5.9. Location of mutations in EL4. EL4 is shown in orange, TM5 shown in yellow, TM7 shown in purple, and TM8 shown in teal. **A.** In plane of the membrane from the reverse face and **B.** Top down. Y550 (cyan spheres) is approximately one turn of the helix up from I545 (green spheres).

All of the acyl amino acids tested had reduced apparent affinity and maximal level of inhibition to the Y550L mutant (Table 5.2), which suggests both binding and ability to cause inhibition is affected. The effect of compounds with larger L-Trp and L-Arg head groups was most striking, with transport in the presence of the acyl amino acid unchanged compared to transport in the absence of inhibitor ($IC_{50} >3 \mu\text{M}$ for Y550L compared to 54.6 nM and 47.9 nM for WT respectively) (Figure 5.10C, D), where smaller head groups (Gly) and aliphatic side chains (L-Leu and L-Val) had IC_{50} values only 1.5-3-fold higher than WT GlyT2.

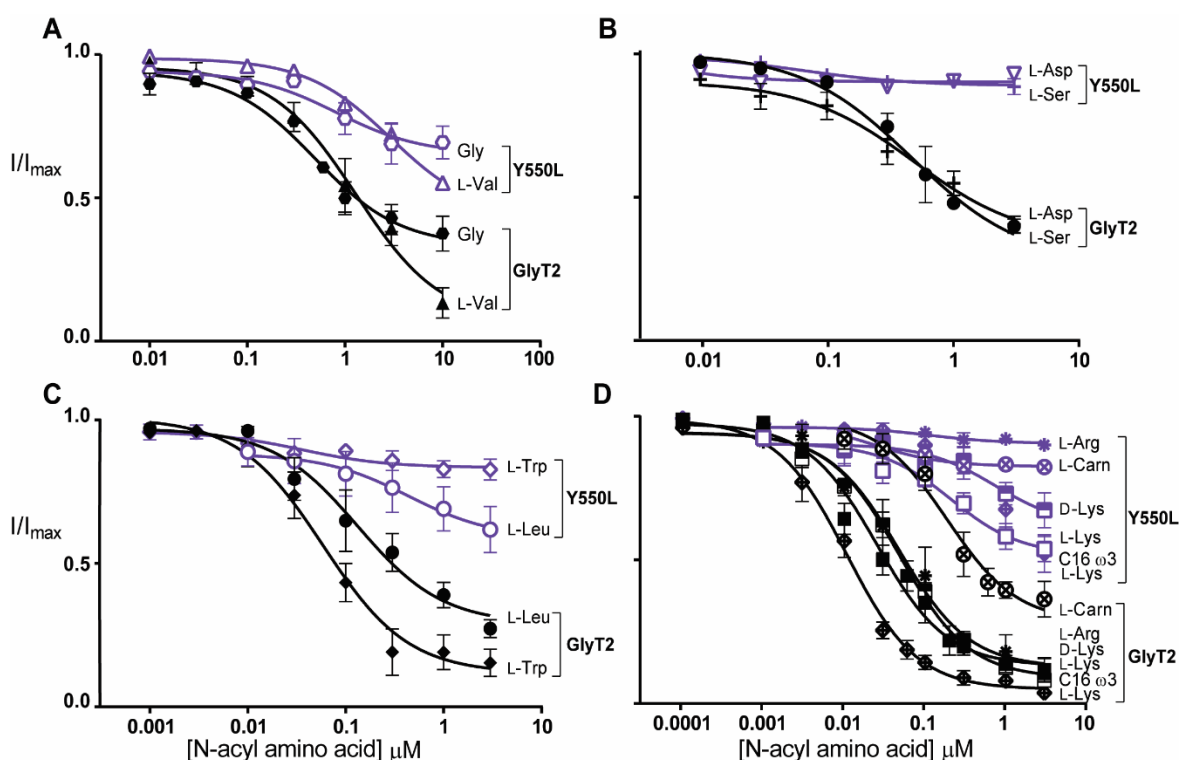


Figure 5.10. Acyl amino acids inhibit glycine transport currents of Y550L mutant GlyT2 transporters expressed in *Xenopus laevis* oocytes. Glycine transport currents were measured in the presence of lipids. **A.** Concentration–inhibition curves for compounds **2** and **23**. **B.** Concentration–inhibition curves for compounds **30** and **32**. **C.** Concentration–inhibition curves for compounds **25** and **41**. **D.** Concentration–inhibition curves for compounds OLCarn, **45**, **47**, **48**, and **56**. The responses are normalized mean values \pm SEM ($n \geq 3$ cells) fit using least-squares analysis. WT GlyT2 data has been shown in the previous chapters but is included for comparison (black curves). Y550L is shown in purple. \circ NOGly Δ L-Val \oplus L-Ser ∇ L-Asp \circ L-Leu \diamond L-Trp \otimes L-Carn $*$ L-Arg \square L-Lys \blacksquare D-Lys \blacklozenge C16 ω 3 L-Lys

5.2.6 Mutations to the top of TM8 disrupt lipid head group interactions

As EL4 shifts into the vestibule, it packs tightly to core helices, including TM8 to close the extracellular gate (Forrest *et al.*, 2008; Krishnamurthy & Gouaux, 2012). I545 and Y550 in EL4 are oriented towards the top half of TM8, near P561 and W563 (Figure 5.11), which were identified to be important in the mechanism of OLCarn inhibition in the initial screen. Inhibition of P561S by Gly and L-Val acyl amino acids is comparable to WT GlyT2, whereas lipids with larger or more sterically restricted head groups (L-Carn, L-Trp, and D-Lys) have reduced apparent affinities (Figure 5.12C, D), similar to the Y550L mutant. P561 is the first residue at the top of TM8, where the helix breaks into a small unwound region before EL4 begins. Mutation of P561 may therefore alter the connection between TM8 and EL4, extending the helix and changing the shape of the gap between the two domains. This could limit the pocket size available to acyl amino acid inhibitors with larger head groups.

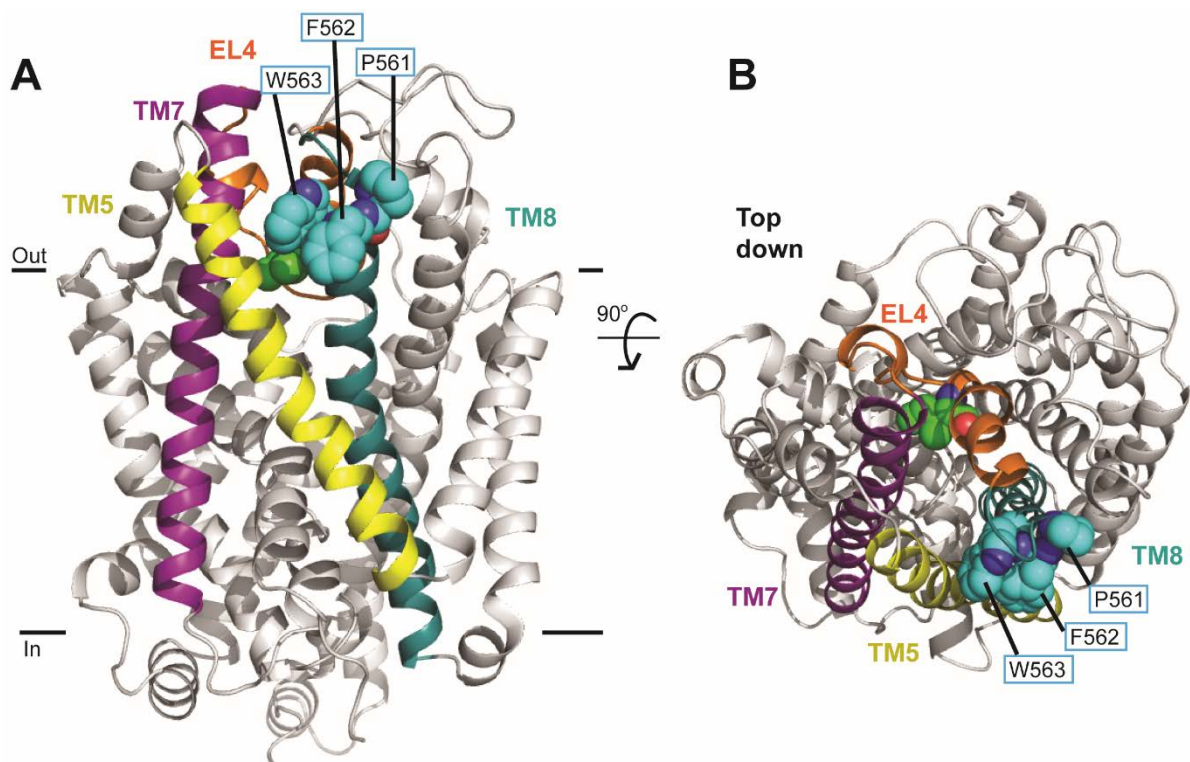


Figure 5.11. Location of mutations at the top of TM8. EL4 is shown in orange, TM5 in yellow, TM7 in purple, and TM8 in teal. **A.** In plane of the membrane from the reverse face **B.** Top down. Mutated residues are shown in cyan spheres. I545 is in green spheres.

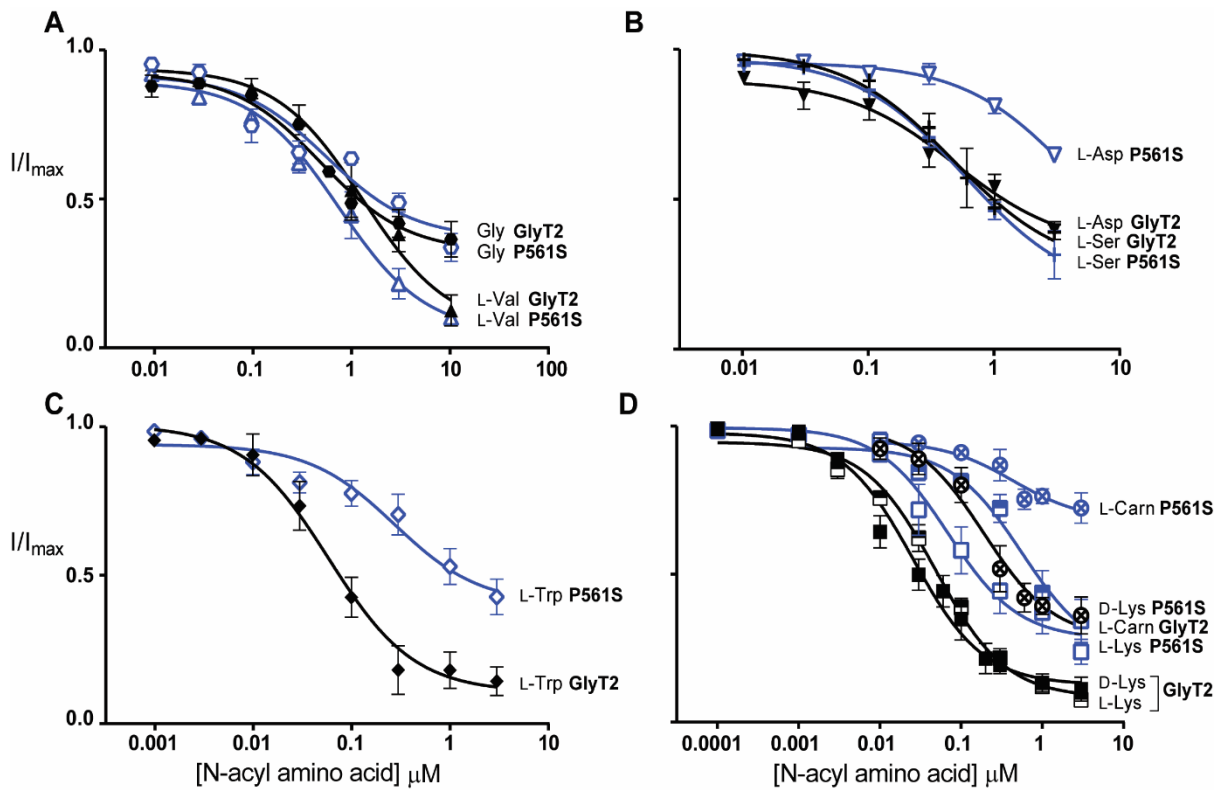


Figure 5.12. Acyl amino acids inhibit glycine transport currents of P561S mutant GlyT2 transporters expressed in *Xenopus laevis* oocytes. Glycine transport currents were measured in the presence of lipids. **A.** Concentration–inhibition curves for compounds **2** and **23**. **B.** Concentration–inhibition curves for compounds **25** and **41**. **C.** Concentration–inhibition curves for compound **41**. **D.** Concentration–inhibition curves for compounds OLCarn, **47** and **48**. The responses are normalized mean values \pm SEM ($n \geq 3$ cells) fit using least-squares analysis. WT GlyT2 data has been shown in the previous chapters but is included for comparison (black curves). P561S is shown in blue. \circ NOGly Δ L-Val $+$ L-Ser ∇ L-Asp \diamond L-Trp \otimes L-Carn \square L-Lys \blacksquare D-Lys

Tryptophan residues at the intra- and extra- cellular edges of helices often interact with polar head groups of membrane phospholipids (Yau *et al.*, 1998). W563 lies two residues down at the top of TM8 (Figure 5.11) and may have a capacity to interact with amphipathic lipid inhibitor compounds. Mutation to a leucine (W563L) has no effect on inhibition by the nucleophilic or acidic acyl amino acids, L-Ser and L-Asp (Figure 5.13B). Conversely, the activity of L-Trp

(Figure 5.13C), L-Lys, D-Lys, and L-Carn (Figure 5.13D) lipid inhibitors were all reduced compared to WT GlyT2. The difference in selectivity for this tryptophan residue may be due to the contribution of π electrons for π - π and cation- π interactions with aromatic or positively charged head groups respectively. The differential selectivity of P561S and W563L for acyl inhibitors containing different amino acids suggests they may comprise part of the binding site that coordinate the head group.

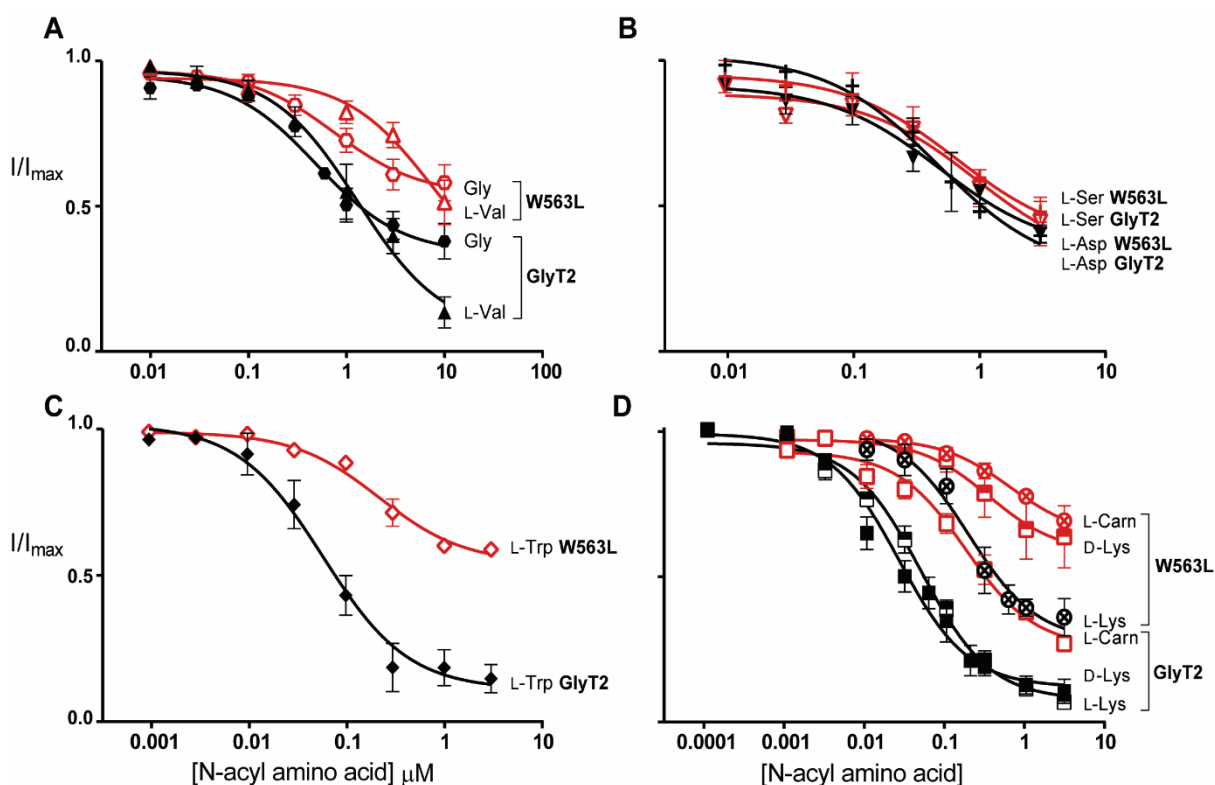


Figure 5.13. Acyl amino acids inhibit glycine transport currents of W563L mutant GlyT2 transporters expressed in *Xenopus laevis* oocytes. Glycine transport currents were measured in the presence of lipids. **A.** Concentration–inhibition curves for compounds **2** and **23**. **B.** Concentration–inhibition curves for compounds **25** and **41**. **C.** Concentration–inhibition curves for compound **41**. **D.** Concentration–inhibition curves for compounds OLCarn, **47** and **48**. The responses are normalized mean values \pm SEM ($n \geq 3$ cells) fit using least-squares analysis. WT GlyT2 data has been shown in the previous chapters but is included for comparison (black curves). W563L is shown in red. \circ NOGly Δ L-Val $+$ L-Ser ∇ L-Asp \diamond L-Trp \otimes L-Carn \square L-Lys \blacksquare D-Lys

5.2.7 Mutations of membrane exposed medial TM5 and TM8 residues disrupt lipid tail group interactions

Because of the relatively slow rate of onset by lipid inhibitors it was postulated that the site may be formed or partially formed with membrane exposed regions of GlyT2. L569 (TM8) and F428 (TM5) are located approximately medial on each transmembrane helix (Figure 5.14), and are likely to be buried in the hydrophobic core of the lipid bilayer. Both the L569F and F428A mutant transporters had reduced inhibition by acyl inhibitors containing the C18 ω 9 “oleoyl” tail, but had no effect on NAGly which contains instead a polyunsaturated C20 “arachidonyl” tail (Figure 5.15, Figure 5.16). This effect was most pronounced for F428A, and so this mutant was further explored using a range of acyl-glycine compounds from Chapter 3 (Figure 5.16).

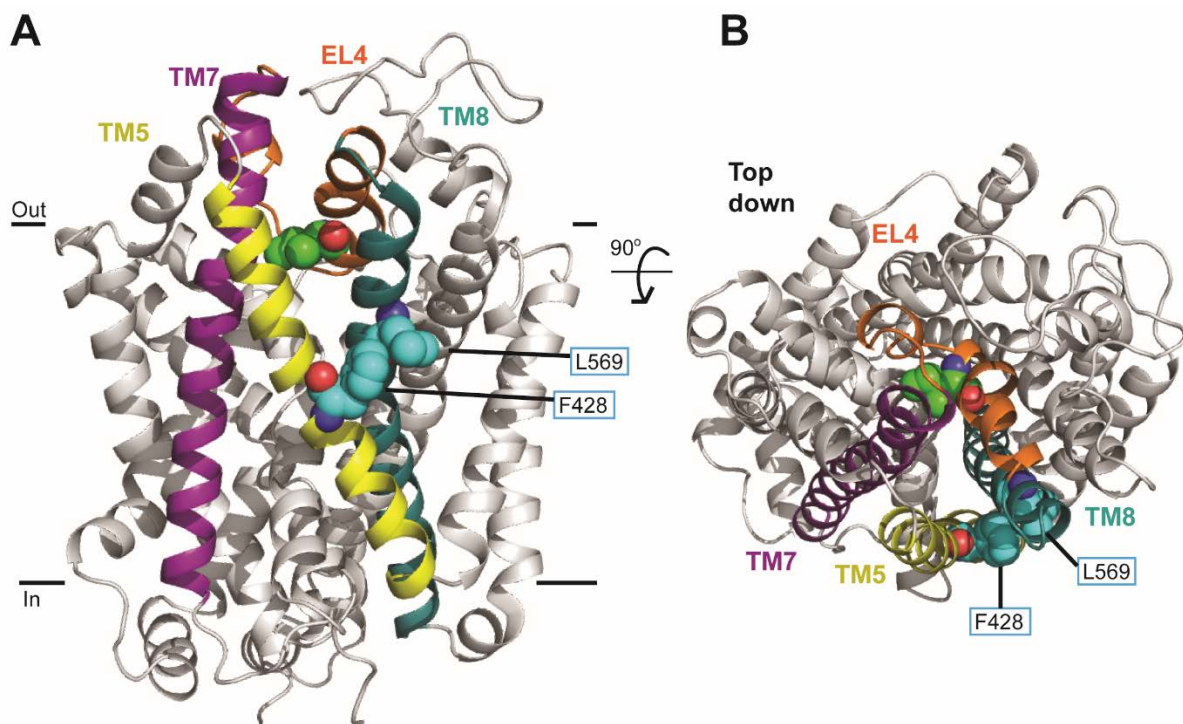


Figure 5.14. Location of membrane exposed mutants in TM5 and TM8. EL4 is shown in orange, TM5 in yellow, TM7 in purple, and TM8 in teal. **A.** In plane of the membrane from the reverse face **B.** Top down. Mutants are shown in cyan spheres. I545 is in green spheres.

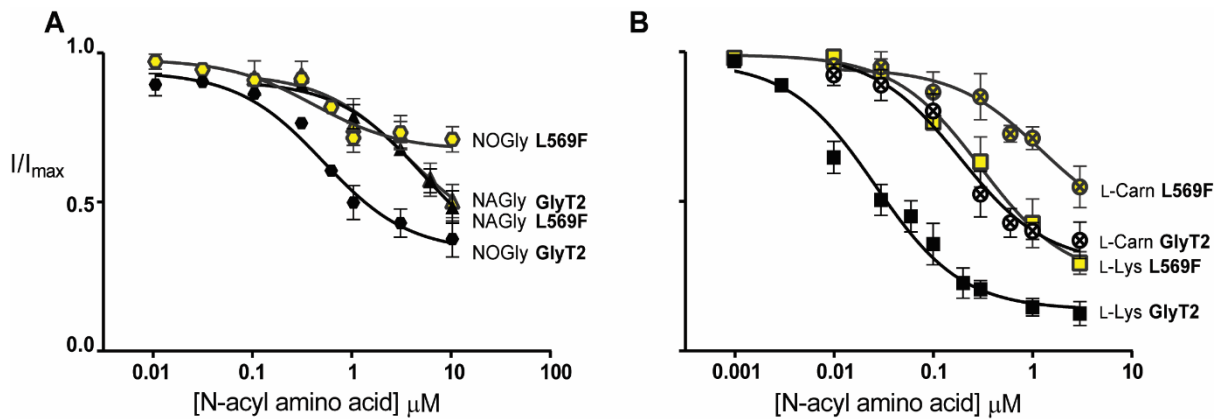


Figure 5.15. Acyl amino acids inhibit glycine transport currents of L569F mutant GlyT2 transporters expressed in *Xenopus laevis* oocytes. Glycine transport currents were measured in the presence of lipids. **A.** Concentration–inhibition curves for compounds **1** and **2**. **B.** Concentration–inhibition curves for compound OLCarn **47**. The responses are normalized mean values \pm SEM ($n \geq 3$ cells) fit using least-squares analysis. WT GlyT2 data has been shown in the previous chapters but is included for comparison (black curves). L569F is shown in yellow. Δ NAGly \circ NOGly \otimes L-Carn \square L-Lys

All C18 acyl-glycines had reduced apparent affinities on F428A. A comparison between acyl-glycines with double bonds in the ω 8, 9 and 10 positions showed a striking relationship demonstrating that acyl-glycine with a double bond in ω 8 position was markedly affected whilst the acyl-glycine with a double bond in the ω 10 position was only mildly affected by the mutation (Figure 5.15B) For C16 acyl-glycines, the activity was also altered by the position of the double bond; the ω 11 compound had activity on F428A comparable to WT GlyT2, but shifting the double bond to the ω 7 position considerably reduced the IC_{50} (5.8 μ M) and max. inhibition (56.5%). Sensitivity of F428A to the only C14 acyl glycerine was also reduced ($IC_{50} > 30 \mu$ M).

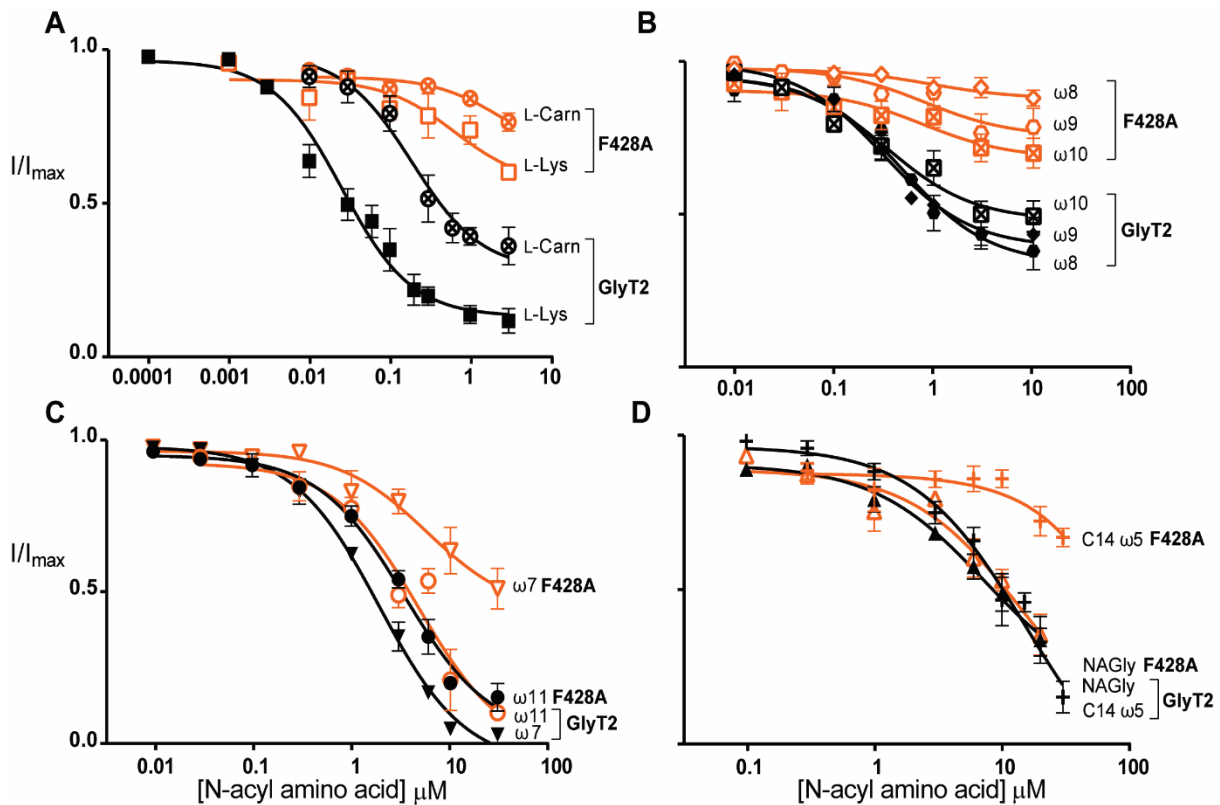


Figure 5.16. Acyl amino acids inhibit glycine transport currents of F428A mutant GlyT2 transporters expressed in *Xenopus laevis* oocytes. Glycine transport currents were measured in the presence of lipids. **A.** Concentration–inhibition curves for positively charged compounds OLCarn and **47**. **B.** Concentration–inhibition curves for C18 acyl-glycine compounds **2**, **7**, and **8**. **C.** Concentration–inhibition curves for C16 acyl-glycine compounds **16** and **18**. **D.** Concentration–inhibition curves for acyl-glycine compounds **1** and **20**. The responses are normalized mean values \pm SEM ($n \geq 3$ cells) fit using least-squares analysis. WT GlyT2 data has been shown in the previous chapters but is included for comparison (black curves). F428A is shown in orange. \otimes L-Carn \square L-Lys \diamond C18 ω 8Gly \circ NOGly \boxtimes C18 ω 10Gly ∇ C16 ω 7Gly \circ C16 ω 11Gly Δ NAGly $+$ C14 ω 5Gly

The compounds that had reduced activity at F428A transporters all possessed a double bond the approximate same distance from the head group (Figure 5.17). F428 may therefore comprise part of the lipid binding site where the double bond interacts, or where the kink in the acyl tail ideally fits into a cavity. The distance from the side chains of W563 in TM8 and

F428 in TM5 is approximately 10 Å (in our GlyT2 model), which is similar to the chain length of 9 carbons between the head group and double bond (assuming a C-C bond length of 1.5 Å and an angle of ~110°). This supports the head specific (W563L) and tail specific (F428A) mutant data, and suggests the binding site may lie within this region.

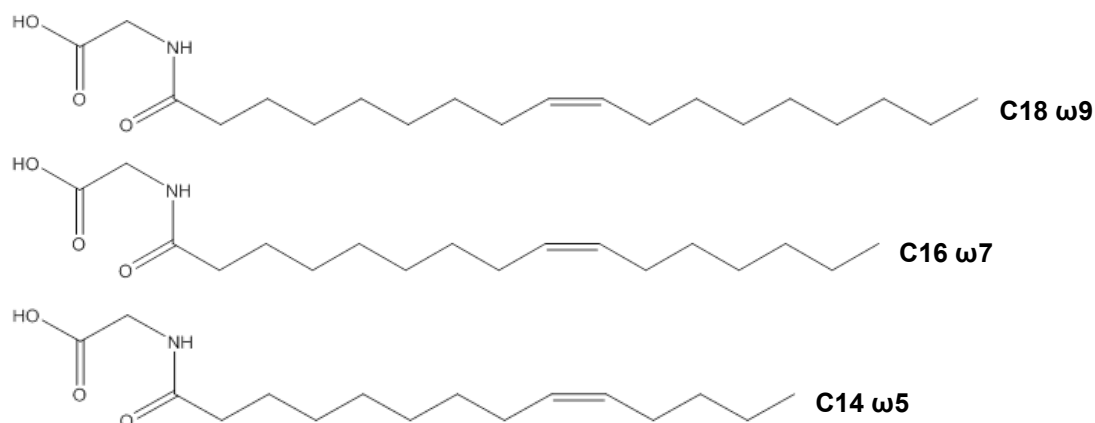


Figure 5.17. Structures of select acyl-glycine analogues: where acyl chains of different lengths possess double bonds the same distance from the head group

5.2.8 Docking of oleoyl D-Lys suggests a lipid binding cavity comprised of residues from EL4, TM5, and TM8

In order to better understand the proposed binding site, dynamic docking of our GlyT2 model with C18 ω9 D-Lys was performed by Mitchell Blyth and Dr Megan O'Mara at the Australian National University. Residues identified by mutagenesis were defined as potential sites of interaction and allowed to move during the simulation. Top scoring binding locations and orientations were then docked into the protein structure. Two binding sites were observed (Figure 5.18). One of the sites consists of a cavity comprised of EL4, TM5, and TM8, with the D-Lys headgroup sandwiched between EL4 and the top of TM8, and the acyl tail buried among conserved aliphatic residues behind TM5 and TM8 ("site A"; purple spheres; Figure 5.18C).

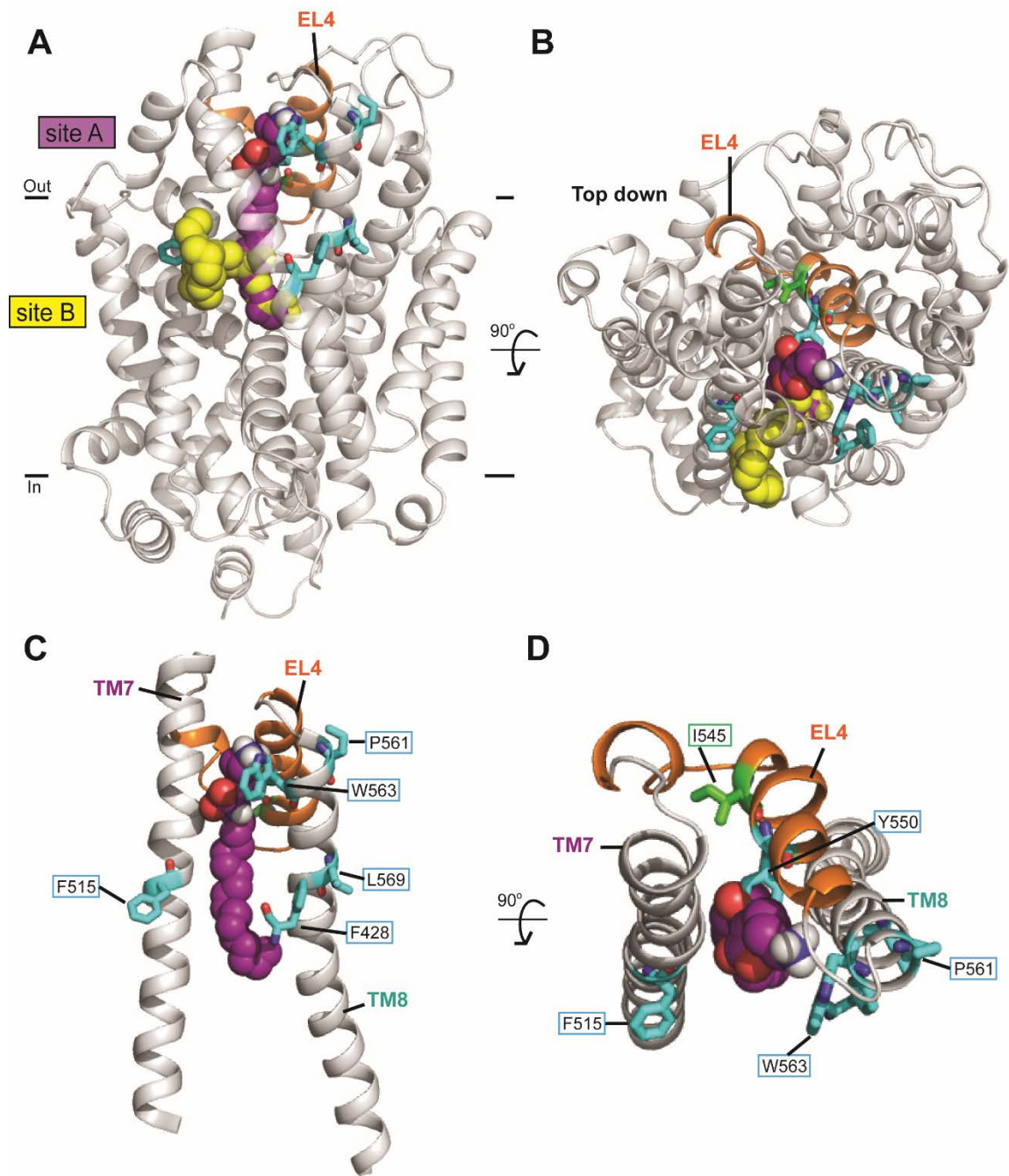


Figure 5.18. GlyT2 model with oleoyl D-Lys docked in site A (purple spheres) and site B (yellow spheres). A. Reverse face in plane of the membrane **B.** Top down. **C.** Close up of "site A": EL4, TM7, and TM8 with mutated residues and **D.** Top down view. EL4 is shown in orange, mutants are shown in cyan sticks, and I545 is shown in green sticks. A Monte Carlo search algorithm was employed to determine potential binding locations and ligand orientations of oleoyl D-Lys on the GlyT2 model. VinaDock was then used to assemble the final docked structure. Docking performed by Mitchell Blyth (ANU).

Aromatic residues, Y550 and W563, appear to directly interact with the head group (Figure 5.18D), which may account for the high potency of acyl inhibitors with a positively charged or aromatic head groups with the potential for form cation- π and π - π interactions respectively. While the hydrophobic tail makes contacts with TM5 and TM8, it did not appear to directly interact with the side chains of L569 or F428. These residues may therefore be indirectly involved, forming the shape of the binding site. The unsaturated acyl tail would have a substantial kink and may only be accommodated by a certain shaped binding cavity; mutations that may alter the shape of the cavity could therefore only affect inhibitors with certain tails which could explain the tail selectivity of these mutants. Alternatively, the docking may be unreliable if the binding site is on the outside of the transporter, partially comprised of membrane phospholipids. A high resolution structure of GlyT2 with a lipid inhibitor bound would provide further insight into inhibitor-transporter interaction.

5.2.9 Comparison with lipid binding membrane proteins

The “site A” cavity is not aqueously accessible, and poses the question of how lipid inhibitors are able to access this site. This is reminiscent of the G-protein coupled receptor family, where ligands have been crystallised in pockets occluded from the aqueous surroundings (Chrencik *et al.*, 2015; Hanson *et al.*, 2012; Hua *et al.*, 2016; Taniguchi *et al.*, 2017). For example, the sphingosine-1-phosphate receptor has a large N-terminal helix which sits above the 7 transmembrane helices and the antagonist ML056 has been resolved in a cavity below this N-terminal cap (Figure 5.19; Hanson *et al.*, 2012). There is an opening between TM1 and TM7 which would provide an opening for ligands to access the final binding site by first inserting into the bilayer and squeezing between membrane exposed helices. It is possible that lipid inhibitors of GlyT2 access the aqueously inaccessible “site A” via a similar mechanism.

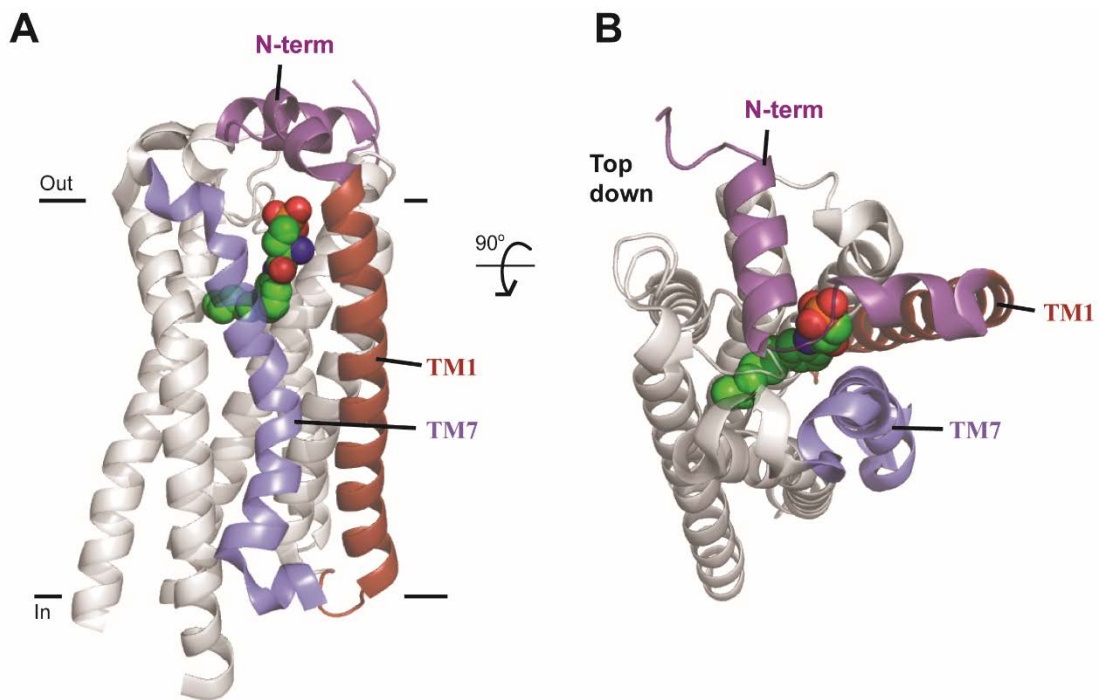


Figure 5.19. Sphingosine-1-phosphate receptor bound to antagonist ML056 (green spheres). A. In plane of the membrane, **B.** Top down. N-terminal helix shown in purple, TM1 in red, and TM7 in blue (Hanson et al., 2012) (adapted from PDB: 3V2Y).

Similarly, the recent crystal structure of the lysophosphatidic acid receptor 6 (LPA₆) possesses a large vertical gap in TM4 and TM5 that spans the length of the extracellular membrane leaflet (Tanigushi *et al.*, 2017). This gap appears to be occupied by a monoolein molecule which may overlap with the LPA acyl chain binding site. Subsequent docking of this site with 2-LPA (2-linoleoyl (18:2)-LPA) proposes 3 potential binding models (Figure 5.20) with the acyl tail in the TM4-TM5 cleft surrounded by aliphatic residues, and the head group in either the central cavity (Figure 5.20 **a, b**), or on the outer surface of the receptor (Figure 5.20**c**). Mutation of potential head group residues suggests the head group lies in the central cavity (**a** or **b**), and acyl chain stretched into the membrane cleft. It is suggested that selectivity for LPA acyl chains is due to structural features (shape/size) of this cleft.

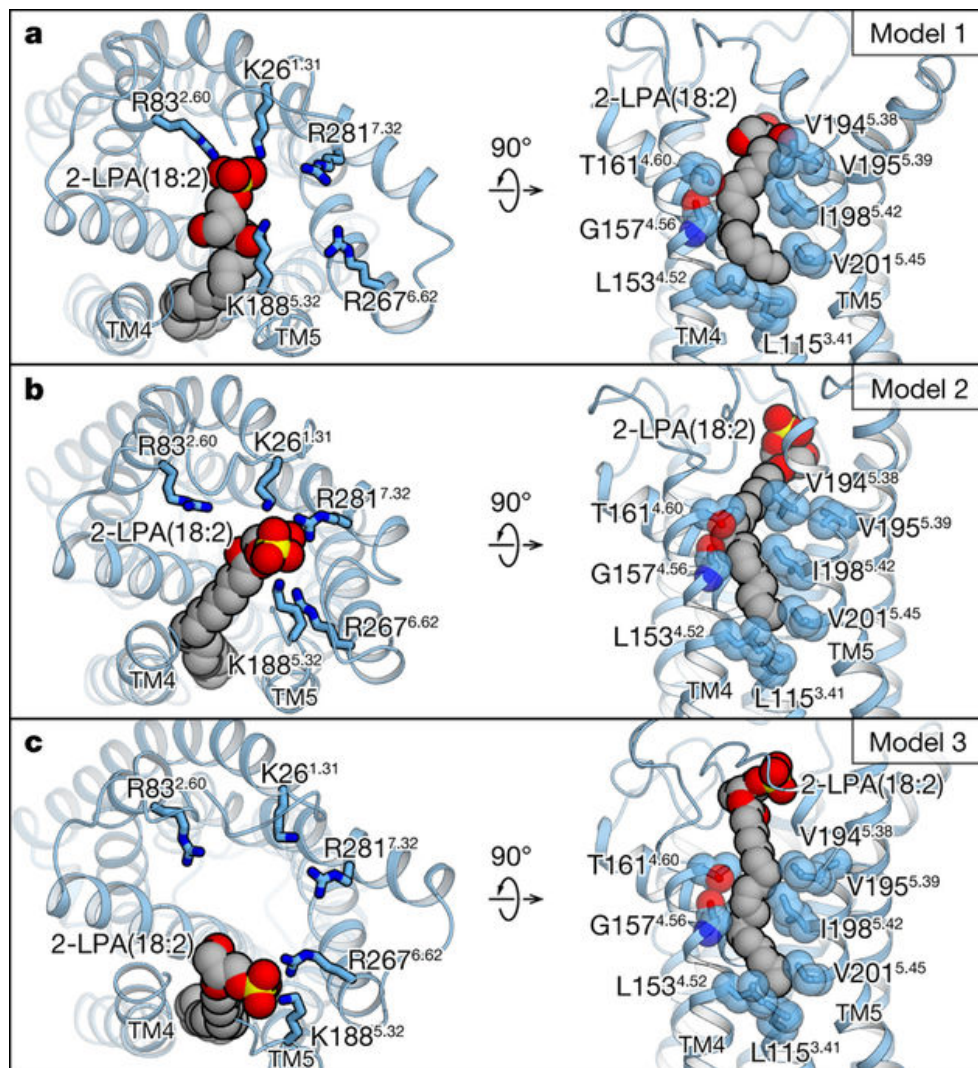


Figure 5.20. Potential LPA binding (3 models a-c) obtained from docking simulations from top down (left) and in plane of the membrane (right). 2-LPA is in spheres with carbons (grey), phosphates (yellow). Potential head group residues are shown in blue sticks. Tail binding residues are shown in blue sticks and semi-transparent spheres. (Taniguchi *et al.*, 2017).

Head group and tail group selective GlyT2 mutants suggest that acyl amino acids bind with their head group towards the central cavity (between EL4 and TM8), and their tail groups adjacent to membrane bound helices (TM5 and TM8). As it does not line “site A”, it is predicted that the F428A mutant GlyT2 is selecting for certain tails through changes in the shape of the acyl binding pocket. An additional lipid site was also observed in the oleoyl D-Lys docked

GlyT2 model where the head group is buried between helices TM5, TM7, and TM8 with the acyl tail extending out into the membrane (“site B”; yellow spheres; Figure 5.18). While mutant data suggests “site A” is more likely, one of the residues identified in the initial mutant screen, F515, appears to stick out into the membrane (Figure 5.21) adjacent to oleoyl D-Lys in “site B”. Converse to other mutant GlyT2 transporters, F515W appeared to have increased inhibition by 1 μ M OLCarn (Figure 5.5).

5.2.10 F515W in TM7 increases efficacy and the reversibility of OLCarn

On WT GlyT2, NAGly, NOGly, and OLCarn are partial inhibitors (Wiles *et al.*, 2006; Carland *et al.*, 2013) (Figure 5.22A). On The F515W mutant however, these compounds are able to act as full inhibitors at high concentrations (Figure 5.22B). F515W increases the % max. level of inhibition, but not the apparent affinities (Table 5.2), which suggests this residue may not be important for binding, but is important in the mechanism of inhibition.

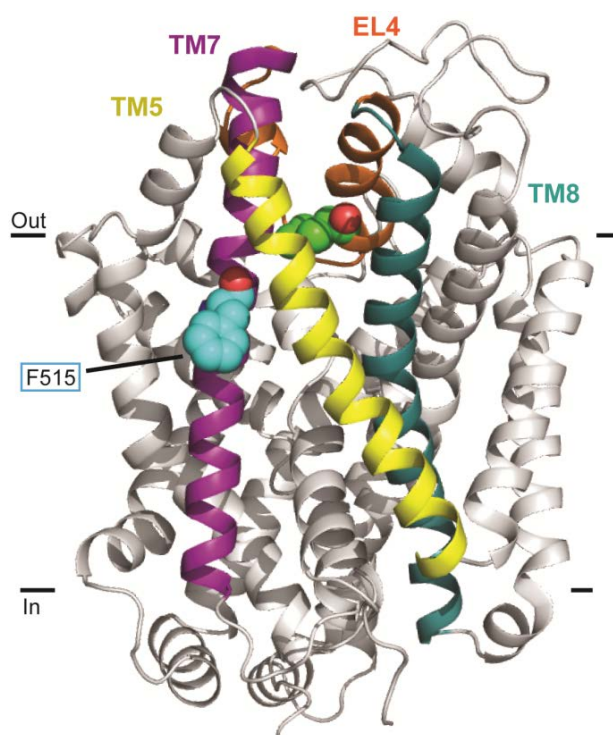


Figure 5.21. Location of F515 on GlyT2 in plane of the membrane. EL4 is shown in orange, TM7 shown in purple, and TM8 shown in teal. F515 is shown in cyan spheres. I545 is shown in green spheres.

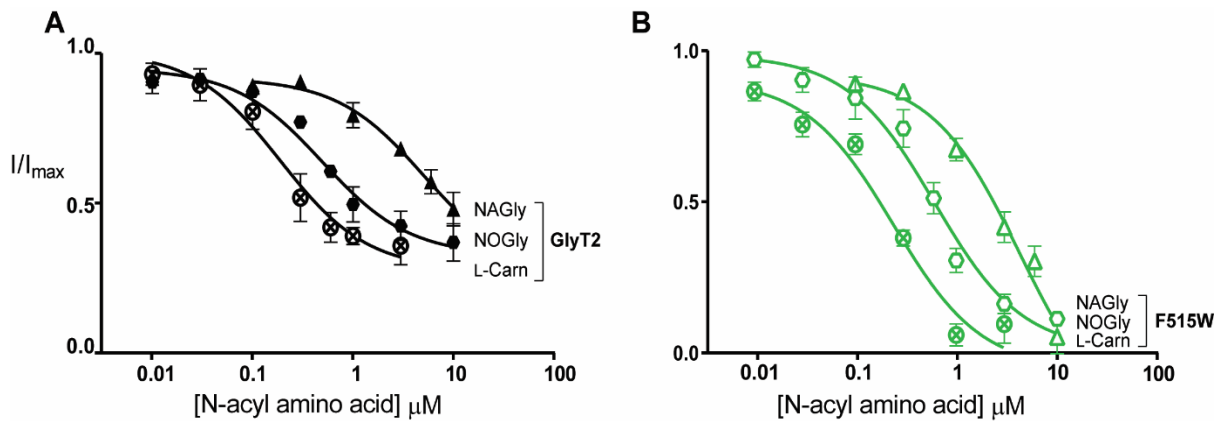


Figure 5.22. Acyl amino acids inhibit glycine transport currents of F515W mutant GlyT2 transporters expressed in *Xenopus laevis* oocytes. Glycine transport currents were measured in the presence of NAGly (1), NOGly (2), and OLCarn. **A.** Concentration–inhibition curves for GlyT2 **B.** Concentration–inhibition curves for F515W. The responses are normalized mean values \pm SEM ($n \geq 3$ cells) fit using least-squares analysis. WT GlyT2 data is included for comparison (black curves). F515W is shown in green.

Δ NAGly \circ NOGly \otimes L-Carn

Acyl-glycine inhibitors, including NAGly and NOGly, are fully reversible 5 minutes post inhibition, as indicated by a restoration of glycine transport currents. OLCarn however, is very slowly reversible, and currents do not return to pre-exposure levels in the timeframe of the assay (Figure 5.23A). At time 0, F515W had a higher level of inhibition compared to WT GlyT2, and therefore begins the washout time course with a lower I/I_{max} . Despite this, transport recovery is much faster for F515W (Figure 5.23B); this mutation not only converts OLCarn into a full inhibitor but also increases reversibility.

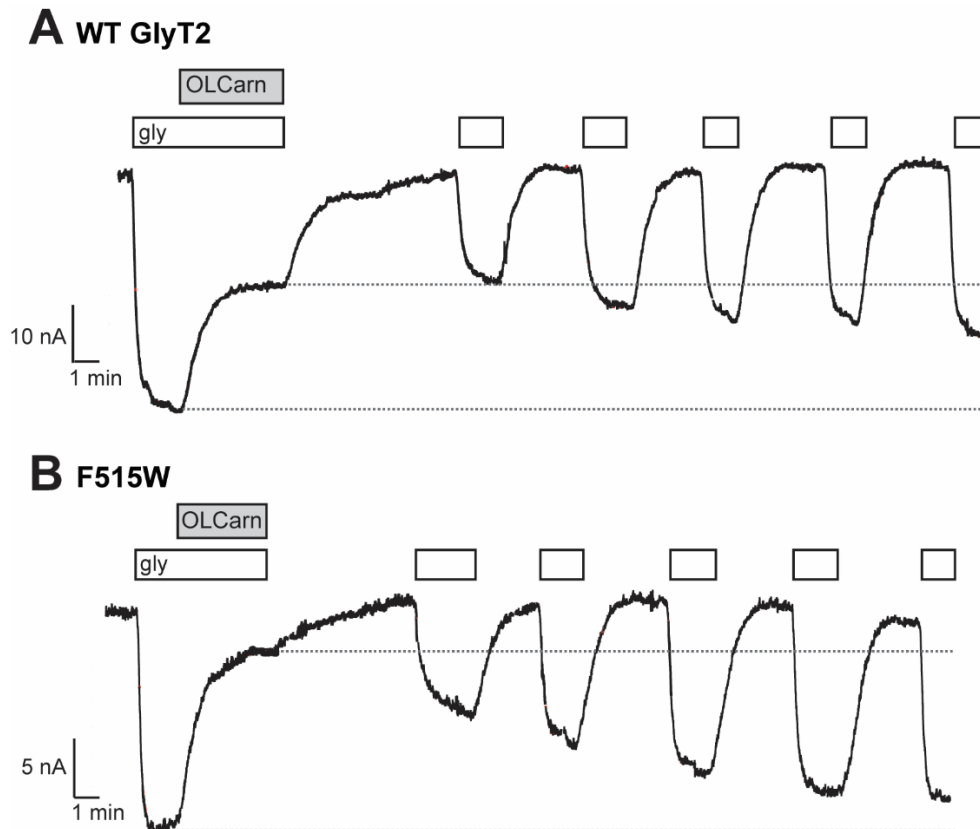


Figure 5.23. Washout of 1 μ M OLCarn on WT GlyT2 and TM7 F515W mutant GlyT2 transporters. Glycine (open bar) is applied to generate an inward current which is inhibited by 1 μ M OLCarn (grey bar) for 4 minutes. 30 μ M glycine was applied at 5 minute intervals throughout a 25 minute wash with ND96 buffer. Maximal transport current and subsequent level of inhibition are marked with grey dashed lines.

I propose that the increase in efficacy and rate of washout is related to the mechanism of access for lipid inhibitors to their site. In the inward-open LeuT structure, TM7 partially forms a 3_{10} helix where F515 (I in LeuT) is located (Krishnamurthy & Gouaux, 2012). These atypical 3_{10} helices are longer, thinner, and more likely to unravel. TM5 has similarly been shown to partially unwind in the multi-hydrophobic amino acid transporter (MhsT) from *Bacillus halodurans*, where unwinding is triggered by a GlyX₉Pro motif that opens an intracellular pathway (Malinauskaite *et al.*, 2014). GlyT2 shares this TM5 GlyX₉Pro motif and unwinding in both TM5 and TM7 may facilitate insertion of acyl inhibitors.

It has also been shown by Dr Megan O'Mara (ANU, unpublished data) that in molecular dynamics simulations of acyl amino acids in a typical POPC membrane, compounds insert into the membrane and distribute themselves on both the extracellular and intracellular leaflets (Figure 5.24). Compounds were then observed to dip below the phospholipid head groups. F515 lies approximately adjacent to the phospholipid head group:acyl chain interface of the surrounding membrane, and is suitably located to be the first point of contact for burrowing lipids. It is proposed that acyl amino acids must first traverse the cell membrane where they interact with F515 and insert between helices in "site B, compounds are then able to access their final binding site "site A" to cause inhibition. The F515W mutation may accelerate this insertion by favouring amphipathic interactions. Tryptophan residues are also known to facilitate movements of proteins within the membrane (Kachel *et al.*, 1995), and therefore may favour certain conformations where lipid inhibitors bind.

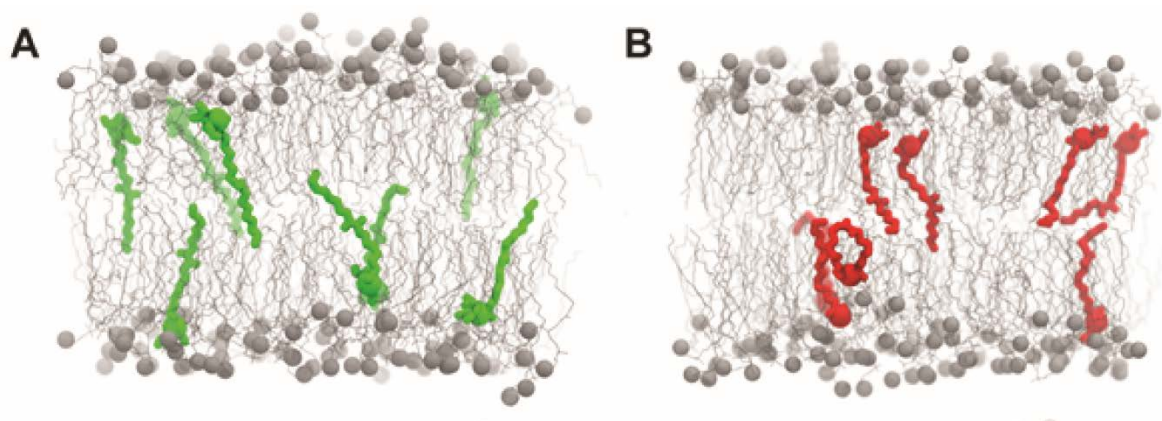


Figure 5.24. Molecular dynamics simulation of acyl inhibitors in a POPC/cholesterol membrane. POPC membranes with 20% cholesterol and 5% acyl inhibitor were run in atomistic simulations for 100 ns. **A.** NAGly. **B.** OLCarn. MD simulations were performed by Michael Thomas (ANU).

Table 5.2. IC₅₀ values and % max. inhibition for mutant GlyT2 transporters

Mutation	Compound	IC₅₀ (nM)	% Max. inhibition
GlyT2			
I545L	oleoyl L-Val	>10 μM ^a	22.5 ± 8.0 ^{b****}
	oleoyl L-Asp	>10 μM ^a	4.9 ± 6.4 ^{****}
	oleoyl L-Trp	>10 μM ^a	20.2 ± 1.7 ^{****}
	oleoyl L-Lys	443 (270 – 804)	80.7 ± 4.8
Y550L	NOGly	829 (65.0 – 4170)	34.8 ± 9.1 ^{**}
	OLCarn	>3 μM ^a	17.3 ± 1.4 ^{****}
	oleoyl L-Val	2930 (1680 – 5130)	57.0 ± 5.1 ^{**}
	oleoyl L-Leu	437 (214 – 8920)	41.1 ± 6.2 [*]
	oleoyl L-Ser	>3 μM ^a	11.2 ± 1.6 ^{****}
	oleoyl L-Asp	>3 μM ^a	7.0 ± 0.8 ^{b****}
	oleoyl L-Trp	>3 μM ^a	16.5 ± 1.7 ^{****}
	oleoyl L-Arg	>3 μM ^a	9.3 ± 1.4 ^{****}
	oleoyl L-Lys	210 (78.6 – 559)	48.2 ± 4.1 ^{****}
	oleoyl D-Lys	>3 μM ^a	38.4 ± 10.0 ^{***}
	C16 ω3 L-Lys	1040 (420 – 2560)	63.1 ± 9.9 [*]
	P561S	NOGly	564 (245 – 1300)
OLCarn		>3 μM ^a	31.6 ± 5.2 ^{****}
oleoyl L-Val		753 (455 – 1250)	94.5 ± 4.7
oleoyl L-Ser		580 (276 – 1220)	80.3 ± 7.3
oleoyl L-Asp		2540 (1490 – 4350)	58.2 ± 4.7
oleoyl L-Trp		318 (153 – 663)	61.4 ± 4.2 ^{***}
oleoyl L-Lys		69.2 (31.8 – 151)	71.5 ± 4.8
oleoyl D-Lys		558 (247 – 1260)	76.7 ± 8.1
W563L	NOGly	755 (317 – 1800)	46.6 ± 4.0
	OLCarn	>3 μM ^a	34.7 ± 3.2 ^{***}
	oleoyl L-Val	7510 (1090 – 52000)	56.3 ± 9.1 ^b

	oleoyl L-Ser	661 (221 – 1980)	62.3 ± 5.3
	oleoyl L-Asp	1160 (477 – 2800)	74.9 ± 7.5
	oleoyl L-Trp	>3 µM ^a	42.9 ± 2.6 ^{****}
	oleoyl L-Lys	175 (110 – 277)	73.5 ± 3.3
	oleoyl D-Lys	>3 µM ^a	42.1 ± 7.7 ^{**}
L569F	NAGly	3590 (430 – 30200)	63.7 ± 19.0
	NOGly	>10 µM ^a	32.5 ± 3.6 ^{****}
	OLCarn	1200 (267 – 5360)	45.5 ± 7.0 ^{b***}
	oleoyl L-Lys	301 (157 – 577)	76.8 ± 5.8
F428A	NAGly	14400 (3540 – 58600)	64.7 ± 6.6 ^b
	NOGly	>10 µM ^a	25.4 ± 4.9 ^{****}
	OLCarn	>3 µM ^a	22.7 ± 3.0 ^{b****}
	oleoyl L-Lys	>3 µM ^a	39.2 ± 2.3 ^{b****}
	C18 ω8 Gly	>10 µM ^{a*}	13.2 ± 2.7 ^{****}
	C18 ω10 Gly	776 (83.8 – 7180)	25.3 ± 5.3 ^{**}
	C16 ω7 Gly	5760 (2220 – 1490)	56.5 ± 7.8 ^{**}
	C16 ω11 Gly	4810 (2620 – 8830)	103 ± 7.7
	C14 ω5 Gly	>30 µM ^a	33.4 ± 3.0 ^{b****}
F515W	NAGly	4240 (2000 – 8980)	94.4 ± 5.6 ^b
	NOGly	612 (391 – 957)	89.6 ± 4.9 [*]
	OLCarn	239 (125 – 456)	105 ± 6.0 ^{***}
GlyT1			
L425I	NAGly	>10 µM ^a	31.6 ± 6.9
	NOGly	>10 µM ^a	28.5 ± 5.3 ^b
	OLCarn	195 (92.4 – 411)	74.6 ± 5.3 ^{***}

Compounds were tested for inhibition of glycine transport on *Xenopus laevis* oocytes expressing mutant GlyT1 and GlyT2 transporters. n ≥ 3 with measurements taken from at least 2 batches of oocytes. Data presented are mean and 95% confidence intervals or mean ± SEM.

^aWhere significant inhibition was not reached, IC₅₀ are presented as greater than the maximum concentration of each compound applied.

^bWhere inhibition was insignificant and could not be accurately calculated by curve fitting values given are the % inhibition at the highest concentration of inhibitor used.

p values are represented from one way ANOVAs or two-tailed t-tests as described in Methods.

5.3 Conclusions

In this chapter I identified a number of residues important for acyl amino acid binding and their mechanism of inhibition. Docking of oleoyl D-Lys revealed 2 potential binding sites: site A is a buried cavity comprised of residues in EL4, TM5, and TM8; and site B is partially membrane exposed, where the head group embeds between TM5 and TM7 and the acyl tail extends into the lipid bilayer. I propose that both sites are functionally relevant to the mechanism of inhibition. Firstly, the acyl inhibitors insert into the membrane (Figure 5.25; 1) and snorkel below the phospholipid head groups (2). Compounds can then enter GlyT2 via site B (3), to access the buried site A cavity (4). Once in the final binding site, transport is arrested (5).

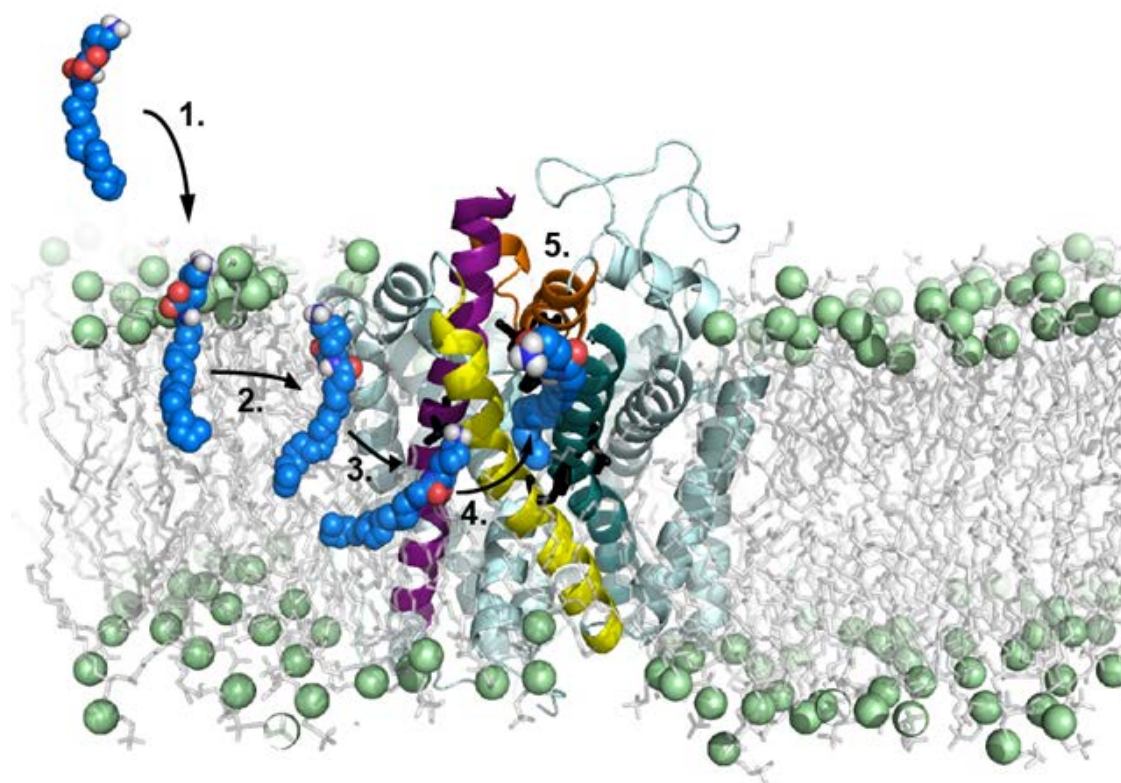


Figure 5.25. Proposed mechanism of inhibition by acyl inhibitors of GlyT2. Lipids insert into the bilayer (1), migrate within the membrane and dip below phospholipid head groups (2), interact with F515 and enter site B (3), wiggle between helices to site A (4), bind between TM8 and EL4 to prevent transport (5).

Mutations to residues at the top of TM8 and in EL4 possess differential selectivity for head groups and may form part of the head group binding site. Aromatic residues in this area may sandwich head groups, and explain the high potency for acyl amino acids with positively charged and aromatic head groups. Similarly, mutations to the medial regions of TM5 and TM8 cause acyl tail group selective disruption of inhibition, and may form a hydrophobic pocket that is restricted by size and/or shape and only allows certain tail configurations to fit. As GlyT2 transitions to the inward facing conformation, EL4 shifts closer towards TM8. Lipid binding between EL4 and TM8 may “glue” these two regions together, creating a transporter that is stable in a transport-unfavourable conformation. In a similar manner to how cholesterol stabilises an outward facing conformation of dDAT by preventing the movement of TM1a (Hong & Amara, 2010; Penmatsa *et al.*, 2013; Zeppelin *et al.*, 2018), I hypothesize that acyl inhibitors stabilise GlyT2 by preventing further movement of EL4. Many acyl amino acids are only partial inhibitors, which suggests there is flexibility in the lipid bound conformation to allow for some glycine transport. While the mutagenesis data presented in this thesis is highly suggestive, combining this data with visualisation of acyl inhibitor bound GlyT2 would unambiguously discern the inhibitor binding site.

Chapter 6: Final discussion and future directions

6.1 Summary of key findings

In this thesis, I have designed two series of lipid compounds and determined their structure activity relationship for a number of inhibitory characteristics that are important in determining optimal inhibition of GlyT2. A number of relatively high potency inhibitors were identified, one of which has since been tested in preliminary studies of an animal model of neuropathic pain. I have also explored the molecular determinants of GlyT2 lipid inhibition to tease out the binding site and potential mechanism of action.

The first study outlined in chapter 3, described a series of compounds where the glycine head group was conjugated to acyl tails of varying length (C14-C18) and saturation. I found that reduction in tail length resulted in a loss of apparent affinity, with the most potent compound possessing a C18 tail with a medial double bond. It was also shown that shifting the double bond to the lateral ends of the C18 carbon chain produced compounds that were inactive. Inactivity was also conferred for compounds with a double bond in the *trans* configuration which suggests that *cis* tails provide a kink that fits ideally within a defined acyl binding site. For C16 compounds, the position of the double bond governed whether inhibition was full or partial, an important consideration when designing therapeutics that target GlyT2.

In chapter 4, a potent C18 tail with a medial double bond (oleoyl) was attached to amino acid head groups that were aliphatic, negatively charged, polar, aromatic, or positively charged. It was shown that compounds with positively charged or aromatic head groups conferred the highest apparent affinity, while those with an aliphatic or negatively charged head group possessed no improved affinity compared to the simplest amino acid, glycine. It was also observed that L- are more active than D- enantiomers with activity decreasing as side chains became larger, particularly for D- aromatic compounds which did not significantly inhibit GlyT2. In addition to the amino acid sidechain being a significant binding moiety, the backbone carboxylic acid was also determined to provide important binding interactions.

A number of lysine-like compounds were designed which displayed a reduction in apparent affinity as the carbon linking the NH_3^+ group became shorter. Conjugation of the L-Lys head to tails of varying length and saturation still produced potent GlyT2 inhibitors, even in the case of C18 ω 5, which was shown to produce an inactive compound in chapter 3 when conjugated to a glycine. Designing lipid inhibitors is not as straightforward as pick-and-mix; where a tail with a certain desired characteristic (full or partial) can be attached to a head group of high potency in order to produce an ideal inhibitor. Any next generation of lipid compounds will therefore need to be tested in a similar assay to determine their activity. It would be of worth however, to produce a new series where the L-Lys (or D-Lys) head is conjugated to varying acyl tails, as it has been shown that C16 ω 3 L-Lys confers a higher potency (10.5 nM). In the low nanomolar range even small shifts can push the boundaries to make a compound more efficacious. In this study oleoyl D-Lys was further examined and shown to be stable in plasma and microsomes; able to cross the BBB; and produce analgesia in a preliminary rat model of neuropathic pain.

Lastly, in chapter 5, I investigated residues that were either in close proximity to EL4, or were in a position to alter conformational dynamics of EL4, to determine their role in inhibition by lipid inhibitors. Using site-directed mutagenesis, and subsequent dynamic docking, it was determined that residues in EL4, TM5, and TM8 comprise the putative lipid inhibitor binding site (site A); where the head group is coordinated by Y550 and W563, and the acyl tail lines an hydrophobic cavity that is shaped by F428 and L569. Using dynamic docking, a second lipid binding site (site B) was observed in a membrane exposed cavity that overlaps with site A (Figure 6.1), where a membrane facing residue F515, when mutated, can alter the maximal level of inhibition and reversibility of compounds.

I propose that site A is the high affinity inhibitor binding site, as alteration of single residues within this site abolish or drastically alter inhibitor activity. The majority of residues lining site A are branched chain aliphatic residues (Figure 6.1B) which would define the shape of the binding cavity and provide hydrophobic interactions for the acyl tail. In addition to Y550 and

W563, a third aromatic residue (F567) points in towards the head group and may influence binding of lipid inhibitors, which could be further explored using mutagenesis. The effect of altering aliphatic residues in the hydrophobic cavity may be difficult to discern, as the tail groups of these compounds are flexible and may be able to adopt subtly different binding conformations. Lipid tails would also provide many points of contact for a large number of hydrophobic interactions, and altering one point of interaction may be insufficient to observe changes in activity. Perhaps an approach to increase the bulk of side chains to plug this cavity will adequately obstruct lipid binding.

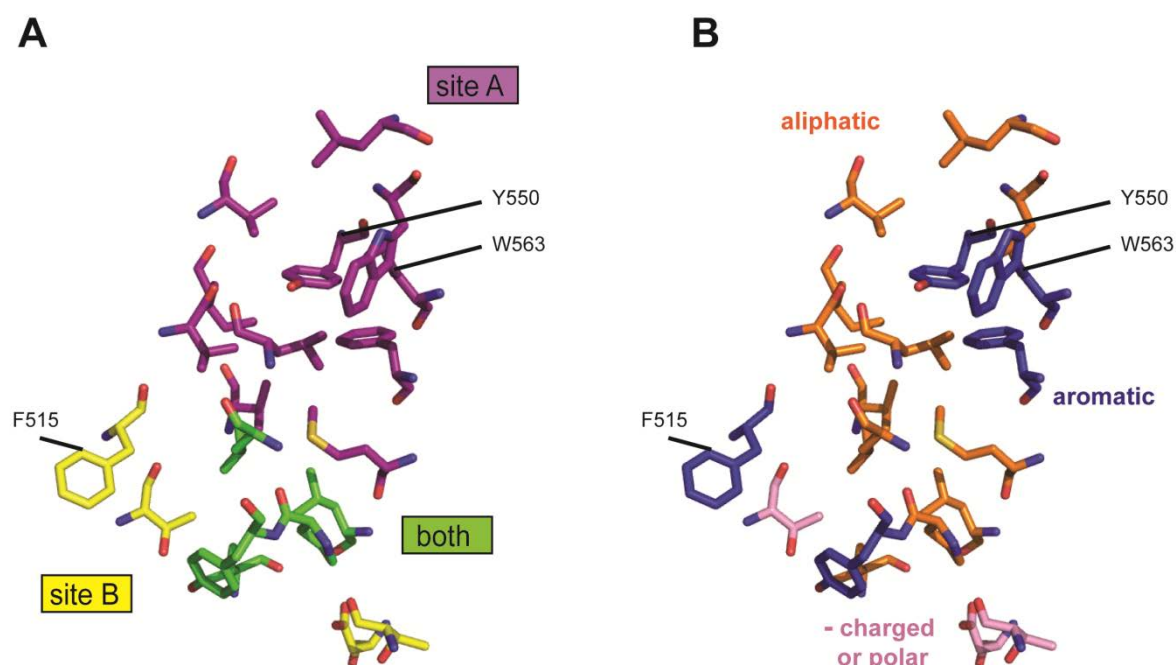


Figure 6.1. Residues lining (within 3 Å) the oleoyl D-Lys site A and site B. Residues are shown in sticks and coloured **A.** purple (site A), yellow (site B), and green (overlapping site). **B.** aliphatic (orange), aromatic (blue), and negatively charged or polar (pink).

Aromatic residues are also present at the proposed entrance point where F515 lies. As aromatic residues appear to coordinate the head group in site A and confer high affinity binding, aromatic residues in site B may attract lipids within the membrane and facilitate their insertion in between TM helices. I propose that site B is a transient site of access where lipids first diffuse into the bilayer before worming between helices TM5 and TM7, to reach site A.

Once bound in site A, lipid inhibitors stick between aromatic residues in both TM8 and EL4 to glue these regions together and prevent transport of glycine.

6.2 Future Directions: Resolving protein-lipid interactions

The research presented in this thesis has identified a large pool of lipid GlyT2 inhibitors that could be developed for the treatment of neuropathic pain. In order to further improve these compounds it would be instructive to understand in more detail how allosteric lipids interact with GlyT2 to cause inhibition. In the following sections I will discuss different approaches in the study of protein-lipid interactions (sections 6.2 and 6.3) and then discuss the ideal properties of a GlyT2 inhibitor for optimal use *in vivo* (section 6.4).

6.2.1 Measuring lipid binding to membrane proteins

Using an IC_{50} value to measure the activity of lipid inhibitors gives information on the compounds relative potencies, which allows for comparison within the series and can identify any changes in activity on a mutant transporter. Inhibition response curves also inform the effectiveness of an inhibitor, and can indicate how transport may be affected *in vivo* to reduce glycine reuptake. This approach does not however directly measure binding, which is required to measure interactions between ligand and protein. It is more difficult to measure binding of a ligand to a membrane protein in its native environment and requires functional, folded protein.

Isothermal titration calorimetry (ITC) is a technique that can be used to measure thermodynamic parameters to describe binding with high sensitivity, and has been applied to the study of protein interactions with small ligands and ions, and to larger macromolecules including nucleic acids and other proteins (Leavitt & Freire, 2001). ITC does not require labelling of the protein or ligand, and a single titration can be used to calculate binding affinity and stoichiometry (Rajaratnam & Rosgen, 2014). More recently, ITC has been used successfully to monitor ligand binding to membrane proteins, including the human glycine

receptor (Wohri *et al.*, 2013) and the *E. coli* Na⁺/H⁺ antiporter NhaA (Maes *et al.*, 2012). ITC was also used to locate ion binding sites in NhaA by comparing the thermodynamic signatures of WT and mutant antiporters (Maes *et al.*, 2012).

For membrane proteins, ITC is carried out on detergent solubilised protein, and protein-detergent interactions can contribute to or mask the signal of binding events (Rajaratnam & Rosgen, 2014). This may complicate the measurement of lipid inhibitor binding to GlyT2, as specific protein-lipid interactions may be difficult to interpret. Nonetheless, ITC would be an interesting approach to study GlyT2 and may provide information on lipid binding, as well as indicate the ordering of flexible lipid tails. While mutant data in this thesis suggests that inhibition of GlyT2 is via a single high specificity site, it remains that lipids are often found bound to multiple sites on a protein. Multiple binding events and their strength of interaction could be observed using this technique.

Another technique to monitor protein-lipid interactions involves using mass spectrometry of intact membrane proteins (native-MS), where purified protein is ionised and liberated from detergent micelles into the gas phase, where it remains folded and can be resolved on a typical mass-charge spectrum (Laganowsky *et al.*, 2013). As the detergent micelle is stripped via collisional activation, any lipids that remain are tightly bound and can be observed in the spectrum. Since its development, native-MS has been integral in increasing the understanding of how lipids influence the structure and function of membrane proteins (Bechara *et al.*, 2015; Bechara & Robinson, 2015; Cong *et al.*, 2016; Laganowsky *et al.*, 2014; Laganowsky *et al.*, 2013; Landreh *et al.*, 2016; Liu *et al.*, 2017; Patrick *et al.*, 2018; Pliotas *et al.*, 2015).

While folded membrane proteins can exist in the gas phase, unfolding can occur under high collisional activation (Laganowsky *et al.*, 2013). A study by Laganowsky *et al.*, (2014) used this principle to measure lipid binding through their ability to maintain the stability of folded protein. It was found that in all cases different numbers of bound lipids conferred stability and that each membrane protein possessed different selectivity. Lipid binding to the

mechanosensitive channel was non-selective, whereas stabilisation of the ammonia channel (AmtB) was head group selective; with cardiolipin and phosphatidylglycerol providing increased stability, while phosphatidic acid and phosphatidylserine did not. Subsequent crystallisation of AmtB in the presence of PG, revealed a structure which was similar to the previously detergent crystallised AmtB (Khademi *et al.*, 2004), but with a loop region forming a specific PG binding site. Asparagine and glutamate residues were observed to cradle the head group while a phenylalanine residue interacted with an acyl tail. A tryptophan residue was also shifted 4 Å and rotated 160° to a position which would interact with membrane phospholipid groups.

In addition to identifying lipids bound to membrane proteins, their strength of interactions can also be quantified using native-MS at a controlled temperature to measure thermodynamic parameters to represent binding modes and conformational ordering (Cong *et al.*, 2016). Lipids with 1-palmitoyl-2-oleoyl (PO) tails and a range of head groups were applied to AmtB which was previously shown to possess lipid head group selectivity. It was observed that there was greater enthalpy upon binding of POPG, and a corresponding decrease in entropy which is believed to be due to rearrangement of AmtB to form the lipid-bound conformation. Lipids with a PG head group attached to 1-, 2- saturated C12-, C14-, or C16- tails were then examined for changes in binding; as tails became longer, the entropy became more favourable which was accompanied by an enthalpic penalty indicative of more hydrophobic interactions. Native-MS of proteins at a set temperature allows for the determination of an equilibrium dissociation constant (K_d) of binding. This is a direct measure of affinity, rather than effective inhibitory concentrations (IC_{50}). Binding of multiple lipid types and their influence on subsequent binding events can also be monitored using this technique (Patrick *et al.*, 2018). It was found for AmtB that different lipid pairs produced different allosteric modulation (indicated by a “coupling factor”), and that most lipid combinations had a positive coupling factor, however some possessed negative coupling factors, which suggests that lipid binding can force both favourable and unfavourable conformations for subsequent binding events.

Lipid inhibition of GlyT2 is non-competitive and proposed to act via an allosteric site. Native-MS is a valuable tool to elucidate specific membrane protein-lipid interactions and would be a useful approach for studying interactions between lipid inhibitors and GlyT2. Native-MS may inform how lipid inhibitors bind, and with what affinity; and could also help in understanding their mechanism of action.

6.2.2 Advances in structural biology to study membrane proteins in a more native environment

Membrane protein structural biology remains a challenging field as a result of the inherent instability of these proteins outside their membrane environment. There are a number of factors contributing to the instability of membrane proteins; their surfaces are highly amphipathic and must be supported by a lipid or detergent scaffold, and they contain highly flexible regions which can hinder crystal formation (Carpenter *et al.*, 2008). While X-ray crystallography has typically been utilised to visualise membrane proteins, there are a number of newer techniques which attempt to circumvent these problems to obtain protein structures.

Traditional X-ray crystallography often requires the use of thermostable mutants where residues are substituted or entire flexible sections removed, as in the case of NSS transporters where the first 20 amino acids of the N-terminus and 42 amino acids from EL2 were removed to capture the structure of dDAT (Penmatsa *et al.*, 2013). Unlike X-ray crystallography, cryo-electron microscopy (cryo-EM) can obtain structures from non-crystalline proteins. In cryo-EM, proteins are rapidly frozen in their flexible, native states and can accommodate flexible regions of proteins. High energy electrons are then used to capture 2D images of these flash frozen proteins from which 3D structures can be constructed (Spiegel *et al.*, 2015; Vinothkumar, 2015). GlyT2 possesses the longest flexible regions of proteins in this family (199 and 102 amino acids in N-terminus and EL2 respectively), which have been excluded from the homology model used in Chapter 5 of this thesis as they are not present in the template dDAT structure (Penmatsa *et al.*, 2013). Visualisation of native GlyT2 by traditional

methods is therefore unlikely and perhaps cryo-EM could be useful in observing more of the flexible regions of this protein.

The use of Cryo-EM has been limited by low resolution limits ($\sim 3 \text{ \AA}$) and size limits ($>100 \text{ kDa}$), but with the advent of new technologies proteins have recently been visualised at atomic resolution (Vinothkumar, 2015). Cryo-EM has traditionally been used to elucidate structures of large protein complexes as errors occur when aligning individual images for smaller proteins, which may hinder visualisation of monomeric LeuT ($\sim 58 \text{ kDa}$) and GlyT2 ($\sim 88 \text{ kDa}$). Recently, a cryo-EM structure of haemoglobin (64 kDa , 3.2 \AA) has been revealed using a phase plate, which improves signal-to-noise and reduces the image contrast problem (Khoshouei *et al.*, 2017). With improvements in this technology, visualisation of smaller proteins, such as GlyT2, may be possible.

To prepare membrane proteins for structural analysis they must be purified from the host cell membrane. Isolation of membrane proteins typically involves detergent solubilisation to mimic lipid bilayers and maintain a protein folded in a functional conformation (Carpenter *et al.*, 2008). As previously discussed, many membrane proteins specifically bind lipids that are essential for their function, therefore solubilising membrane proteins in detergent may remove tightly bound lipids and hold a protein in its non-native state. As a result of this purification process there are few X-ray structures of membrane proteins resolved with lipids bound. One such structure is the trimeric betaine transporter (BetP) which has been solved with 8 POPG lipids mimicking the lipid bilayer or bound in areas thought to mediate oligomeric interactions and gating (Koshy *et al.*, 2013). Structural evidence from X-ray crystallography can suggest roles for lipid interactions which can be strengthened using other techniques. For example, Fourier transform infrared (FTIR) spectroscopy of proteins reconstituted into closely packed two-dimensional crystals of lipids can be used to monitor the stretching modes of lipid head groups and acyl tails for different transport conditions (Lewis & McElhaney, 2013). Using this technique to monitor K^+ binding to BetP reconstituted in negatively charged lipids shows

phospholipid head groups changing their electrostatic and H-bonds in a K^+ dependent manner which supports the original crystallographic data (Güler *et al.*, 2016).

Detergents also may not cover all hydrophobic areas of the protein and this can cause hydrophobic mismatch, causing proteins to aggregate. It has previously been shown that the function of LeuT can be affected by surrounding lipids; the presence of a single membrane exposed residue of LeuT causes hydrophobic mismatch in membranes (Mondal *et al.*, 2013); and by titrating concentrations of the detergent, n-dodecyl- β -D-maltoside, the stoichiometry of transport can be altered (LeVine *et al.*, 2016). Clearly, the membrane environment can alter the functional and structural biology of membrane proteins and should be considered in their studies.

Techniques that study membrane proteins in a more membrane-like environment, such as lipidic cubic phase (LCP) crystallisation and incorporation into nanodiscs can help to capture native states. Following their isolation, membrane proteins can be reconstituted into LCPs, which forms a matrix that closely mimics lipid bilayers and supports membrane proteins (Landau & Rosenbusch, 1996). LCP crystals form in these bilayers with additional protein-protein crystal contacts that are stabilised by the presence of lipid (usually monoolein). LCP often yields stable protein crystals which can be used to determine X-ray crystal structures (Zabara *et al.*, 2017).

Nanodiscs are high density lipoprotein particles made by solubilising a membrane protein with detergent in the presence of phospholipids and an amphipathic membrane scaffold protein (MSP). Following detergent removal, nanodiscs self-assemble with the protein embedded within phospholipids, held together by the MSP (Civjan *et al.*, 2003). As the lipid composition of nanodiscs can be engineered, they are useful tools to study specific lipid-protein interactions (Bayburt & Sligar, 2010).

While LCP and nanodiscs minimise detergent exposure, detergents are still required to initially extract proteins from the host cell membrane. A new strategy to form lipoprotein particles,

without the use of detergents, employs styrene maleic acid (SMA) copolymers which self-assemble into nanoparticles (Scheidelaar *et al.*, 2015). SMA copolymers are membrane solubilising agents that utilise the hydrophobic effect to wrap around planar bilayer fragments to extract and purify membrane proteins with their surrounding lipids to form SMA lipo-particles (SMALPS). Using this technique, membrane proteins never leave the lipid bilayer. It has been shown the tetrameric K⁺ channel (KcsA) can be directly reconstituted into planar lipid bilayers forming SMALPS, and single channel measurements performed using electrophysiology (Dörr *et al.*, 2014). Additionally, crystal structures of bacteriorhodopsin (Broecker *et al.*, 2017) and the *E. coli* multi drug efflux transporter (Parmar *et al.*, 2018) purified by SMA copolymers have recently been solved using LCP and cryo-EM.

Many functional and structural studies require purified protein, a challenge that is yet to be overcome for many mammalian membrane proteins, including GlyT2. The use of detergent-minimising techniques such as LCP, or the incorporation of proteins into lipoparticles formed using MSP mediated nanodiscs or SMA copolymers, may be a promising tool to purify GlyT2 for the study of lipid-protein interactions.

6.3 Monitoring conformational dynamics of transport and inhibition

Mutagenesis data and subsequent docking of lipid inhibitors onto the GlyT2 model have established that EL4 has an important role in inhibition. Because it is proposed that EL4 undergoes large movements from the outward-facing to the inward-facing states, a mechanism of inhibition was suggested wherein lipid inhibitors stabilise EL4 and prevent critical conformational changes. There are a number of crystal structures of LeuT in various states of the transport cycle which can help to infer structural changes; however X-ray crystallography is insufficient to visualise dynamic conformational changes, and by relying solely on these structures data can be over-extrapolated. Comparison of LeuT crystal structures show TM1a tilted by ~45° in the inward-open structure relative to the closed state (Krishnamurthy & Gouaux, 2012), and authors suggested that this movement is required for

substrate release. Recent research using conformational dynamics has observed TM1a movement to be much smaller, and also identify the N-terminus as a region important for intracellular gating (Kazmier *et al.*, 2014; Terry *et al.*, 2018). Dynamic studies of membrane proteins are therefore required to understand more about conformational changes of transport, and could help to propose how lipid-mediated GlyT2 inhibition may occur.

Single molecule [Förster] fluorescence resonance energy transfer (smFRET) and double electron-electron resonance (DEER; also called pulsed electron-electron double resonance) are biophysical techniques which measure molecular scale distances (1-10 nm) to describe conformational dynamics and intramolecular interactions (Jeschke *et al.*, 2002; Juetten *et al.*, 2014; McHaourab *et al.*, 2011; Sasmal *et al.*, 2016). smFRET relies on donor and acceptor fluorophores which are linked to certain areas of the protein; where fluorescence of the acceptor and quenching of the donor indicates their relative positions (Juetten *et al.*, 2014). Distance measurements are similarly measured in DEER where spin-labelled residues produce electron paramagnetic resonance spectra which reflect their local environment (G. Jeschke, 2012). These techniques can help to capture transient conformations; provide information on relative populations of each state and the timing of conformational transitions; as well as monitor how each state changes upon binding of substrate, ions, and inhibitors. Both smFRET and DEER have been used to monitor alternating access by LeuT to identify regions important for transport (Kazmier *et al.*, 2014; Terry *et al.*, 2018; Zhao *et al.*, 2010; Zhao *et al.*, 2011).

smFRET on detergent solubilised LeuT revealed a partially inward-facing intermediate structure which is associated with Na⁺ release from the Na₂ site (Terry *et al.*, 2018). In substrate free conditions, this state was only sampled 13% of the time, which suggests it may be a more rare conformation that is difficult to obtain using traditional crystallographic techniques. It was also shown that pre-incubation with Na⁺ causes thinning of the extracellular vestibule which hinders the access of leucine, but not alanine, of the primary substrate site.

smFRET has enabled the visualisation of how occupation of certain sites (in this case Na⁺) can allosterically alter substrate binding.

In a study by Kazmier *et al.*, (2014), using DEER, substrate and Na⁺ concentrations were used to drive isomerisation of LeuT from outward-open to inward-open. It was shown that EL4 shifted between outward-facing and occluded and is an important region to drive transport. By using either n-octyl-β-D-glucopyranoside or n-dodecyl-β-D-maltoside the populations of states could be shifted, with n-octyl-β-D-glucopyranoside favouring the outward open state.

Lipid inhibitors of GlyT2 may act by binding allosterically to GlyT2 and changing access or the shape of the primary substrate binding site. They may also stabilise the transporter in a certain state that is not transport-favourable. By using dynamic techniques that monitor conformational transitions, perhaps an inhibited state could be captured and the mechanism of inhibition better understood. DEER spin-labelling and smFRET fluorophores generally rely on labelling either native or engineered cysteine residues. GlyT2 contains 23 native cysteines which would make creation of a functional cysteine-less template very difficult. Alternative labelling strategies, for example incorporation of unnatural amino acids, may help in the use of these methods.

Another approach to monitor dynamic movements of proteins is using computational MD studies. MD uses classical equations of motion and energy for each particle in the system to observe protein changes. For a typical membrane protein in its native environment the system is comprised of not only the protein and aqueous compartments, but the lipid bilayer. This requires calculations on ~10⁵ atoms for atomic simulations (Dror *et al.*, 2012). Lipid motions (lipid diffusion, flip-flopping, bilayer self-assembly) are slow which makes them difficult to detect within the time frame of a simulation (Kandt *et al.*, 2007). To capture each of the proposed steps in the mechanism of lipid inhibition of GlyT2, longer simulations will need to be performed.

The more stable a protein is, the longer it can be run in an MD simulation with confidence that conformational changes are genuine (Kandt *et al.*, 2007). Homology models are less stable than protein data bank (PDB) structures and their quality is entirely dependent on the quality of the template structure (Koehler *et al.*, 2015). For GlyT2, the homology model used in this thesis for the docking of oleoyl D-Lys is based on the outward-occluded dDAT structure (PDB: 4M48) and was developed using a protein fold recognition (or threading) approach (Subramanian *et al.*, 2016). GlyT2 shares ~50% sequence identity with dDAT and the dDAT structure and GlyT2 homology model overlap with an RMSD of 1.37 Å, which is appropriate for accurate MD simulations (Leman *et al.* 2015). In order to run simulations of a homology model for suitably long to observe lipid movements, coarse-grain MD can be used, where particles are defined as groups of atoms (for example a residue) (Kandt *et al.*, 2007).

A recent study by Zeppelin *et al.*, (2018), used both atomistic and coarse-grain MD to examine the role cholesterol possesses in altering conformational dynamics of dDAT, hDAT, hSERT, and the human noradrenalin transporter from either crystal structures or homology models. It was observed that in the absence of cholesterol DAT commences the first steps of transport, whereas in the presence of cholesterol no conformational changes take place. This suggests that cholesterol stabilises the outward-open conformation to prevent transport, which was predicted from the first dDAT structure (Penmatsa *et al.*, 2013). It was also found that cholesterol-mediated inhibition was conserved at this site in the SERT and noradrenalin transporters. A similar approach for GlyT2 lipid inhibitors could be employed, where conformational changes of the oleoyl D-Lys docked protein structure could be compared to GlyT2 with no lipid present. MD simulations may help to further discern the mechanism of inhibition at GlyT2, which is currently only visualised in a static docked model.

6.4 Functional implications of glycine transport inhibitors

Nerve injury and alteration in synaptic pathways within the dorsal horn can give rise to neuropathic pain, and a loss of inhibitory neurotransmission can cause disinhibition of pain

signalling (Latremoliere & Woolf, 2009; Takazawa & MacDermott, 2010). Inhibitory GABAergic neurons are distributed throughout the CNS, while glycinergic neurons expressing GlyR and GlyT2 are abundant within the spinal cord dorsal horn. Here, glycine acts in a feed-forward inhibitory circuit that separates the innocuous and noxious sensory pathways (Lu *et al.*, 2013).

It has been shown that following peripheral inflammation there is reduced frequency of GlyR-mediated currents and a reduction in inhibitory control of spinal lamina I neurons, and that this loss of control is via a presynaptic mechanism (Müller *et al.*, 2003). More recently, it was observed that there is a loss of glycinergic control over excitatory radial neurons in spinal lamina II (Imlach *et al.*, 2016).

Partial, non-competitive inhibition of presynaptic GlyT2 glycine transporters prolongs the time-course of glycine at inhibitory synapses in the superficial dorsal horn, which then remains to activate GlyRs and increase inhibitory tone (Jeong *et al.*, 2010). Full inhibition, however, has been shown to alter the ratio of GABA to glycine release (Xu *et al.*, 2005). It is thought that complete blockage of GlyT2 results in an imbalance of GABA:glycine loading into vesicles by VIAAT, which ultimately reduces glycine release and inhibitory glycinergic signalling in the spinal cord dorsal horn. For therapeutics targeting GlyT2 to be successful, full vs. partial inhibition must be addressed; but the question remains – how partial is partial? That is, what is the ideal level of inhibition that will provide a balance between slowing reuptake, and still allow appropriate glycine recycling? A partial, non-competitive inhibitor should in theory not change the equilibrium intracellular glycine concentration, but rather alter the time taken to reach equilibrium. In this thesis I identified a large range of allosteric lipid inhibitors with differences in maximal level of inhibition and reversibility characteristics. It would be valuable to study a few key compounds in brain slices containing inhibitory glycinergic synapses, where inhibition of GlyT2 would either increase or decrease glycine in the synapse following prolonged exposure. This would help to identify efficacious compounds with ideal characteristics that may reduce any adverse side effects when introduced into animal models of neuropathic pain.

The failure of potential therapeutics can also be due to ineffectiveness as well as an adverse side effect profile. Lipid analgesics could be tested in a number of models of chronic pain, for example, inflammatory pain induced using a subcutaneous injection of Freund's Complete Adjuvant into the plantar surface of the paw, as in previous studies of NAGly (Succar et al., 2007). Validating the use of N-acyl amino acids as analgesics in multiple animal models may increase the likelihood of their activity as analgesics in humans. While oleoyl D-Lys has been shown to cross the BBB via IP injection, the oral bioavailability should be examined, which may direct further chemistry to improve the permeability and solubility of lipid inhibitors while retaining efficacy, and will become an important consideration in the development of the next generation of GlyT2 inhibitors.

6.5 Conclusion

The objective of this thesis was to contribute to the understanding of how lipid compounds can inhibit the membrane bound transporter, GlyT2. I have greatly expanded the known pool of lipid GlyT2 inhibitors, and identified compounds with a broad range of inhibitory properties, which can be used as tools to determine ideal *in vivo* activity. I have also used site-directed mutagenesis to begin to unravel the molecular mechanism of inhibition. Further understanding of the mechanism of inhibition and design of more effective inhibitors will require the use of recent advances in functional and structural biochemical techniques to visualise lipid inhibitors bound to GlyT2, and to appreciate the conformational dynamics underlying transport. These approaches will greatly contribute to the study of lipid-membrane protein interactions. It is hoped that further development of the compounds characterised in this thesis will produce clinically relevant therapeutics for the treatment of chronic neuropathic pain.

References

- Access Economics Pty Limited for MBF Foundation in collaboration with University of Sydney Pain Management Research Institute, November 2007. *The high price of pain: the economic impact of persistent pain in Australia.*
- Ahmadi, S., Kotalla, C., Gühring, H., Takeshima, H., Pahl, A., & Zeilhofer, H.U. (2001). Modulation of synaptic transmission by nociceptin/orphanin FQ and nocistatin in the spinal cord dorsal horn of mutant mice lacking the nociceptin/orphanin FQ receptor. *Mol Pharmacol.*, 59(3):612-618
- Aponte-Santamaria, C., Briones, R., Schenk, A. D., Walz, T., & de Groot, B. L. (2012). Molecular driving forces defining lipid positions around aquaporin-0. *Proc Natl Acad Sci U S A*, 109(25), 9887-9892.
- Aragon, C., & Lopez-Corcuera, B. (2005). Glycine transporters: crucial roles of pharmacological interest revealed by gene deletion. *Trends Pharmacol Sci*, 26(6), 283-286.
- Bai, J. Y., Ding, W. G., Kojima, A., Seto, T., & Matsuura, H. (2015). Putative binding sites for arachidonic acid on the human cardiac Kv 1.5 channel. *Br J Pharmacol*, 172(22), 5281-5292.
- Bayburt, T. H., & Sligar, S. G. (2010). Membrane protein assembly into Nanodiscs. *FEBS Lett*, 584(9), 1721-1727.
- Bechara, C., Noll, A., Morgner, N., Degiacomi, M. T., Tampe, R., & Robinson, C. V. (2015). A subset of annular lipids is linked to the flippase activity of an ABC transporter. *Nat Chem*, 7(3), 255-262.
- Bechara, C., & Robinson, C. V. (2015). Different modes of lipid binding to membrane proteins probed by mass spectrometry. *J Am Chem Soc*, 137(16), 5240-5247.
- Beno, B. R., Yeung, K. S., Bartberger, M. D., Pennington, L. D., & Meanwell, N. A. (2015). A Survey of the Role of Noncovalent Sulfur Interactions in Drug Design. *J Med Chem*, 58(11), 4383-4438.
- Berglund, B. A., Boring, D. L., Wilken, G. H., Makriyannis, A., Howlett, A. C., & Lin, S. (1998). Structural requirements for arachidonylethanolamide interaction with CB1 and CB2 cannabinoid receptors: pharmacology of the carbonyl and ethanolamide groups. *Prostaglandins Leukot Essent Fatty Acids*, 59(2), 111-118.

- Bhadani, A., Iwabata, K., Sakar, K., Koura, S., Sakai, H., & Abe, A. (2017) Sustainable oleic acid and stearic acid based biodegradable surfactants. *RCS Adv*, 7, 10433-10442.
- Bornheim, L. M., Kim, K. Y., Chen, B., & Correia, M. A. (1995). Microsomal cytochrome P450-mediated liver and brain anandamide metabolism. *Biochem Pharmacol*, 50(5), 677-686.
- Bradaia, A., Schlichter, R., & Trouslard, J. (2004). Role of glial and neuronal glycine transporters in the control of glycinergic and glutamatergic synaptic transmission in lamina X of the rat spinal cord. *J Physiol*, 559(Pt 1), 169-186.
- Bradshaw, H. B., Rimmerman, N., Hu, S. S., Benton, V. M., Stuart, J. M., Masuda, K., . . . Walker, J. M. (2009). The endocannabinoid anandamide is a precursor for the signaling lipid N-arachidonoyl glycine by two distinct pathways. *BMC Biochem*, 10, 14.
- Brinkmann, V., Billich, A., Baumruker, T., Heining, P., Schmouder, R., Francis, G., . . . Burtin, P. (2010). Fingolimod (FTY720): discovery and development of an oral drug to treat multiple sclerosis. *Nat Rev Drug Discov*, 9(11), 883-897.
- Broecker, J., Eger, B. T., & Ernst, O. P. (2017). Crystallogensis of Membrane Proteins Mediated by Polymer-Bounded Lipid Nanodiscs. *Structure*, 25(2), 384-392.
- Brunner, J. D., Lim, N. K., Schenck, S., Duerst, A., & Dutzler, R. (2014). X-ray structure of a calcium-activated TMEM16 lipid scramblase. *Nature*, 516(7530), 207-212.
- Carland, J. E., Mansfield, R. E., Ryan, R. M., & Vandenberg, R. J. (2013). Oleoyl-L-carnitine inhibits glycine transport by GlyT2. *Br J Pharmacol*, 168(4), 891-902.
- Carland, J. E., Thomas, M., Mostyn, S. N., Subramanian, N., O'Mara, M. L., Ryan, R. M., & Vandenberg, R. J. (2018). Molecular Determinants for Substrate Interactions with the Glycine Transporter GlyT2. *ACS Chem Neurosci*, 9(3), 603-614.
- Carpenter, E. P., Beis, K., Cameron, A. D., & Iwata, S. (2008). Overcoming the challenges of membrane protein crystallography. *Curr Opin Struct Biol*, 18(5), 581-586.
- Carta, E., Chung, S. K., James, V. M., Robinson, A., Gill, J. L., Remy, N., . . . Harvey, R. J. (2012). Mutations in the GlyT2 gene (SLC6A5) are a second major cause of startle disease. *J Biol Chem*, 287(34), 28975-28985.

- Caulfield, W. L., Collie, I. T., Dickins, R. S., Epemolu, O., McGuire, R., Hill, D. R., . . . Sundaram, H. (2001). The first potent and selective inhibitors of the glycine transporter type 2. *J Med Chem*, *44*(17), 2679-2682.
- Chen, R., & Chung, S. H. (2015). Molecular dynamics simulations of Na(+) and leucine transport by LeuT. *Biochem Biophys Res Commun*, *464*(1), 281-285.
- Chrencik, J. E., Roth, C. B., Terakado, M., Kurata, H., Omi, R., Kihara, Y., . . . Hanson, M. A. (2015). Crystal Structure of Antagonist Bound Human Lysophosphatidic Acid Receptor 1. *Cell*, *161*(7), 1633-1643.
- Civjan, N. R., Bayburt, T. H., Schuler, M. A., & Sligar, S. G. (2003). Direct solubilization of heterologously expressed membrane proteins by incorporation into nanoscale lipid bilayers. *Biotechniques*, *35*(3), 556-560, 562-553.
- Coleman, J. A., Green, E. M., & Gouaux, E. (2016). X-ray structures and mechanism of the human serotonin transporter. *Nature*, *532*(7599), 334-339.
- Cong, X., Liu, Y., Liu, W., Liang, X., Russell, D. H., & Laganowsky, A. (2016). Determining Membrane Protein-Lipid Binding Thermodynamics Using Native Mass Spectrometry. *J Am Chem Soc*, *138*(13), 4346-4349.
- Console-Bram, L., Ciuciu, S. M., Zhao, P., Zipkin, R. E., Brailoiu, E., & Abood, M. E. (2017). N-arachidonoyl glycine, another endogenous agonist of GPR55. *Biochem Biophys Res Commun*, *490*(4), 1389-1393.
- Corcelli, A. (2009). The cardiolipin analogues of Archaea. *Biochim Biophys Acta*, *1788*(10), 2101-2106.
- Costigan, M., Scholz, J., & Woolf, C. J. (2009). Neuropathic pain: a maladaptive response of the nervous system to damage. *Annu Rev Neurosci*, *32*, 1-32.
- Cravatt, B. F., Giang, D. K., Mayfield, S. P., Boger, D. L., Lerner, R. A., & Gilula, N. B. (1996). Molecular characterization of an enzyme that degrades neuromodulatory fatty-acid amides. *Nature*, *384*, 83.
- Dersh, J., Gatchel, R. J., Polatin, P., & Mayer, T. (2002). Prevalence of psychiatric disorders in patients with chronic work-related musculoskeletal pain disability. *J Occup Environ Med*, *44*(5), 459-468.
- Dörr, J. M., Koorengevel, M. C., Schafer, M., Prokofyev, A. V., Scheidelaar, S., van der Cruisen, E. A., . . . Killian, J. A. (2014). Detergent-free isolation, characterization, and functional reconstitution of a tetrameric K⁺ channel: the power of native nanodiscs. *Proc Natl Acad Sci U S A*, *111*(52), 18607-18612.

- Dror, R. O., Dirks, R. M., Grossman, J. P., Xu, H., & Shaw, D. E. (2012). Biomolecular simulation: a computational microscope for molecular biology. *Annu Rev Biophys*, 41, 429-452.
- Edington, A. R., McKinzie, A. A., Reynolds, A. J., Kassiou, M., Ryan, R. M., & Vandenberg, R. J. (2009). Extracellular loops 2 and 4 of GLYT2 are required for N-arachidonylglycine inhibition of glycine transport. *J Biol Chem*, 284(52), 36424-36430.
- Efremov, R. G., Gatsogiannis, C., & Raunser, S. (2017). Lipid Nanodiscs as a Tool for High-Resolution Structure Determination of Membrane Proteins by Single-Particle Cryo-EM. *Methods Enzymol*, 594, 1-30.
- Eulenburg, V., Arnsen, W., Betz, H., & Gomeza, J. (2005). Glycine transporters: essential regulators of neurotransmission. *Trends Biochem Sci*, 30(6), 325-333.
- Eulenburg, V., Becker, K., Gomeza, J., Schmitt, B., Becker, C. M., & Betz, H. (2006). Mutations within the human GLYT2 (SLC6A5) gene associated with hyperekplexia. *Biochem Biophys Res Commun*, 348(2), 400-405.
- Evans, J. F., & Hutchinson, J. H. (2010). Seeing the future of bioactive lipid drug targets. *Nat Chem Biol*, 6(7), 476-479.
- Fornasari, D. (2017). Pharmacotherapy for Neuropathic Pain: A Review. *Pain Ther*, 6(Suppl 1), 25-33.
- Forrest, L. R., Zhang, Y. W., Jacobs, M. T., Gesmonde, J., Xie, L., Honig, B. H., & Rudnick, G. (2008). Mechanism for alternating access in neurotransmitter transporters. *Proc Natl Acad Sci U S A*, 105(30), 10338-10343.
- Fowler, C. J. (2013). Transport of endocannabinoids across the plasma membrane and within the cell. *The FEBS Journal*, 280(9), 1895-1904.
- Funari, S. S., Barcelo, F., & Escriba, P. V. (2003). Effects of oleic acid and its congeners, elaidic and stearic acids, on the structural properties of phosphatidylethanolamine membranes. *J Lipid Res*, 44(3), 567-575.
- Gatchel, R. J., Peng, Y. B., Peters, M. L., Fuchs, P. N., & Turk, D. C. (2007). The biopsychosocial approach to chronic pain: scientific advances and future directions. *Psychol Bull*, 133(4), 581-624.
- Giang, D. K., & Cravatt, B. F. (1997). Molecular characterization of human and mouse fatty acid amide hydrolases. *Proc Natl Acad Sci U S A*, 94(6), 2238-2242.

- Gomez, J., Hulsmann, S., Ohno, K., Eulenburg, V., Szoke, K., Richter, D., & Betz, H. (2003a). Inactivation of the glycine transporter 1 gene discloses vital role of glial glycine uptake in glycinergic inhibition. *Neuron*, *40*(4), 785-796.
- Gomez, J., Ohno, K., Hulsmann, S., Armsen, W., Eulenburg, V., Richter, D. W., . . . Betz, H. (2003b). Deletion of the mouse glycine transporter 2 results in a hyperekplexia phenotype and postnatal lethality. *Neuron*, *40*(4), 797-806.
- Gonen, T., Cheng, Y., Sliz, P., Hiroaki, Y., Fujiyoshi, Y., Harrison, S. C., & Walz, T. (2005). Lipid-protein interactions in double-layered two-dimensional AQP0 crystals. *Nature*, *438*(7068), 633-638.
- Güler, G., Gartner, R. M., Ziegler, C., & Mantele, W. (2016). Lipid-Protein Interactions in the Regulated Betaine Symporter BetP Probed by Infrared Spectroscopy. *J Biol Chem*, *291*(9), 4295-4307.
- Gupta, K., Donlan, J. A. C., Hopper, J. T. S., Uzdaviny, P., Landreh, M., Struwe, W. B., . . . Robinson, C. V. (2017). The role of interfacial lipids in stabilizing membrane protein oligomers. *Nature*, *541*(7637), 421-424.
- Hanson, M. A., Roth, C. B., Jo, E., Griffith, M. T., Scott, F. L., Reinhart, G., . . . Stevens, R. C. (2012). Crystal structure of a lipid G protein-coupled receptor. *Science*, *335*(6070), 851-855.
- Haranishi, Y., Hara, K., Terada, T., Nakamura, S., & Sata, T. (2010). The antinociceptive effect of intrathecal administration of glycine transporter-2 inhibitor ALX1393 in a rat acute pain model. *Anesth Analg*, *110*(2), 615-621.
- Harroun, T. A., Heller, W. T., Weiss, T. M., Yang, L., & Huang, H. W. (1999a). Experimental evidence for hydrophobic matching and membrane-mediated interactions in lipid bilayers containing gramicidin. *Biophys J*, *76*(2), 937-945.
- Harroun, T. A., Heller, W. T., Weiss, T. M., Yang, L., & Huang, H. W. (1999b). Theoretical analysis of hydrophobic matching and membrane-mediated interactions in lipid bilayers containing gramicidin. *Biophys J*, *76*(6), 3176-3185.
- Hermanns, H., Muth-Selbach, U., Williams, R., Krug, S., Lipfert, P., Werdehausen, R., . . . Bauer, I. (2008). Differential effects of spinally applied glycine transporter inhibitors on nociception in a rat model of neuropathic pain. *Neurosci Lett*, *445*(3), 214-219.

- Hong, W. C., & Amara, S. G. (2010). Membrane cholesterol modulates the outward facing conformation of the dopamine transporter and alters cocaine binding. *J Biol Chem*, 285(42), 32616-32626.
- Hua, T., Vemuri, K., Pu, M., Qu, L., Han, G. W., Wu, Y., . . . Liu, Z. J. (2016). Crystal Structure of the Human Cannabinoid Receptor CB1. *Cell*, 167(3), 750-762 e714.
- Huang, Bisogno, T., Petros, T. J., Chang, S. Y., Zavitsanos, P. A., Zipkin, R. E., . . . Walker, J. M. (2001). Identification of a new class of molecules, the arachidonyl amino acids, and characterization of one member that inhibits pain. *J Biol Chem*, 276(46), 42639-42644.
- Huang, W., & Simpson, R. K. (2000). Long-term intrathecal administration of glycine prevents mechanical hyperalgesia in a rat model of neuropathic pain. *Neurol Res*, 22(2), 160-164.
- Hunter, S. F., Bowen, J. D., & Reder, A. T. (2016). The Direct Effects of Fingolimod in the Central Nervous System: Implications for Relapsing Multiple Sclerosis. *CNS Drugs*, 30(2), 135-147.
- Hurst, D. P., Grossfield, A., Lynch, D. L., Feller, S., Romo, T. D., Gawrisch, K., . . . Reggio, P. H. (2010). A lipid pathway for ligand binding is necessary for a cannabinoid G protein-coupled receptor. *J Biol Chem*, 285(23), 17954-17964.
- Imlach, W. L., Bholra, R. F., Mohammadi, S. A., & Christie, M. J. (2016). Glycinergic dysfunction in a subpopulation of dorsal horn interneurons in a rat model of neuropathic pain. *Sci Rep*, 6, 37104.
- Inano, A., Sai, Y., Nikaido, H., Hasimoto, N., Asano, M., Tsuji, A., & Tamai, I. (2003). Acetyl-L-carnitine permeability across the blood-brain barrier and involvement of carnitine transporter OCTN2. *Biopharm Drug Dispos*, 24(8), 357-365.
- Jeong, H.J., Jang, I.S., Moorhouse, A.J., Akaike N. (2003). Activation of presynaptic glycine receptors facilitates glycine release from presynaptic terminals synapsing onto rat spinal sacral dorsal commissural nucleus neurons. *J Physiol.*, 550(2): 373–383.
- Jeong, H. J., Vandenberg, R. J., & Vaughan, C. W. (2010). N-arachidonyl-glycine modulates synaptic transmission in superficial dorsal horn. *Br J Pharmacol*, 161(4), 925-935.
- Jeschke, G. (2012). DEER distance measurements on proteins. *Annu Rev Phys Chem*, 63, 419-446.

- Jeschke, G., Pannier, M., & Spiess, H. W. (2002). Double electron-electron resonance *Distance Measurements in Biological Systems by EPR* (pp. 493-512): Springer.
- Juette, M. F., Terry, D. S., Wasserman, M. R., Zhou, Z., Altman, R. B., Zheng, Q., & Blanchard, S. C. (2014). The bright future of single-molecule fluorescence imaging. *Curr Opin Chem Biol*, 20, 103-111.
- Julius, D., & Basbaum, A. I. (2001). Molecular mechanisms of nociception. *Nature*, 413(6852), 203-210.
- Kachel, K., Asuncion-Punzalan, E., & London, E. (1995). Anchoring of tryptophan and tyrosine analogs at the hydrocarbon-polar boundary in model membrane vesicles: parallax analysis of fluorescence quenching induced by nitroxide-labeled phospholipids. *Biochemistry*, 34(47), 15475-15479.
- Kandt, C., Ash, W. L., & Tieleman, D. P. (2007). Setting up and running molecular dynamics simulations of membrane proteins. *Methods*, 41(4), 475-488.
- Kazmier, K., Sharma, S., Quick, M., Islam, S. M., Roux, B., Weinstein, H., . . . McHaourab, H. S. (2014). Conformational dynamics of ligand-dependent alternating access in LeuT. *Nat Struct Mol Biol*, 21(5), 472-479.
- Khademi, S., O'Connell, J., 3rd, Remis, J., Robles-Colmenares, Y., Miercke, L. J., & Stroud, R. M. (2004). Mechanism of ammonia transport by Amt/MEP/Rh: structure of AmtB at 1.35 Å. *Science*, 305(5690), 1587-1594.
- Khoshouei, M., Radjainia, M., Baumeister, W., & Danev, R. (2017). Cryo-EM structure of haemoglobin at 3.2 Å determined with the Volta phase plate. *Nat Commun*, 8, 16099.
- Koehler, L. J., Ulmschneider, M. B., & Gray, J. J. (2015). Computational modeling of membrane proteins. *Proteins*, 83(1), 1-24.
- Kohno, M., Hasegawa, H., Inoue, A., Muraoka, M., Miyazaki, T., Oka, K., & Yasukawa, M. (2006). Identification of N-arachidonylglycine as the endogenous ligand for orphan G-protein-coupled receptor GPR18. *Biochem Biophys Res Commun*, 347(3), 827-832.
- Koshy, C., Schweikhard, E. S., Gartner, R. M., Perez, C., Yildiz, O., & Ziegler, C. (2013). Structural evidence for functional lipid interactions in the betaine transporter BetP. *EMBO J*, 32(23), 3096-3105.

- Kotarsky, K., Nilsson, N. E., Flodgren, E., Owman, C., & Olde, B. (2003). A human cell surface receptor activated by free fatty acids and thiazolidinedione drugs. *Biochem Biophys Res Commun*, 301(2), 406-410.
- Krishnamurthy, H., & Gouaux, E. (2012). X-ray structures of LeuT in substrate-free outward-open and apo inward-open states. *Nature*, 481(7382), 469-474.
- Krishnamurthy, H., Piscitelli, C. L., & Gouaux, E. (2009). Unlocking the molecular secrets of sodium-coupled transporters. *Nature*, 459(7245), 347-355.
- Kristensen, A. S., Andersen, J., Jorgensen, T. N., Sorensen, L., Eriksen, J., Loland, C. J., . . . Gether, U. (2011). SLC6 neurotransmitter transporters: structure, function, and regulation. *Pharmacol Rev*, 63(3), 585-640.
- Laganowsky, A., Reading, E., Allison, T. M., Ulmschneider, M. B., Degiacomi, M. T., Baldwin, A. J., & Robinson, C. V. (2014). Membrane proteins bind lipids selectively to modulate their structure and function. *Nature*, 510(7503), 172-175.
- Laganowsky, A., Reading, E., Hopper, J. T., & Robinson, C. V. (2013). Mass spectrometry of intact membrane protein complexes. *Nat Protoc*, 8(4), 639-651.
- Landau, E. M., & Rosenbusch, J. P. (1996). Lipidic cubic phases: a novel concept for the crystallization of membrane proteins. *Proc Natl Acad Sci U S A*, 93(25), 14532-14535.
- Landreh, M., Marty, M. T., Gault, J., & Robinson, C. V. (2016). A sliding selectivity scale for lipid binding to membrane proteins. *Curr Opin Struct Biol*, 39, 54-60.
- Latremoliere, A., & Woolf, C. J. (2009). Central sensitization: a generator of pain hypersensitivity by central neural plasticity. *J Pain*, 10(9), 895-926.
- Leavitt, S., & Freire, E. (2001). Direct measurement of protein binding energetics by isothermal titration calorimetry. *Curr Opin Struct Biol*, 11(5), 560-566.
- LeVine, M. V., Khelashvili, G., Shi, L., Quick, M., Javitch, J. A., & Weinstein, H. (2016). Role of Annular Lipids in the Functional Properties of Leucine Transporter LeuT Proteomicelles. *Biochemistry*, 55(6), 850-859.
- Lewis, R. N., & McElhaney, R. N. (2013). Membrane lipid phase transitions and phase organization studied by Fourier transform infrared spectroscopy. *Biochim Biophys Acta*, 1828(10), 2347-2358.

- Lin, S., Khanolkar, A. D., Fan, P., Goutopoulos, A., Qin, C., Papahadjis, D., & Makriyannis, A. (1998). Novel analogues of arachidonylethanolamide (anandamide): affinities for the CB1 and CB2 cannabinoid receptors and metabolic stability. *J Med Chem*, 41(27), 5353-5361.
- Lipinski, C.A., Lombardo, F., Dominy, B.W., Feeney, P.J. (1997). Experimental and computational approaches to estimate solubility and permeability in drug discovery and development settings. *Adv. Drug Deliv. Rev.* 23:3-25
- Liu, X., Mitrovic, A. D., Vandenberg, R. J (2009). Glycine transporter 1 associates with cholesterol-rich membrane raft microdomains. *Biochem. Biophys. Res. Commun.* 384(4) 530-534.
- Liu, Y., Cong, X., Liu, W., & Laganowsky, A. (2017). Characterization of Membrane Protein-Lipid Interactions by Mass Spectrometry Ion Mobility Mass Spectrometry. *J Am Soc Mass Spectrom*, 28(4), 579-586.
- Liu, Y., Liu, D., Heath, L., Meyers, D. M., Krafte, D. S., Wagoner, P. K., . . . Curran, M. E. (2001). Direct activation of an inwardly rectifying potassium channel by arachidonic acid. *Mol Pharmacol*, 59(5), 1061-1068.
- Lu, Y., Dong, H., Gao, Y., Gong, Y., Ren, Y., Gu, N., . . . Xiong, L. (2013). A feed-forward spinal cord glycinergic neural circuit gates mechanical allodynia. *J Clin Invest*, 123(9), 4050-4062.
- Luchicchi, A., & Pistis, M. (2012). Anandamide and 2-arachidonoylglycerol: pharmacological properties, functional features, and emerging specificities of the two major endocannabinoids. *Mol Neurobiol*, 46(2), 374-392.
- Lynch, J. W. (2004). Molecular structure and function of the glycine receptor chloride channel. *Physiol Rev*, 84(4), 1051-1095.
- Maccarrone, M., Fiori, A., Bari, M., Granata, F., Gasperi, V., De Stefano, M. E., . . . Strom, R. (2005). Regulation by cannabinoid receptors of anandamide transport across the blood-brain barrier and through other endothelial cells. *Thrombosis and Haemostasis*.
- Maes, M., Rimon, A., Kozachkov-Magrisso, L., Friedler, A., & Padan, E. (2012). Revealing the ligand binding site of NhaA Na⁺/H⁺ antiporter and its pH dependence. *J Biol Chem*, 287(45), 38150-38157.
- Makriyannis, A. (1995). *Cannabinoid Receptors* (R. G. Pertwee, ed Ed. Vol. 87-115): Academic Press, London.

- Malinauskaite, L., Quick, M., Reinhard, L., Lyons, J. A., Yano, H., Javitch, J. A., & Nissen, P. (2014). A mechanism for intracellular release of Na⁺ by neurotransmitter/sodium symporters. *Nature Structural & Molecular Biology*, 21, 1006.
- Malosio, M.L., Marquèze-Pouey, B., Kuhse, J., & Betz H. (1991). Widespread expression of glycine receptor subunit mRNAs in the adult and developing rat brain. *EMBO J*, 10(9):2401-9
- Manzke, T., Niebert, M., Koch, U.R., Caley, A., Vogelgesang, S., Hülsmann, S., Ponimaskin, E., Müller, U., Smart, T.G., Harvey, R.J., Richter, D.W. (2010). Serotonin receptor 1A-modulated phosphorylation of glycine receptor $\alpha 3$ controls breathing in mice. *J Clin Invest.*, 120(11):4118-28
- McHaourab, Hassane S., Steed, P. R., & Kazmier, K. (2011). Toward the Fourth Dimension of Membrane Protein Structure: Insight into Dynamics from Spin-Labeling EPR Spectroscopy. *Structure*, 19(11), 1549-1561.
- Mi, W., Li, Y., Yoon, S. H., Ernst, R. K., Walz, T., & Liao, M. (2017). Structural basis of MsbA-mediated lipopolysaccharide transport. *Nature*, 549(7671), 233-237.
- Mingorance-Le Meur, A., Ghisdal, P., Mullier, B., De Ron, P., Downey, P., Van Der Perren, C., . . . Courade, J. P. (2013). Reversible inhibition of the glycine transporter GlyT2 circumvents acute toxicity while preserving efficacy in the treatment of pain. *Br J Pharmacol*, 170(5), 1053-1063.
- Mitchell, R. W., On, N. H., Del Bigio, M. R., Miller, D. W., & Hatch, G. M. (2011). Fatty acid transport protein expression in human brain and potential role in fatty acid transport across human brain microvessel endothelial cells. *J Neurochem*, 117(4), 735-746.
- Mondal, S., Khelashvili, G., Shi, L., & Weinstein, H. (2013). The cost of living in the membrane: a case study of hydrophobic mismatch for the multi-segment protein LeuT. *Chem Phys Lipids*, 169, 27-38.
- Montigny, C., Lyons, J., Champeil, P., Nissen, P., & Lenoir, G. (2016). On the molecular mechanism of flippase- and scramblase-mediated phospholipid transport. *Biochim Biophys Acta*, 1861(8 Pt B), 767-783.
- Morita, K., Motoyama, N., Kitayama, T., Morioka, N., Kifune, K., & Dohi, T. (2008). Spinal antiallodynia action of glycine transporter inhibitors in neuropathic pain models in mice. *J Pharmacol Exp Ther*, 326(2), 633-645.

- Morrow, J. A., Collie, I. T., Dunbar, D. R., Walker, G. B., Shahid, M., & Hill, D. R. (1998). Molecular cloning and functional expression of the human glycine transporter GlyT2 and chromosomal localisation of the gene in the human genome. *FEBS Lett*, 439(3), 334-340.
- Müller, F., Heinke, B., & Sandkuhler, J. (2003). Reduction of glycine receptor-mediated miniature inhibitory postsynaptic currents in rat spinal lamina I neurons after peripheral inflammation. *Neuroscience*, 122(3), 799-805.
- Nedeljkovic, S. S., Correll, D. J., Bao, X., Zamor, N., Zeballos, J. L., Zhang, Y., . . . Lee, D. H. (2017). Randomised, double-blind, parallel group, placebo-controlled study to evaluate the analgesic efficacy and safety of VVZ-149 injections for postoperative pain following laparoscopic colorectal surgery. *BMJ Open*, 7(2), e011035.
- Omori, Y., Nakajima, M., Nishimura, K., Takahashi, E., Arai, T., Akahira, M., . . . Kainoh, M. (2015). Analgesic effect of GT-0198, a structurally novel glycine transporter 2 inhibitor, in a mouse model of neuropathic pain. *J Pharmacol Sci*, 127(3), 377-381.
- Ormel, J., VonKorff, M., Ustun, T. B., Pini, S., Korten, A., & Oldehinkel, T. (1994). Common mental disorders and disability across cultures. Results from the WHO Collaborative Study on Psychological Problems in General Health Care. *JAMA*, 272(22), 1741-1748.
- Pal, D., & Chakrabarti, P. (2001). Non-hydrogen bond interactions involving the methionine sulfur atom. *J Biomol Struct Dyn*, 19(1), 115-128.
- Pang, M. H., Kim, Y., Jung, K. W., Cho, S., & Lee, D. H. (2012). A series of case studies: practical methodology for identifying antinociceptive multi-target drugs. *Drug Discov Today*, 17(9-10), 425-434.
- Patrick, J. W., Boone, C. D., Liu, W., Conover, G. M., Liu, Y., Cong, X., & Laganowsky, A. (2018). Allostery revealed within lipid binding events to membrane proteins. *Proc Natl Acad Sci U S A*, 115(12), 2976-2981.
- Pei, Y., Mercier, R. W., Anday, J. K., Thakur, G. A., Zvonok, A. M., Hurst, D., . . . Makriyannis, A. (2008). Ligand-binding architecture of human CB2 cannabinoid receptor: evidence for receptor subtype-specific binding motif and modeling GPCR activation. *Chem Biol*, 15(11), 1207-1219.
- Penmatsa, A., & Gouaux, E. (2014). How LeuT shapes our understanding of the mechanisms of sodium-coupled neurotransmitter transporters. *J Physiol*, 592(5), 863-869.

- Penmatsa, A., Wang, K. H., & Gouaux, E. (2013). X-ray structure of dopamine transporter elucidates antidepressant mechanism. *Nature*, *503*(7474), 85-90.
- Penmatsa, A., Wang, K. H., & Gouaux, E. (2015). X-ray structures of *Drosophila* dopamine transporter in complex with nisoxetine and reboxetine. *Nat Struct Mol Biol*, *22*(6), 506-508.
- Pliotas, C., Dahl, A. C., Rasmussen, T., Mahendran, K. R., Smith, T. K., Marius, P., . . . Naismith, J. H. (2015). The role of lipids in mechanosensation. *Nat Struct Mol Biol*, *22*(12), 991-998.
- Prusakiewicz, J. J., Kingsley, P. J., Kozak, K. R., & Marnett, L. J. (2002). Selective oxygenation of N-arachidonylglycine by cyclooxygenase-2. *Biochem Biophys Res Commun*, *296*(3), 612-617.
- Rajaratnam, K., & Rosgen, J. (2014). Isothermal titration calorimetry of membrane proteins - progress and challenges. *Biochim Biophys Acta*, *1838*(1 Pt A), 69-77.
- Rees, M. I., Harvey, K., Pearce, B. R., Chung, S. K., Duguid, I. C., Thomas, P., . . . Harvey, R. J. (2006). Mutations in the gene encoding GlyT2 (SLC6A5) define a presynaptic component of human startle disease. *Nat Genet*, *38*(7), 801-806.
- Rosenblum, A., Marsch, L. A., Joseph, H., & Portenoy, R. K. (2008). Opioids and the treatment of chronic pain: controversies, current status, and future directions. *Exp Clin Psychopharmacol*, *16*(5), 405-416.
- Ross, H. R., Gilmore, A. J., & Connor, M. (2009). Inhibition of human recombinant T-type calcium channels by the endocannabinoid N-arachidonoyl dopamine. *Br J Pharmacol*, *156*(5), 740-750.
- Roux, M. J., & Supplisson, S. (2000). Neuronal and glial glycine transporters have different stoichiometries. *Neuron*, *25*(2), 373-383.
- Sasmal, D. K., Pulido, L. E., Kasal, S., & Huang, J. (2016). Single-molecule fluorescence resonance energy transfer in molecular biology. *Nanoscale*, *8*(48), 19928-19944.
- Scheidelaar, S., Koorengel, M. C., Pardo, J. D., Meeldijk, J. D., Breukink, E., & Killian, J. A. (2015). Molecular model for the solubilization of membranes into nanodisks by styrene maleic Acid copolymers. *Biophys J*, *108*(2), 279-290.
- Scholz, J., Broom, D. C., Youn, D. H., Mills, C. D., Kohno, T., Suter, M. R., . . . Wolf, C. J. (2005). Blocking caspase activity prevents transsynaptic neuronal

apoptosis and the loss of inhibition in lamina II of the dorsal horn after peripheral nerve injury. *J Neurosci*, 25(32), 7317-7323.

Scholz, J., & Woolf, C. J. (2002). Can we conquer pain? *Nat Neurosci*, 5 Suppl, 1062-1067.

Shashoua, V. E., & Hesse, G. W. (1996). N-docosahexaenoyl, 3 hydroxytyramine : A dopaminergic compound that penetrates the blood-brain barrier and suppresses appetite. *Life Sciences*, 58(16), 1347-1357.

Sheskin, Hanus L., Slager J., Vogel Z., & R., M. (1997). Structural requirements for binding of anandamide-type compounds to the brain cannabinoid receptor. *J Med Chem*, 40, 659-667.

Shimizu, T. (2009). Lipid mediators in health and disease: enzymes and receptors as therapeutic targets for the regulation of immunity and inflammation. *Annu Rev Pharmacol Toxicol*, 49, 123-150.

Spiegel, M., Duraisamy, A. K., & Schroder, G. F. (2015). Improving the visualization of cryo-EM density reconstructions. *J Struct Biol*, 191(2), 207-213.

Srivastava, A., Yano, J., Hirozane, Y., Kefala, G., Gruswitz, F., Snell, G., . . . Okada, K. (2014). High-resolution structure of the human GPR40 receptor bound to allosteric agonist TAK-875. *Nature*, 513(7516), 124-127.

Stollznow Research for Pfizer Australia: Chronic Pain. April 2010

Stubbs, C. D., & Smith, A. D. (1984). The modification of mammalian membrane polyunsaturated fatty acid composition in relation to membrane fluidity and function. *Biochim Biophys Acta*, 779(1), 89-137.

Subramanian, N., Scopelitti, A. J., Carland, J. E., Ryan, R. M., O'Mara, M. L., & Vandenberg, R. J. (2016). Identification of a 3rd Na⁺ Binding Site of the Glycine Transporter, GlyT2. *PLoS One*, 11(6), e0157583.

Succar, R., Mitchell, V. A., & Vaughan, C. W. (2007). Actions of N-arachidonyl-glycine in a rat inflammatory pain model. *Mol Pain*, 3, 24.

Supplisson, S., & Bergman, C. (1997). Control of NMDA receptor activation by a glycine transporter co-expressed in *Xenopus* oocytes. *J Neurosci*, 17(12), 4580-4590.

Takahashi, E., Arai, T., Akahira, M., Nakajima, M., Nishimura, K., Omori, Y., . . . Hayashi, R. (2014). The discovery of potent glycine transporter type-2

- inhibitors: design and synthesis of phenoxymethylbenzamide derivatives. *Bioorg Med Chem Lett*, 24(18), 4603-4606.
- Takazawa, T., & MacDermott, A. B. (2010). Synaptic pathways and inhibitory gates in the spinal cord dorsal horn. *Ann N Y Acad Sci*, 1198, 153-158.
- Tan, B., O'Dell, D. K., Yu, Y. W., Monn, M. F., Hughes, H. V., Burstein, S., & Walker, J. M. (2010). Identification of endogenous acyl amino acids based on a targeted lipidomics approach. *J Lipid Res*, 51(1), 112-119.
- Taniguchi, R., Inoue, A., Sayama, M., Uwamizu, A., Yamashita, K., Hirata, K., . . . Nureki, O. (2017). Structural insights into ligand recognition by the lysophosphatidic acid receptor LPA6. *Nature*, 548(7667), 356-360.
- Tavoulari, S., Margheritis, E., Nagarajan, A., DeWitt, D. C., Zhang, Y. W., Rosado, E., . . . Rudnick, G. (2016). Two Na⁺ Sites Control Conformational Change in a Neurotransmitter Transporter Homolog. *J Biol Chem*, 291(3), 1456-1471.
- Terry, D. S., Kolster, R. A., Quick, M., LeVine, M. V., Khelashvili, G., Zhou, Z., . . . Blanchard, S. C. (2018). A partially-open inward-facing intermediate conformation of LeuT is associated with Na(+) release and substrate transport. *Nat Commun*, 9(1), 230.
- Thomas, B. F., Adams, I. B., Mascarella, S. W., Martin, B. R., & Razdan, R. K. (1996). Structure-activity analysis of anandamide analogs: relationship to a cannabinoid pharmacophore. *J Med Chem*, 39(2), 471-479.
- Tian, X., Guo, J., Yao, F., Yang, D. P., & Makriyannis, A. (2005). The conformation, location, and dynamic properties of the endocannabinoid ligand anandamide in a membrane bilayer. *J Biol Chem*, 280(33), 29788-29795.
- Todd, A. J. (2010). Neuronal circuitry for pain processing in the dorsal horn. *Nat Rev Neurosci*, 11(12), 823-836.
- Trott, O & Olson, A.J. (2010). AutoDock Vina: improving the speed and accuracy of docking with a new scoring function, efficient optimization and multithreading. *J Comput Chem*. 31(2):455-461
- Uchida, Y., Ohtsuki, S., Katsukura, Y., Ikeda, C., Suzuki, T., Kamiie, J., & Terasaki, T. (2011). Quantitative targeted absolute proteomics of human blood-brain barrier transporters and receptors. *J Neurochem*, 117(2), 333-345.
- Ueda, N., Yamamoto, K., Yamamoto, S., Tokunaga, T., Shirakawa, E., Shinkai, H., . . . Saito, H. (1995). Lipoxygenase-catalyzed oxygenation of

- arachidonylethanolamide, a cannabinoid receptor agonist. *Biochimica et Biophysica Acta (BBA) - Lipids and Lipid Metabolism*, 1254(2), 127-134.
- Valley, C. C., Cembran, A., Perlmutter, J. D., Lewis, A. K., Labello, N. P., Gao, J., & Sachs, J. N. (2012). The methionine-aromatic motif plays a unique role in stabilizing protein structure. *J Biol Chem*, 287(42), 34979-34991.
- van Meer, G., Voelker, D. R., & Feigenson, G. W. (2008). Membrane lipids: where they are and how they behave. *Nat Rev Mol Cell Biol*, 9(2), 112-124.
- Vandenberg, R. J., Mostyn, S. N., Carland, J. E., & Ryan, R. M. (2016). Glycine transporter2 inhibitors: Getting the balance right. *Neurochem Int*, 98, 89-93.
- Vandenberg, R. J., Ryan, R. M., Carland, J. E., Imlach, W. L., & Christie, M. J. (2014). Glycine transport inhibitors for the treatment of pain. *Trends Pharmacol Sci*, 35(8), 423-430.
- Vandenberg, R. J., Shaddick, K., & Ju, P. (2007). Molecular basis for substrate discrimination by glycine transporters. *J Biol Chem*, 282(19), 14447-14453.
- Vinothkumar, K. R. (2015). Membrane protein structures without crystals, by single particle electron cryomicroscopy. *Curr Opin Struct Biol*, 33, 103-114.
- Vuong, L. A., Mitchell, V. A., & Vaughan, C. W. (2008). Actions of N-arachidonyl-glycine in a rat neuropathic pain model. *Neuropharmacology*, 54(1), 189-193.
- Wang, K. H., Penmatsa, A., & Gouaux, E. (2015). Neurotransmitter and psychostimulant recognition by the dopamine transporter. *Nature*, 521(7552), 322-327.
- Wiles, A. L., Pearlman, R. J., Rosvall, M., Aubrey, K. R., & Vandenberg, R. J. (2006). N-Arachidonyl-glycine inhibits the glycine transporter, GLYT2a. *J Neurochem*, 99(3), 781-786.
- Wohri, A. B., Hillertz, P., Eriksson, P. O., Mueller, J., Dekker, N., & Snijder, A. (2013). Thermodynamic studies of ligand binding to the human homopentameric glycine receptor using isothermal titration calorimetry. *Mol Membr Biol*, 30(2), 169-183.
- Xu, T. X., Gong, N., & Xu, T. L. (2005). Inhibitors of GlyT1 and GlyT2 differentially modulate inhibitory transmission. *Neuroreport*, 16(11), 1227-1231.
- Yabuuchi, H., Tamai, I., Nezu, J., Sakamoto, K., Oku, A., Shimane, M., . . . Tsuji, A. (1999). Novel membrane transporter OCTN1 mediates multispecific,

- bidirectional, and pH-dependent transport of organic cations. *J Pharmacol Exp Ther*, 289(2), 768-773.
- Yaksh, T. L. (1989). Behavioral and autonomic correlates of the tactile evoked allodynia produced by spinal glycine inhibition: effects of modulatory receptor systems and excitatory amino acid antagonists. *Pain*, 37(1), 111-123.
- Yamashita, A., Singh, S. K., Kawate, T., Jin, Y., & Gouaux, E. (2005). Crystal structure of a bacterial homologue of Na⁺/Cl⁻-dependent neurotransmitter transporters. *Nature*, 437(7056), 215-223.
- Yang, Z., Aubrey, K. R., Alroy, I., Harvey, R. J., Vandenberg, R. J., & Lynch, J. W. (2008). Subunit-specific modulation of glycine receptors by cannabinoids and N-arachidonyl-glycine. *Biochem Pharmacol*, 76(8), 1014-1023.
- Yau, W. M., Wimley, W. C., Gawrisch, K., & White, S. H. (1998). The preference of tryptophan for membrane interfaces. *Biochemistry*, 37(42), 14713-14718.
- Yu, M., Ives, D., & Ramesha, C. S. (1997). Synthesis of prostaglandin E2 ethanolamide from anandamide by cyclooxygenase-2. *J Biol Chem*, 272(34), 21181-21186.
- Zabara, A., Meikle, T. G., Newman, J., Peat, T. S., Conn, C. E., & Drummond, C. J. (2017). The nanoscience behind the art of in-meso crystallization of membrane proteins. *Nanoscale*, 9(2), 754-763.
- Zafra, F., Aragon, C., Olivares, L., Danbolt, N. C., Gimenez, C., & Storm-Mathisen, J. (1995). Glycine transporters are differentially expressed among CNS cells. *J Neurosci*, 15(5 Pt 2), 3952-3969.
- Zeppelin, T., Ladefoged, L. K., Sinning, S., Periole, X., & Schiott, B. (2018). A direct interaction of cholesterol with the dopamine transporter prevents its out-to-inward transition. *PLoS Comput Biol*, 14(1), e1005907.
- Zhao, Y., Terry, D., Shi, L., Weinstein, H., Blanchard, S. C., & Javitch, J. A. (2010). Single-molecule dynamics of gating in a neurotransmitter transporter homologue. *Nature*, 465(7295), 188-193.
- Zhao, Y., Terry, D. S., Shi, L., Quick, M., Weinstein, H., Blanchard, S. C., & Javitch, J. A. (2011). Substrate-modulated gating dynamics in a Na⁺-coupled neurotransmitter transporter homologue. *Nature*, 474(7349), 109-113.